Chapter 5A:

Palladium Schiff-Base Complexes Encapsulated in Zeolite-Y Host: Functionality Controlled by the structure of guest complex

***Abstract**: A series of palladium complexes of tetradendate Schiff base ligands L1' (N,N′-bis(salicylidene)phenylene-1,3-diamine) and its derivatives L5' and L6' have been synthesized by using the "flexible ligand method" within the supercage of zeolite-Y. These complexes in both their free and encapsulated states have been thoroughly characterized with the help of different characterization tools such as XRD, SEM-EDS, BET, thermal analysis, XPS, IR, and UV–Vis spectroscopic studies. All these encapsulated complexes are identified with a dramatic red shift of the d–d transition in their electronic spectra when compared with their free states. Theoretical as well as experimental studies together suggest a substantial modification of the structural parameters of square planar Pd(II)–Schiff base complexes upon encapsulation within the supercage of zeolite-Y. Encapsulated complexes are also subject to show modified catalytic activities toward the Heck reaction. These heterogeneous catalysts can easily be separated from the reaction mixture and reused.*

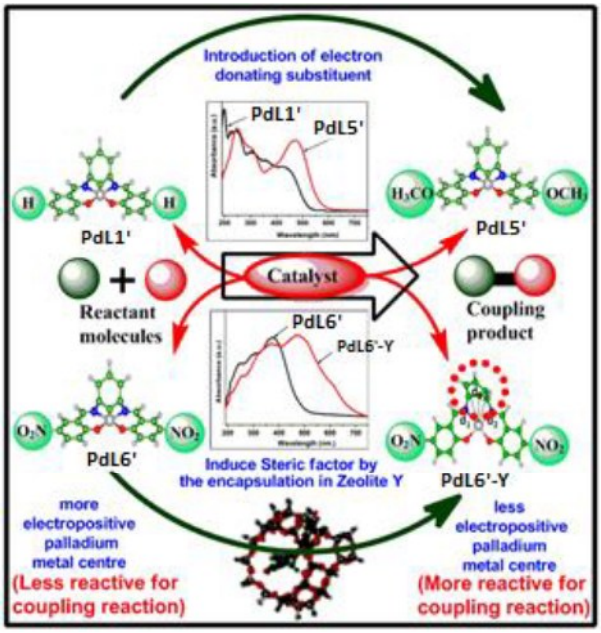

*S. Kumari, K. Maddipoti, B. Das and S. Ray, *Inorg. Chem.*, 2019, **58 (2)**, 1527-1540.

5A.1 INTRODUCTION

Cross-coupling reactions in chemistry are of enormous importance for obvious reasons and to list down the implications, it is mandatory to mention their applications in organic synthesis for the preparation of natural products, biologically active compounds, conducting polymers, pesticides, pharmaceutical intermediates, and liquid crystals.[1-5] Very commonly, these reactions are catalyzed by palladium based compounds. Quite a few numbers of homogeneous palladium complexes have been reported as efficient catalysts for Heck coupling reaction, however, they certainly have some limitations and disadvantages specifically when separation, purification of the products, thermal stability, recyclability of catalyst are concerned and in many cases these catalyst suffer from loss of catalytic activity.[6, 7] In recent times, many researchers are pursuing with several techniques such as support of ionic liquids,[8] immobilized on silica,[9] grafted on polymers,[10] anchored on activated carbon[11] or carbon nanotubes[12] and supported on zeolites[13] and MCM-41[14, 15]etc, specially to recover the catalyst successfully. Several such host-guest chemistry based studies focus on transition metal (M) complexes (M=Co, Ni, Cu and Pd) within the microporous and mesoporous materials.[16-20] Zeolite encapsulated palladium phenanthroline complex exhibited efficient catalytic activity for the aminocarbonylation reaction[21] and zeolite encaged Pd clusters are found to be proficient catalyst for the hydrogen generation.[22]

Palladium (II) Schiff-base complexes have been widely studied because of their diverse applications in catalysis.[23-28] Schiff-base ligands with a largely conjugated architecture of π systems play an important role in inorganic chemistry due to their synthetic flexibility, strong binding ability and excellent chelating nature.[29-31] Palladium salen and salophen complexes prevails as active catalysts for the Heck olefination of aryl iodides and Suzuki reactions under aerobic conditions.[32] An approach for the simultaneous immobilization of a new NHC-Pd/IL matrix on silica has been established. This system was successfully employed as catalyst for the Heck coupling reaction using a broad range of iodo- and bromo- arenes. The system exhibits high thermal stability and can be recycled up to four reaction cycles.[33]

Air and moisture-stable palladium (II) complex of Schiff-base salen-OH ligand has been synthesized and employed as a catalyst for Mizoroki–Heck and decarboxylative coupling reactions. It exhibits high catalytic activities towards both the reactions. Besides, it requires a low loading of catalyst i.e. 2.0 mol% is used for Heck coupling and 0.5 mol% catalyst is used for decarboxylative coupling reactions than the previously examined catalysts.[34] Even lower Pd loading of 0.0188 mol% of palladium complex entrapped

in zeolite-Y is used for the Suzuki–Miyaura cross-coupling reactions quite successfully.[35] In another study, palladium complex loaded in zeolites show high catalytic activity for the Heck coupling reaction where low amount of palladium (0.1 mol%) is sufficient to perform Heck reaction .[36] In the current study, even lesser amount of palladium catalyst i.e. 0.70 mmol% is of interest and is explored as catalyst the Heck coupling reaction.

Very recently, $Fe_3O_4@SiO_2$ core–shell superparamagnetic nanoparticles functionalized palladium salophen complex are synthesized and used as proficient magnetic nanocatalyst for the Heck and Sonogashira cross coupling reactions. The loading content and leaching amounts of palladium metal are analyzed by inductively coupled plasma (ICP) analysis. This heterogeneous catalyst showed a good catalytic activity for the coupling of aryl halides with alkynes (Sonogashira reaction) as well as aryl halides with alkene (Heck reaction). The catalyst can be simply separated from the reaction mixture by an external magnet and reused for eight consecutive runs without any significant loss of activity.[37]

Out of varieties of host materials, zeolite-Y is well known microporous crystalline aluminosilicate material with a pore diameter of 7.4 Å and supercage dimension of 12.47 Å. It provides high surface area and excellent chemical stability with quite a low toxicity. Encapsulation of metal complex is a convenient approach to couple the reactivity of the complex with the stability, specific electronic environment provided by host materials and ease of separation. It is a unique way for the site isolation of the desired catalyst.

Recently, the synthesis of a series of palladium salen complexes inside zeolite-Y has been reported. These encapsulated palladium complexes have been perceived to be efficient catalysts for sulfoxidation of methyl phenyl sulfide compared to their neat analogues and towards the betterment of catalysis, the role of the distorted structure of the encapsulated complexes have been established.[18]

The current work deals with the synthesis of encapsulated palladium Schiff base complexes inside the supercage of zeolite Y *via* the 'flexible ligand method'. This method is already well-established and as discussed before, is found appropriate for the encapsulation of palladium salophen complexes as the salophen ligand having desired flexibility can be introduced into the supercage of zeolite through the channel. Here the un-substituted ligand is *N, N'*-bis(salicylidene)phenylene-1,3-diamine (shown in Figure 5A.1) Once, the complex formed, this ligand also loses the flexibility and hence becomes immobilized inside the supercage unless the zeolite framework being destroyed. Encapsulation of these complexes

inside the host makes it altogether a heterogeneous catalyst. This is a convenient and efficient route to combine the reactivity of palladium complex of this particular ligand with the robustness and stereochemistry of the zeolite framework.

The palladium complexes of interest with the L1′, L5′ and L6′ ligands follow the order of molecular dimension as PdL1′<PdL5′<PdL6′, where L1′ ;*N, N'*-bis(salicylidene)phenylene-1,3-diamine, L5′; *N, N'*-bis(5-methoxysalicylidene)phenylene-1,3-diamine and L6′; *N, N'*-bis(5-nitrosalicylidene)phenylene-1,3-diamine (given in Figure 5A.1). Here, the chosen substituent groups are known of displaying strong electronic effects. The metal in three different complexes with different substituent essentially experience electronic effect differently, as well as are subjected to the different steric constraint imposed by the topology of the zeolite cavity. The host framework induces the structural modification to the guest complex and alters the electronic, magnetic and redox properties of guest metal complex. Therefore, the topology of the host framework has substantial control over the functionality and selectivity of the guest molecule. These hybrid systems are employed as a catalyst for the cross-coupling Heck reaction of bromobenzene with styrene in presence of sodium carbonate as a base to investigate the steric interaction and electronic effect of the substituent's group attached to the complex.

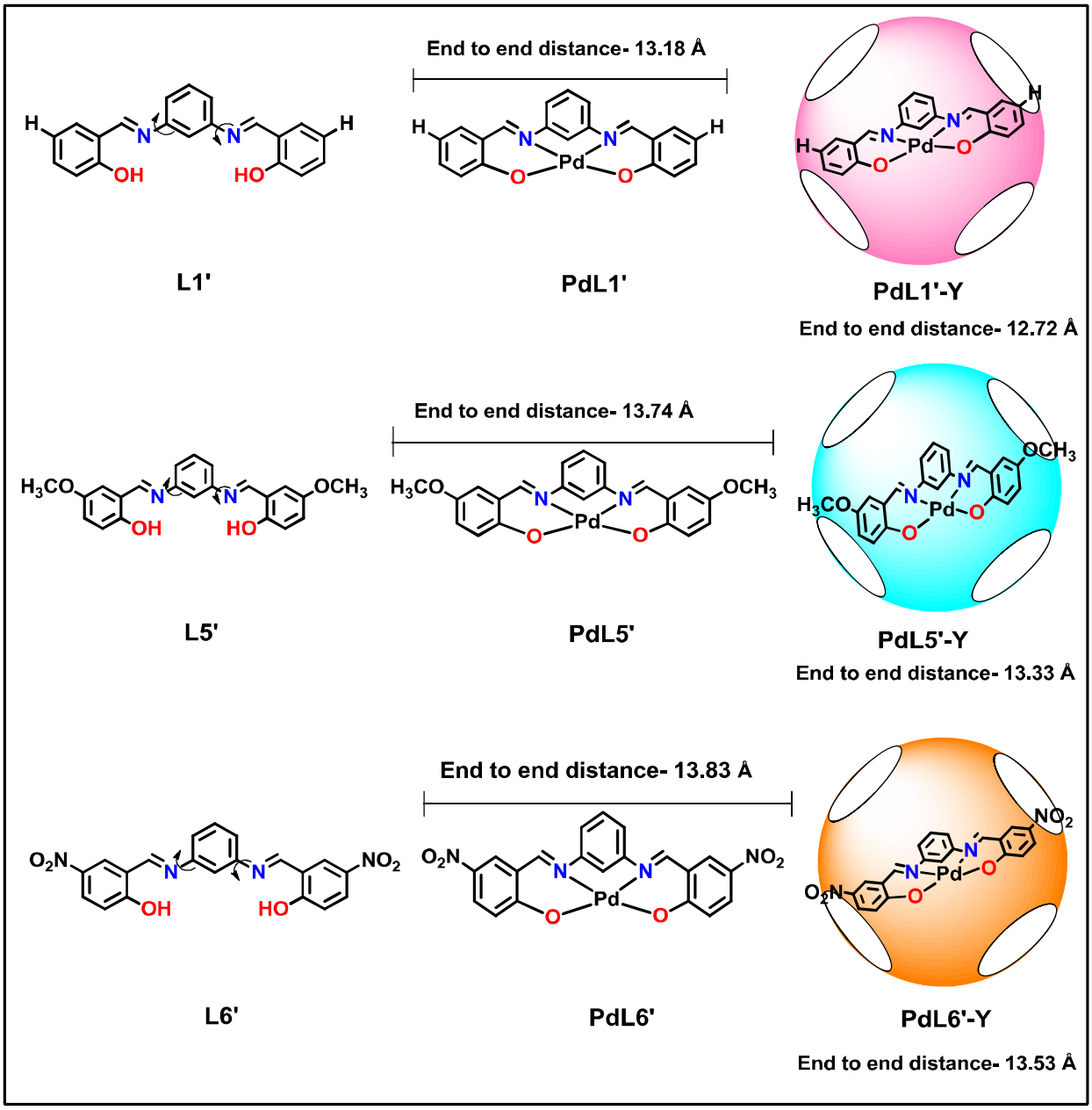

Figure 5A.1: Schematic representation of palladium Schiff-base complexes.

5A.2 RESULTS AND DISCUSSION

Synthesis of ligands and nickel Schiff-base complexes in free or encapsulated states have already discussed in chapter 2 under experimental section (2.2.1-2.2.5).

5A.2.1 Elemental Analysis

The chemical composition of palladium (II)-exchanged zeolite Y and encapsulated palladium complexes (PdL1′-Y, PdL5′-Y, and PdL6′-Y) are analyzed by EDX technique. The Si/Al ratio for unit cell $Na_{52}(AlO_2)_{52}(SiO_2)_{140}.y\ H_2O$ of pure zeolite Y is 2.7. The Si/Al ratio has not been significantly affected during palladium (II)-exchanged reaction as well as during the process of encapsulation as the dealumination during encapsulation are minimal. Results obtained from EDX analysis are given in form of weight % in Table 5A.1. The concentration of palladium metal in the encapsulated complexes as compared to palladium (II)-exchanged zeolite Y is found to be lower. The decrease in palladium content can probably be attributed to the formation of the palladium complex inside the cavity of host as leaching of some of the palladium ion during the encapsulation process is commonly observed phenomenon.

Table 5A.1: Concentration of palladium (wt %) content in the different Samples.

S.No.	Samples	Palladium (wt%)	Si/ Al ratio
1	Zeolite-Y	-	2.90
2	Pd-Y	0.65	2.79
3	PdL1′-Y	0.38	2.86
4	PdL5′-Y	0.41	2.84
5	PdL6′-Y	0.40	2.80

5A.2.2 X-Ray Diffraction and Scanning Electron Microscopy Analysis

The powder X-ray diffraction patterns have been recorded for pure zeolite Y, palladium (II)-exchanged zeolite Y, and zeolite encapsulated complexes (presented in Figure 5A.2) with 2θ varying from 8 to 50 to study the crystallinity, the integrity of the host framework and to ensure encapsulation inside the supercage of zeolite Y. The appearance of very similar XRD patterns for pure zeolite-Y, Pd(II)-Y and zeolite encapsulated palladium Schiff-base complexes positively indicates that the framework of host has not undergone any structural modification after encapsulation of the metal complexes inside the cavity and crystalline nature of host is also not affected.[38] However, there is an interesting observation with the relative intensities of peaks appearing at 2θ values 10° and 12° corresponding to the planes 220 and 311

respectively. For pure and Pd(II)-Y zeolite samples, XRD peak at 10° is more intense than peak at 12° whereas, for encapsulated metal Schiff base complexes, the relation between intensities is just reverse i.e. $I_{220}<I_{311}$. This finding matches with the previously discussed systems in Chapter, 3,is exactly in-line with quite a well-established semi-empirical intensity reversal of the XRD peaks of pure zeolite at 2θ =10° and 12° with large molecule entrapped.[39] This change in the relative intensities may be related with the rearrangement of randomly coordinated free cations in zeolite Y.[40, 41] No new peak is detected for Pd(II)-Y as well as for zeolite with encapsulated palladium complexes confirming a low loading level of metal in host framework.

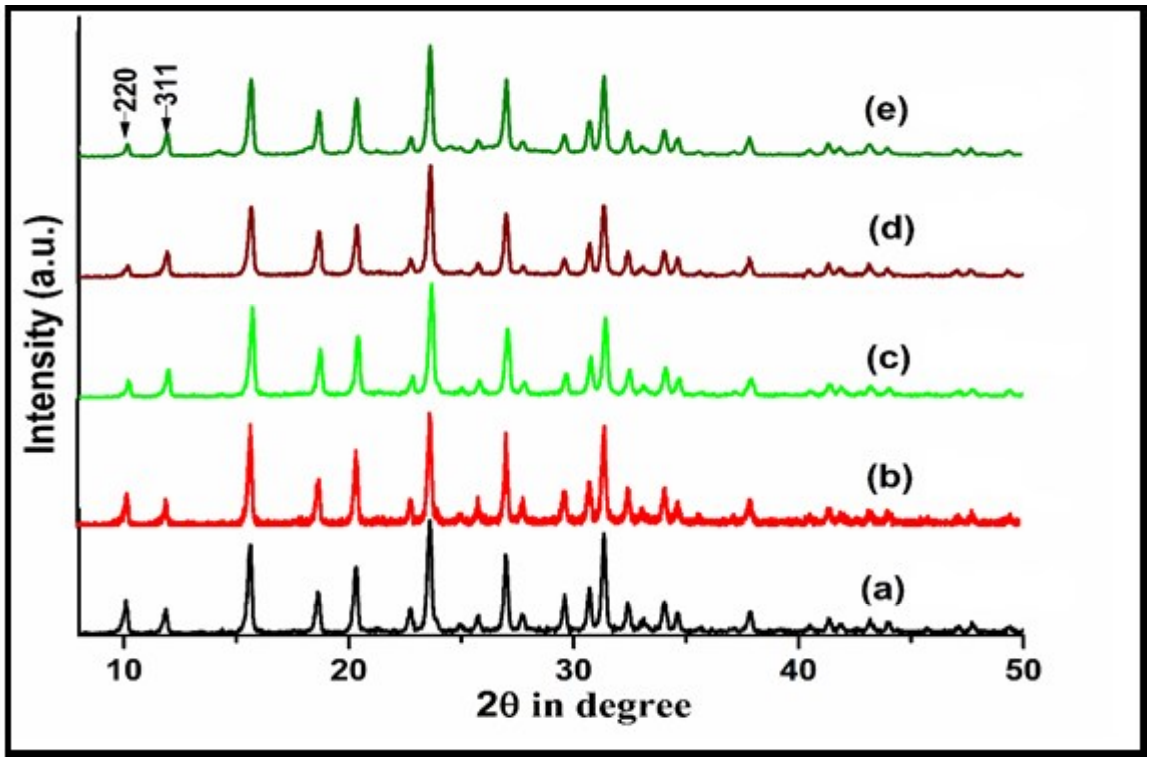

Figure 5A.2: XRD pattern of (a) Pure zeolite-Y, (b) Pd-exchanged zeolite -Y, (c) PdL1′-Y, (d) PdL5′-Y and (e) PdL6′-Y.

From scanning electron microscopy analysis, it has been observed that some impurities are present at the surface of the host in form of complex and unreacted ligand but these impurities have been completely washed from the surface of zeolite Y by extensive Soxhlet extraction. SEM images are given in Figure

5A.3. After Soxhlet extraction, clear boundaries of the host framework are manifest in SEM micrograph. This observation further, suggests that the crystalline nature of the host is conserved during the encapsulation process.

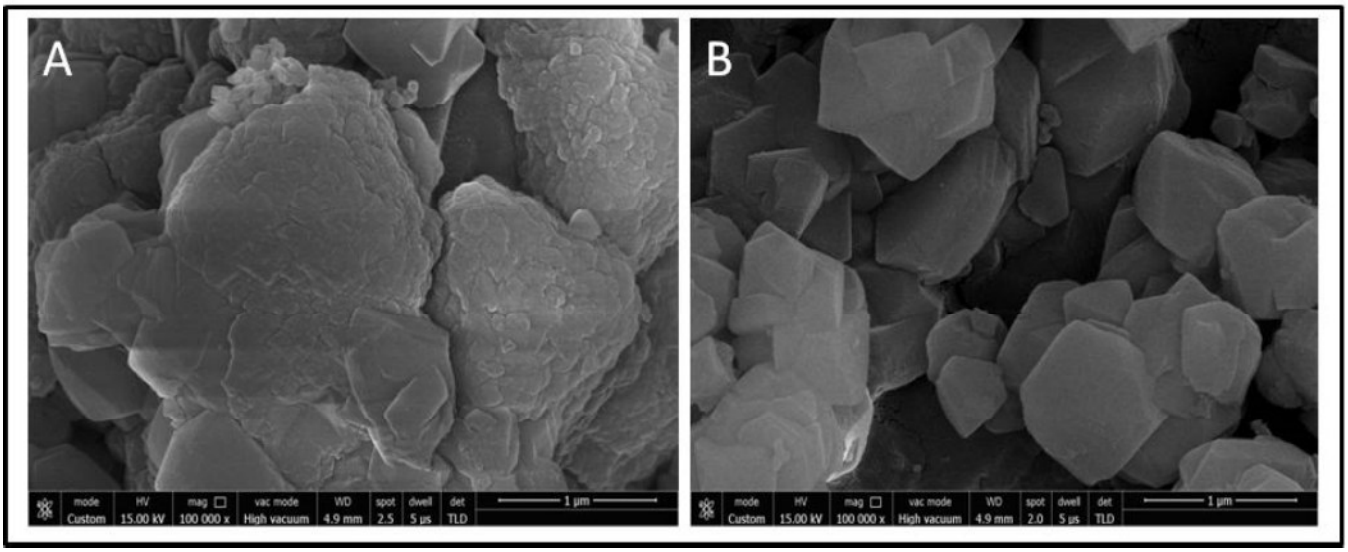

Figure 5A.3: SEM images (A) PdL5′-Y (before Soxhlet extraction) and (B) PdL5′-Y (after Soxhlet extraction).

5A.2.3 BET surface area analysis

The BET surface area analysis has been carried out to determine the surface area and pore volume for the pure zeolite Y and zeolite with encapsulated complexes. The comparative adsorption-desorption isotherms for all encapsulated complexes and zeolite-Y are shown in Figure 5A.4 and the surface area and pore volume data are given in Table 5A.2. The pattern of adsorption-desorption isotherms for all the samples are found to be nearly identical (Figure 5A.4), suggesting that the host framework remains unaffected during the whole process of encapsulation. However, there exists a considerable difference in the surface area and pore volume of zeolite Y and all hybrid systems. In all the encapsulated systems, the BET surface area and pore volume are found to be significantly lower in comparison to those for pure zeolite-Y, which directly indicates the presence of metal complex inside the supercage of zeolite Y rather than adsorbed on

the external surface.[42, 43]All the catalysts have shown type I adsorption-desorption isotherms, which is a characteristic of the microporous material.[44] The lowering of BET surface areas and pore volumes for the hybrid systems are largely depend upon the loading level of metal in zeolites along with the molecular dimension and geometry of the complex encapsulated inside the zeolite supercage.

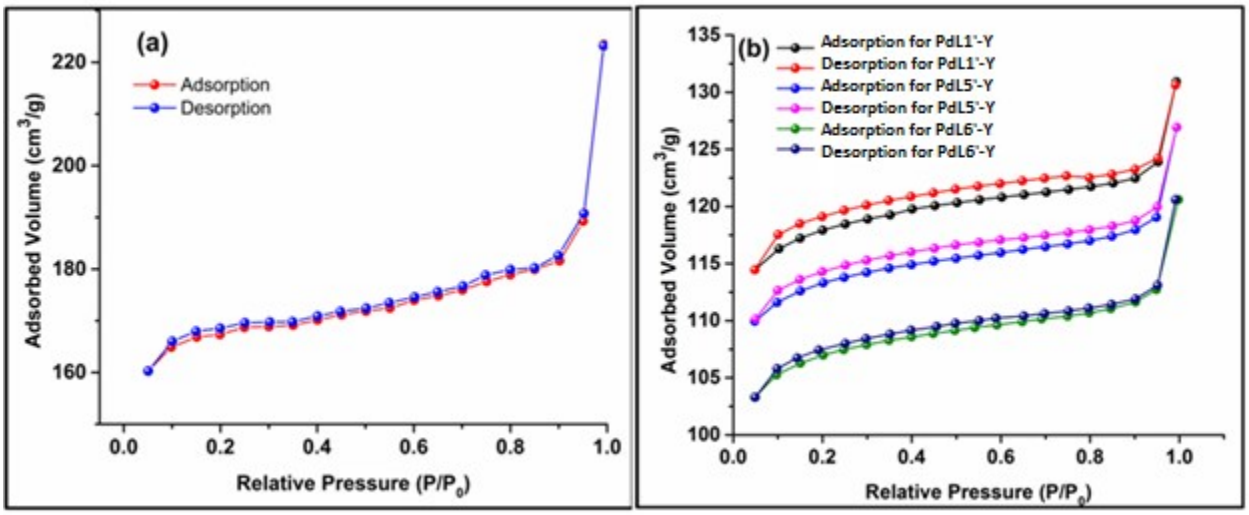

Figure 5A.4: BET isotherms for pure zeolite-Y and zeolite encapsulated complexes: (a) pure zeolite Y, (b) PdL1′-Y, PdL5′-Y and PdL6′-Y.

Table 5A.2: BET surface area and pore volume of pure zeolite Y and encapsulated complexes PdL1′-Y, PdL5′-Y and PdL6′-Y.

S.No.	Sample	BET surface area (m^2/g)	Pore volume (cm^3/g)
1	**Pure zeolite Y**	535	0.3456
2	**PdL1′-Y**	355	0.2025
3	**PdL5′-Y**	342	0.1961
4	**PdL6′-Y**	340	0.1920

5A.2.4 Thermal analysis

Differential thermal analysis and thermo-gravimetric analysis have been used to characterize for all neat and encapsulated palladium complexes. The TG/DTA curves for pure zeolite Y, free-state and encapsulated PdL6′ complexes are presented in Figure 5A.5 and thermal analysis spectra for neat complexes PdL1′, PdL5′ and corresponding encapsulated complexes are represented in Figure 5A.6. Pure zeolite shows only weight loss due to loss of adsorbed water in the temperature range of 70-250 °C. All the three neat complexes exhibit sharp weight loss in a single step. There is a sharp decomposition with highest weight % change at 272 °C for PdL6′ neat complex and this decomposition corresponds to the loss of organic moiety of the complex. However, for the corresponding zeolite encapsulated palladium complexes weight loss occurs in two steps. The first step in the temperature range of 30-150 °C is certainly due to the desorption of physically adsorbed water molecules from host framework,[45] which appears as endothermic peak in DTA curve.[46] The second step in the wide temperature range of 300-800°C is associated with the decomposition of organic part of catalyst as an exothermic phenomenon.[45] The TG/DTA curves show a sharp weight loss occurring for all neat complexes in the exothermic mode[46] but all encapsulated complexes are characterized with plateau type plot, indicating slow and continuous weight loss and process of decomposition extends towards higher temperature. It is quite apparent that upon encapsulation, thermal stability of the complexes is enhanced significantly.[47]

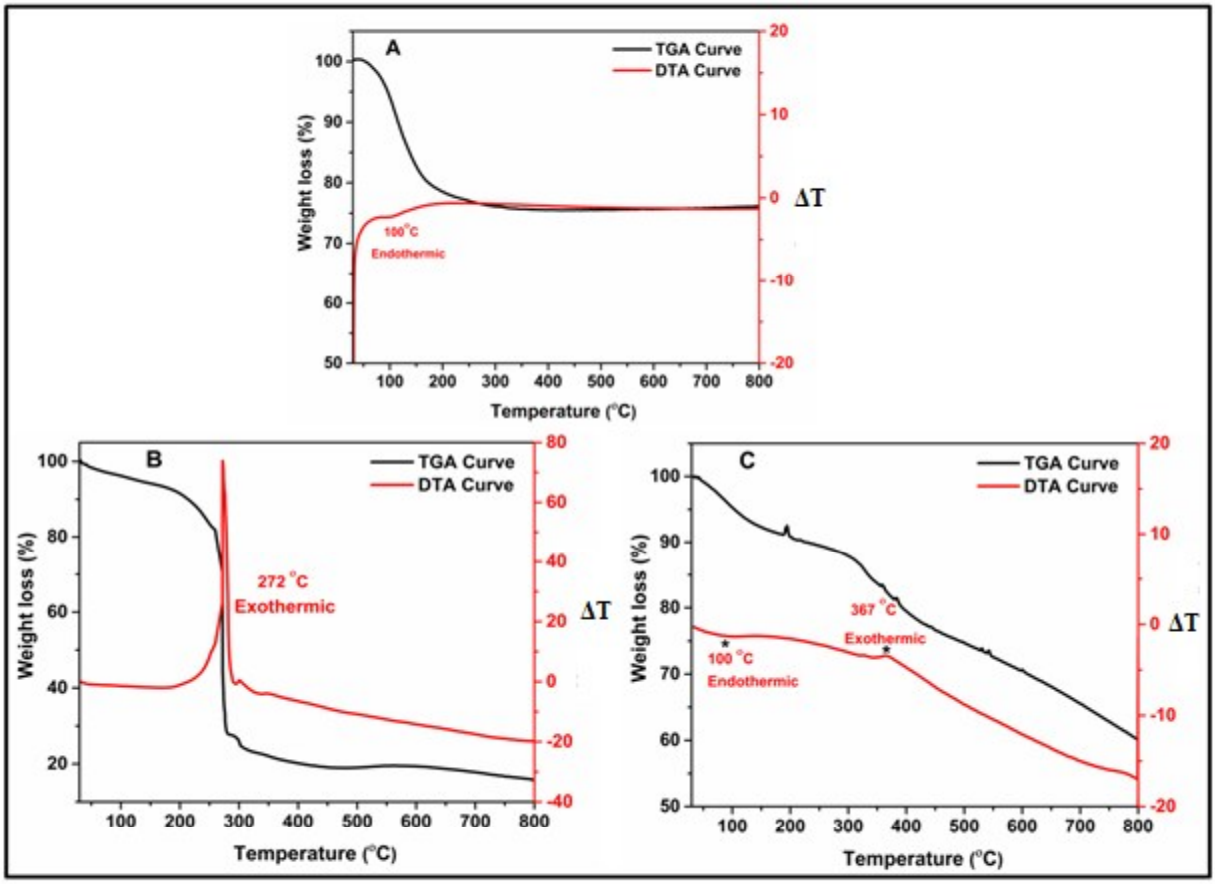

Figure 5A.5: Thermogravimetric analysis (TGA) and Differential thermal analysis (DTA) results for (A) pure zeolite-Y, (B) PdL6′ and (C) PdL6′-Y.

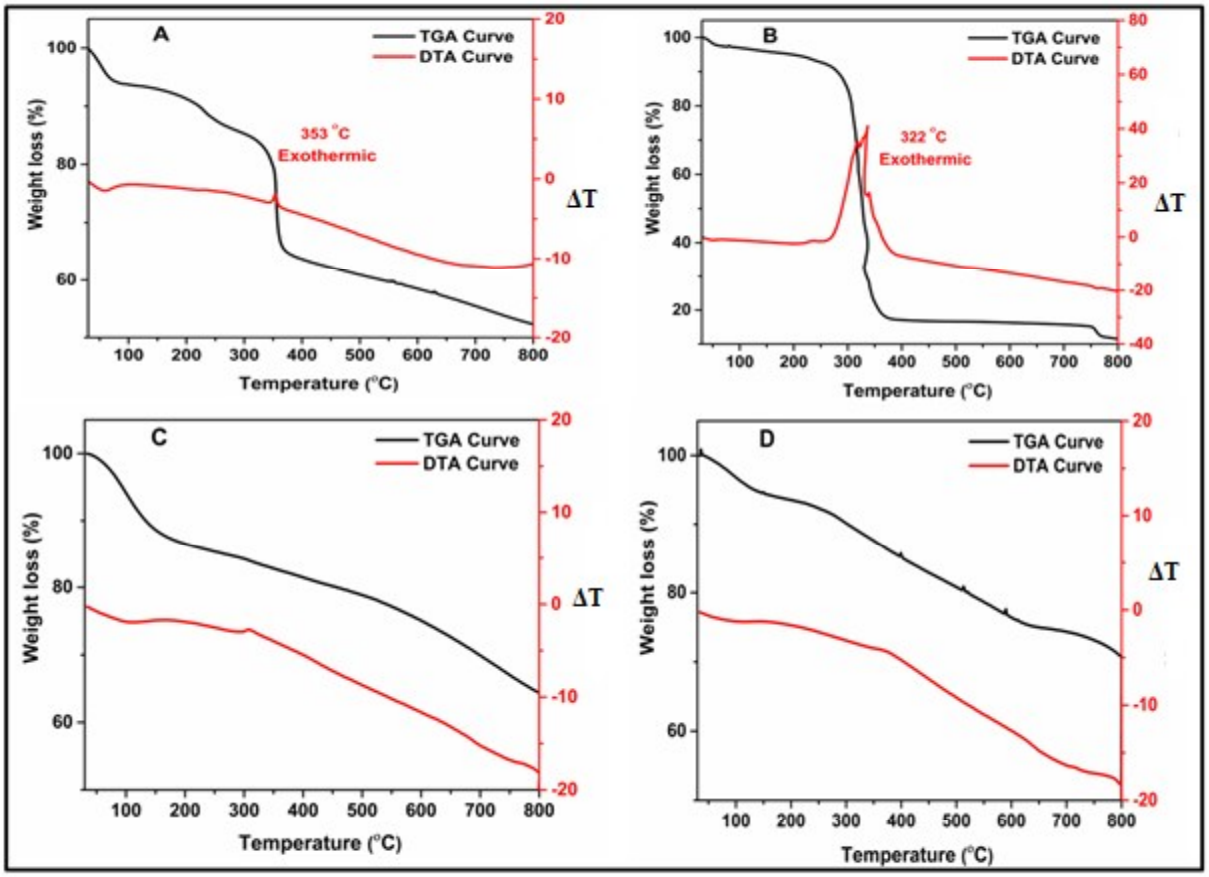

Figure 5A.6: TGA and DTA curves for (A) PdL1′, (B) PdL5′, (C) PdL1′-Y and (D) PdL5′-Y.

5A.2.5 IR Spectroscopic study

The FTIR spectral data of pure zeolite-Y, palladium Schiff-base complexes and zeolite encapsulated palladium complexes are shown in Figure 5A.7 and Table 5A.3. The strong IR peak at 1018 cm^{-1} of pure zeolite Y corresponds to the asymmetric stretching vibrations of $(Si/Al)O_4$ units of host framework. Few important peaks observed at 560, 717 and 786 cm^{-1}, are the signature of T-O bending mode, double ring and symmetric stretching vibrations respectively.[48] In addition, the prominent IR bands appeared at 1643 and 3500 $cm^{-1}$are assigned to lattice water molecules and surface hydroxylic group, respectively.[49] All these characteristics IR bands of zeolite Y remain unaltered after palladium exchange and even after encapsulation reaction, concluding that the host framework maintains its integrity during the whole process of encapsulation of palladium Schiff base complexes. The IR spectral range of 1200 to1600 cm^{-}

[1]appears to be a suitable range for the study of zeolite encapsulated metal complex as in this range, prominent IR bands of the zeolite are absent. Therefore, IR peaks observed are only because of the complexes though the intensity of these IR peaks is very weak definitely indicating low loading level of palladium inside the zeolite cage.

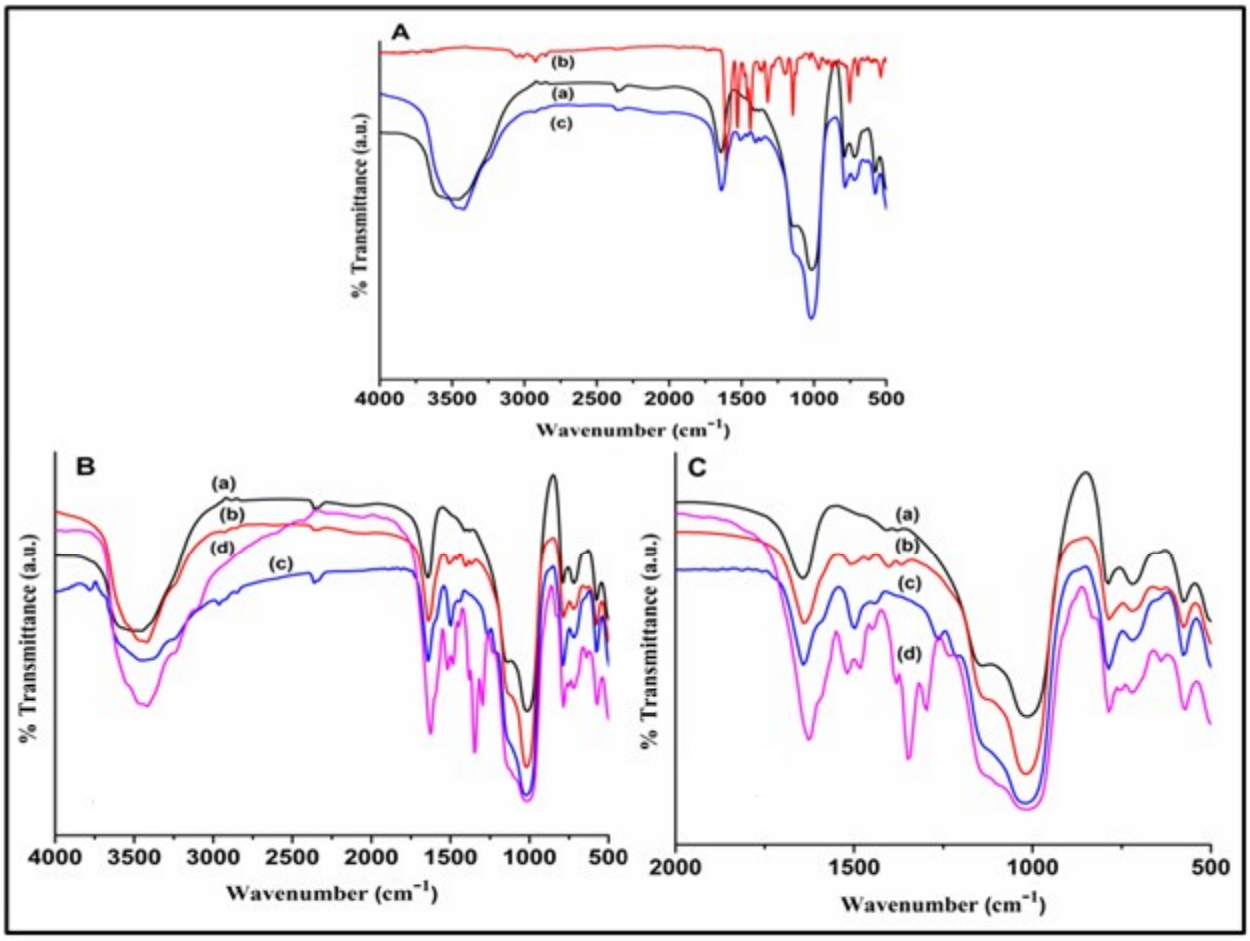

Figure 5A.7: FTIR spectra of (A) (a) pure zeolite-Y, (b) PdL1′ and (c) PdL1′-Y, (B) (a) zeolite-Y, (b) PdL1′-Y, (c) PdL5′-Y and (d) PdL6′-Y and (C) Enlarged view of FTIR spectra in the range of 500 cm^{-1} to 2000 cm^{-1} for (a) pure zeolite-Y, (b) PdL1′-Y, (c) PdL5′-Y and (d) PdL6′-Y.

FT-IR peaks of ligand observed as two strong bands at1612-1620 cm^{-1} and 1273-1296 cm^{-1} are attributed to the C=N and C-O stretching vibrations and these bands are slightly shifted towards lower frequency upon complexation, indicating nitrogen and oxygen coordination inside the cavity of zeolite Y. IR spectra of free state palladium complexes show important peaks at 1528, 1439 cm^{-1} (C=C Stretch.), 1605 cm^{-1}(C=N stretch.), 1278 cm^{-1}(C-O stretch.) and 1358 (ν_{C-H} deformation).[50] Similar IR bands with little shift are also observed in all encapsulated complexes providing indirect evidence for the presence of palladium Schiff base complexes inside the supercage of host. Shifts in some characteristics peaks upon encapsulation are attributed to the effect of host matrix on the metal complex. The shift in ν_{C-H} deformation frequencies obtained in all encapsulated complexes, also provides clear evidence for the encapsulation of metal complex inside the cavity of host.

Table 5A.3: FTIR data of neat and encapsulated complexes.

S. No	Samples	C=N stretching	C=C stretching	C-H deformation	C-O stretching
1	**PdL1′**	1605	1528,1439	1358	1278
2	**PdL1′-Y**	1636	1535,1462	1369	1257
3	**PdL5′**	1589	1528,1466	1366	1257
4	**PdL5′-Y**	1643	1497,1443	1378	1265
5	**PdL6′**	1605	1551,1481	1380	1256
6	**PdL6′-Y**	1628	1520,1481	1383	1234

5A.2.6 X-ray Photoelectron Spectroscopy (XPS)

XPS studies also are found explanatory about the existence of the palladium complex inside the supercage of zeolite Y. XPS data confirms the relative concentration of element and their oxidation states in the neat and encapsulated complexes. It is noticed that the XPS signal for palladium metal in the complex is very weak when it is encapsulated; definitely indicates a very low concentration of palladium in host framework. Observations are just in accordance with those obtained from EDX, IR and UV-Vis

spectroscopic studies. The XPS measurements are carried out for PdL1′ (neat state), PdL1′-Y and PdL5′-Y (encapsulated states). The binding energies(eV) for Pd(3d), C(1s), N(1s), O(1s), Si(2p), Al(2p) and Na(1s) and XPS spectra of PdL1′, PdL1′-Y and PdL5′-Y are presented in Table 5A.4 and Figure 5A.8-5A.10). The binding energies of $Pd3d_{3/2}$ and $Pd3d_{5/2}$, confirm the palladium metal present in +2 oxidation state in all complexes. For PdL1′ complex, these signals appear at 343.6 (Pd $3d_{3/2}$) and 338.2 eV (Pd $3d_{5/2}$),[51] whereas for the encapsulated complexes, these signals are at approximately same binding energies; for the PdL1′-Y, signals have appeared at 342.4, 337.2 eV and for PdL5′-Y complex, signals are observed at 342.5, 336.3 eV with one new XPS signal at higher binding energy of 347.9 eV. The appearance of the new peak after encapsulation is a mere indication of removal of electron density around the palladium center because of obliteration of the delocalization environment driven by the adaptation of square planar geometry of the encapsulated complexes.[52-54] For PdL1′ complex, C (1s) XPS signals appear at 286.4 and 284.5 eV corresponding to sp^3 and sp^2 carbon atoms respectively whereas two different type of N (1s) signals appeared, confirm the presence of M-N and C=N species. O (1s) XPS signal are observed at binding energy value of 534.0 eV.[55] Encapsulated complexes (PdL1′-Y and PdL5′-Y) secure these XPS peaks almost at the identical positions. In both encapsulated complexes, the binding energy signals for Pd(3d), C(1s), N(1s), O(1s), Si(2p), Al(2p) and Na(1s) are observed. PdL1′-Y system has shown zeolitic Si 2p, Al 2p and Na 1s signals at 103.2 eV, 75.5 eV and 1073.3 eV respectively, whereas in PdL5′-Y, zeolitic signals appear at binding energies at 103.5 eV (Si 2p), 74.8 eV (Al 2p) and 1072.6 eV (Na 1s). The binding energy data of Pd 3d peak for all encapsulated complexes ensure the successful encapsulation of palladium Schiff base complex inside the zeolite Y.

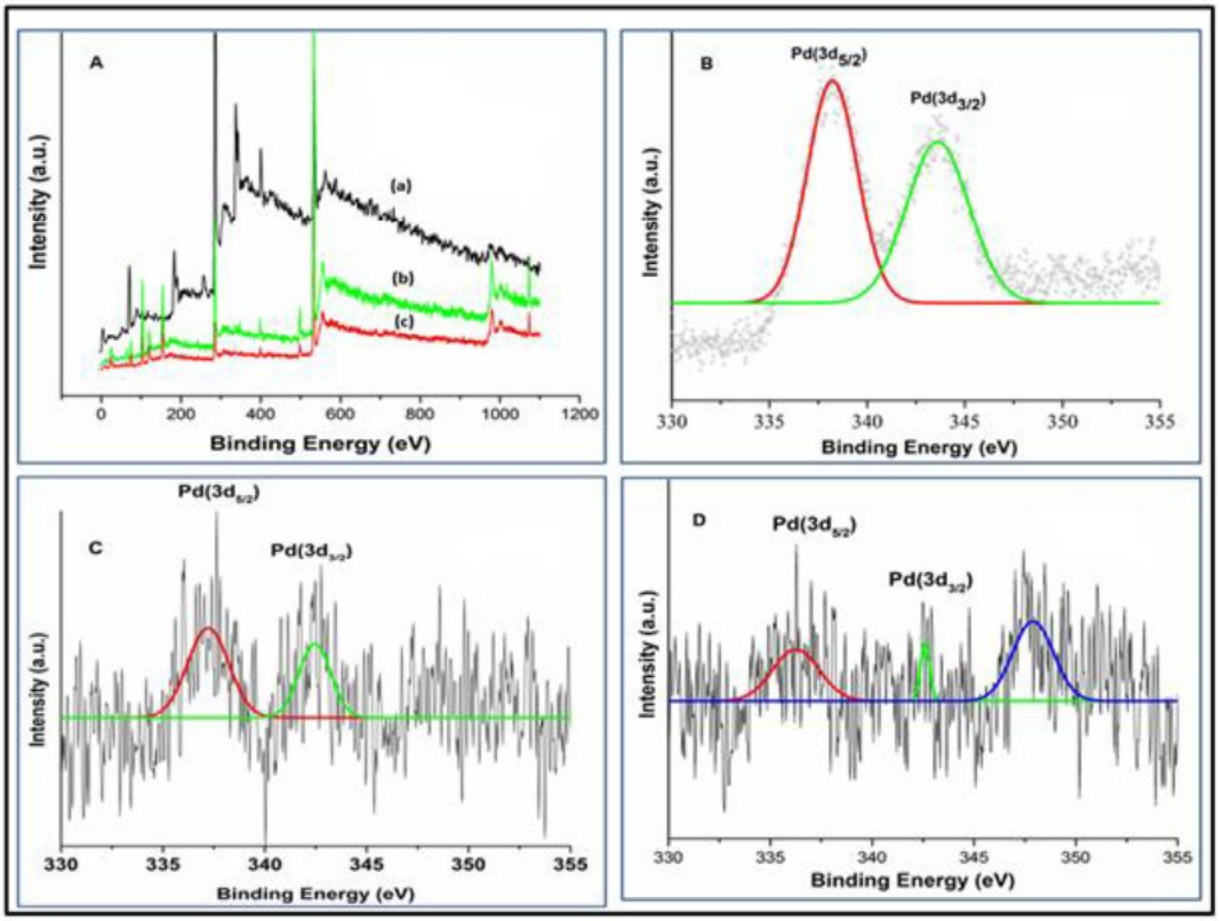

Figure 5A.8: (A) XPS survey spectra for (a) PdL1′ and encapsulated complexes (b) PdL1′-Y and (c) PdL5′-Y. High-resolution XPS signals of Pd (3d) for (B) PdL1′, (C) PdL1′-Y and (D) PdL5′-Y complex.

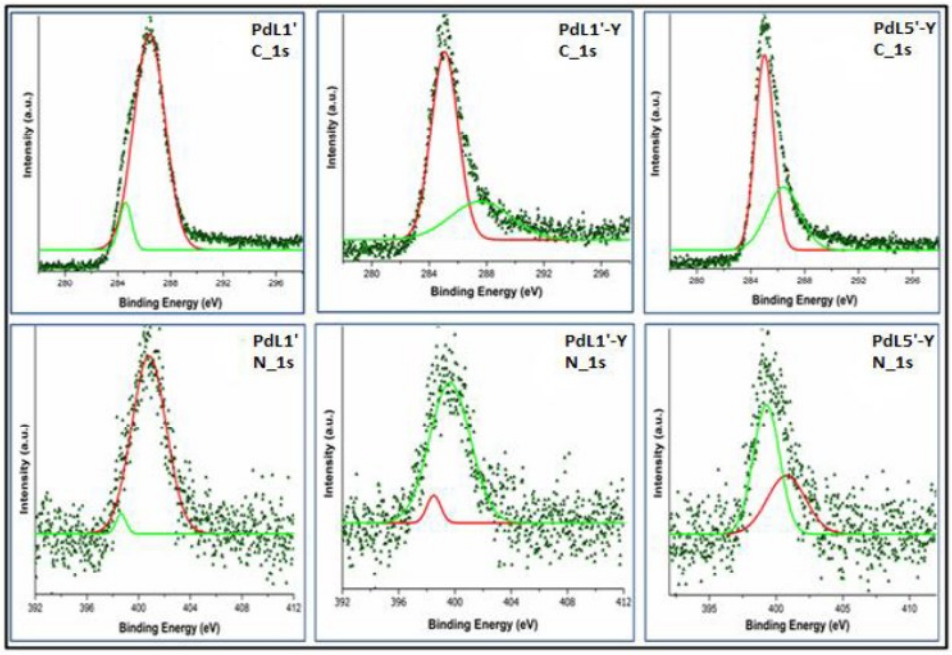

Figure 5A.9: High resolution XPS spectra of C (1s), N (1s) for PdL1′, PdL1′-Y and PdL5′-Y.

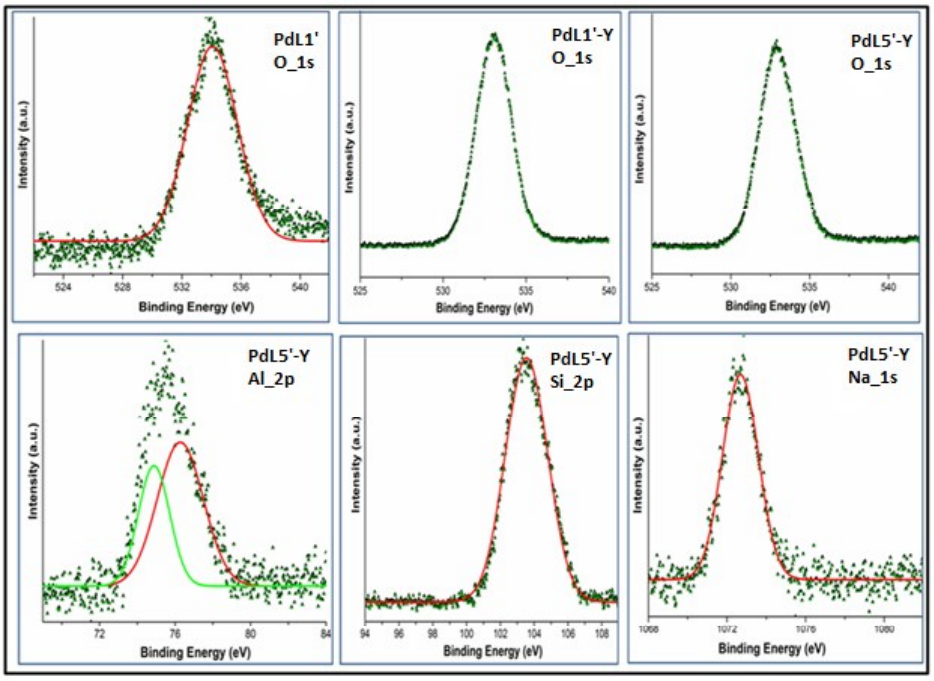

Figure 5A.10: High resolution XPS spectra of O (1s) for PdL1′, PdL1′-Y and PdL5′-Y, Al (2p), Si(2p) and Na(1s) for PdL5′-Y.

Table 5A.4: Binding energy (eV) of neat and encapsulated complexes.

S. No	Samples	Si (2p)	Al (2p)	Na (1s)	C (1s)	N(1s)	O (1s)	Pd(3d5/2)	Pd(3d3/2)
1.	**PdL1′**	-	-	-	286.41, 284.57	400.79, 398.59	534.08	338.24	343.65
2.	**PdL1′-Y**	103.27	70.40, 75.50	1073.31	287.70, 285.08	399.63, 398.49	533.10	337.22	342.40
3.	**PdL5′-Y**	103.53	74.87, 76.30	1072.68	286.37, 285.01	400.84, 399.28	532.92	336.30	342.59 347.96

5A.2.7 UV-Vis/Diffuse Reflectance Spectroscopy (UV−Vis/ DRS)

The UV-Vis spectra of the ligands and free-state palladium Schiff base complexes recorded in $CHCl_3$ have shown few interesting features (presented in Figure 5A.11; spectral data given in Table 5A.5). Intense band observed in the UV-Vis spectra of Schiff base ligand in the range of 232-278 nm in is assigned as π–π* transition and n–π* transition is observed in the range of 302nm- 375nm. Lowest energy band appearing at 401 -468 nm is identified as a transition involving metal i.e. charge transfer transition or d-d transition. The appearance of lowest energy bands therefore, supports strongly the formation of the complex.

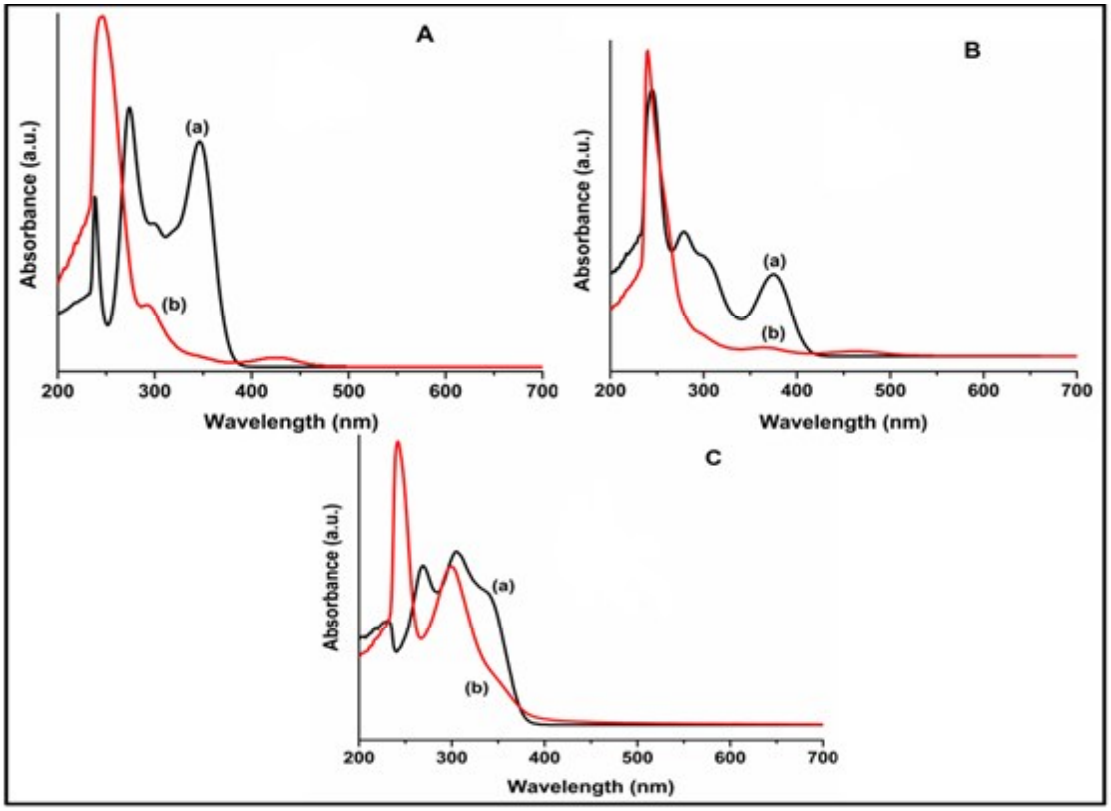

Figure 5A.11: Solution UV-Vis spectra of (A) (a) L1′ and (b) PdL1′, (B) (a) L5′ and (b) PdL5′ and (C) (a) L6′ and (b) PdL6′.

Table 5A.5: Solution UV-Visible data of ligand and neat complexes.

S. No	Samples	π—π^* transitions	n—π^* transitions	CT transitions / d-d transitions
1	**L1′**	237, 273	302,347	-
2	**PdL1′**	245	294,340	429
3	**L5′**	245, 278	306, 375	-
4	**PdL5′**	240	302, 370	468
5	**L6**	232, 268	305,340	-
6	**PdL6′**	241	300,350	401

The solid-state UV-Vis spectrum of PdL1′ exhibits bands at 200, 246, 308 and 360 nm. The first two bands are assigned as π–π* transition and the next two bands are originated from n–π* transition. The peak at 439 nm is assigned as d-d transition and is blue-shifted to a large extent so that eventually is merged with charge transfer. This observation is just in line with fact that being a 4d transition metal Pd always undergoes large d orbital splitting.[56]

On complexation, metal complexes show these transitions slightly shifted; π–π* transition observed at 240 nm-245 nm, n–π* transition observed at 294 nm-370 nm. The presence of similar electronic transitions in the encapsulated states as its neat analogs confirms the complex formation inside the supercage of zeolite Y quite evidently. However, upon encapsulation inside the zeolite matrix, the d–d transitions are found to be red-shifted clearly indicating a different electronic environment experienced by the square planar complex especially around the metal. PdL1′ complex, simply upon encapsulation shows the shift of d-d transition from 439 nm to 468 nm. Similar type of observations are found for all three encapsulated palladium complexes (shown in Figure 5A.12 and Table 5A.6) so the structural modification of all the encapsulated complexes must be very alike. The red shift in d-d transition is practically unexpected and hence noteworthy as it demands an enhanced π-delocalization around the metal center after encapsulation. Encapsulation by some means induces planarity around the central metal atom, thereby, supplements π-delocalization.

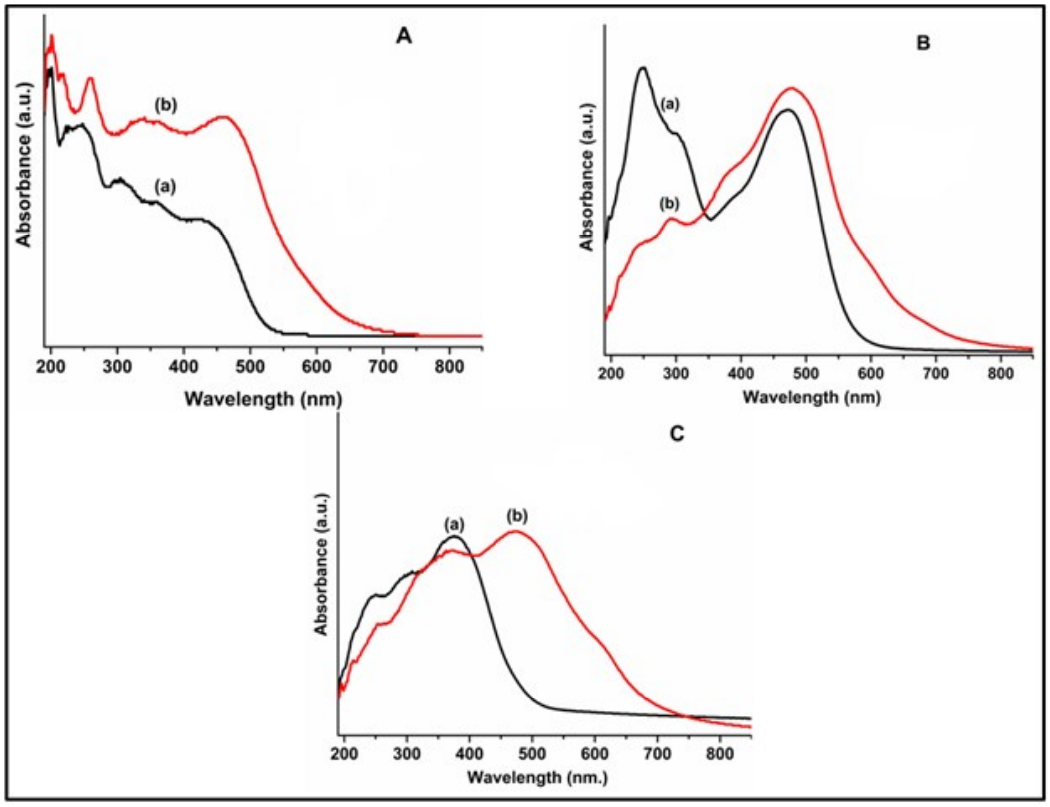

Figure 5A.12: Solid-state UV-Vis spectra of (A) (a) PdL1 and (b) PdL1′-Y, (B) (a) PdL5′ and (b) PdL5′-Y and (C) (c) PdL6 and (b) PdL6′-Y.

Table 5A.6: Solid-state UV-Visible data of neat and encapsulated palladium complexes.

S. No	samples	π—π^* transitions	n—π^* transitions	CT transitions / d-d transitions
1	**PdL1′**	246	308,360	439
2	**PdL1′-Y**	259	328,362	468,598
3	**PdL5′**	250	301,386	471
4	**PdL5′-Y**	252	292,387	480,605
5	**PdL6′**	246	309,375	402
6	**PdL6′-Y**	256	318,371	476,618

5A.2.8 Theoretical Methods

The electronic structure calculations based on Density Functional Theory (DFT) was used to study and analyze the structural and optical properties of the Pd complexes in neat and zeolite encapsulated states. All results presented here are obtained using GAUSSIAN 09 suite of *ab initio* quantum chemistry programs.[57] The details of the theoretical methods have already discussed in chapter 2 under section 2.3.11.

5A.2.8.1 Structure of neat Pd-complexes

Thus the structural studies show, in the free ground state, PdL1′, PdL5′ and PdL6′ complexes are partially planar with central aromatic ring aligned perpendicular and are diamagnetic and singlet, however, the complexes are deformed and bowl-shaped when encapsulated inside the zeolite pore and the distortion helps to stabilize the triplet state. For singlet PdL1′, PdL5′ and PdL6′, the distances d_1 and d_2 (shown in Figure 5A.13) are identical and equal to 2.90-2.91 Å and the distance d_3 is shorter in all the cases (~2.77-2.79 Å). Apart from these distances, we also look into the end-to-end, distances of all the complexes as well, which is a well-defined parameter for the neat singlet complexes. The end-to-end distances for PdL1′, PdL5′ and PdL6′ are 13.18, 13.74 and 13.83 Å respectively (shown in Table 5A.7). It is important to note the decrease in end-to-end distance *w.r.t* the free ligands L1′, L5′ and L6′, which is due to the coiling of the ligand around the metal center. We also look into the <O-Pd-N bond-angle around the Pd atom, which provides some idea about the overall planarity around the metal center and for the singlet, neat molecules; the <O-Pd-N bond angle is ~86 deg. which indicates it's near planarity. In case of the neat molecules, the Pd-O, Pd-N, O-C and N=C bond-distances are 2.01, 2.19, 1.29 and 1.30 Å respectively.

5A.2.8.2 Structure of Pd-complexes in neat and encapsulated states

We theoretically first studied the free ligands, L1′, L5′ and L6′ and observe that the three aromatic rings in the molecule are not co-planar, but the middle ring of m-phenylenediamine is placed at an angle of 40-50 deg, from the two side rings, depending on the substituents (shown in Figure 5A.13a) and the molecule is flexible and stretched. In presence of Pd^{2+} ion, the ligands readily form metal complexes, and encompass the metal atom in a half-circular fashion, where the two side rings of the ligand and the metal atom is co-planar, but the middle aromatic ring of the ligand now bents almost perpendicular to the two terminal aromatic rings (see Figure 5A.13b). The neat PdL1′, PdL5′, and PdL6′ exist as singlet states, without any

unpaired electrons; however, there exist higher energy triplet states with two unpaired electrons for all complexes studied. Structural optimizations are carried out for PdL1′, PdL5′ and PdL6′ complexes in the neat singlet states and then in zeolite encapsulated triplet states and the optimized structures are presented in Figure 5A.13c with the important structural parameters tabulated in Table 5A.7. In the Pd-complex, the central ring itself is no longer completely planar, unlike aromatic rings, but it appears to be somewhat boat-shaped and unique structure-property relationship is observed for this class of complexes. To understand the positioning of this ring with respect to the Pd atom we have defined three distance parameters d_1, d_2 and d_3 marked in the Figure 5A.13b,c. The encapsulated Pd complexes studied are all triplet, and they are bent longitudinally, thus the end-to-end distances decrease by ~0.4 Å (See Table 5A.7). The distortion of the encapsulated complexes as a whole, however, affects the positioning of the central out-of-plane ring behind the Pd atom, the d_1, d_2 distances now differ, and are ~2.80 and ~3.02 Å respectively (Table 5A.7). The shorter distance d_3 is now found to be longer and 2.93 Å. Thus, the whole molecule now resembles a 'bowl' unlike the neat molecules, which indeed were largely planar. Moreover, the central phenylene-1,3-diamine ring is no longer symmetrically placed behind the metal center, and thus Pd-N and N=C distances are different now. The Pd-N distances are 2.07 and 2.13 Å and N=C distances are 1.29 and 1.33 Å respectively (Table 5A.7). On the contrary, the Pd-O and O-C distances for the singlet and the triplet states are very similar.

Thus the structural studies show, in the free ground state, PdL1′, PdL5′ and PdL6′ complexes are partially planar with central aromatic ring aligned almost perpendicular and are diamagnetic and singlet, however, the complexes are deformed and bowl-shaped when encapsulated inside the zeolite pore and the distortion helps to stabilize the triplet state. This, in turn, alters the relative ordering of the molecular orbitals and consequently, optical and catalytic properties of the complexes are modified.

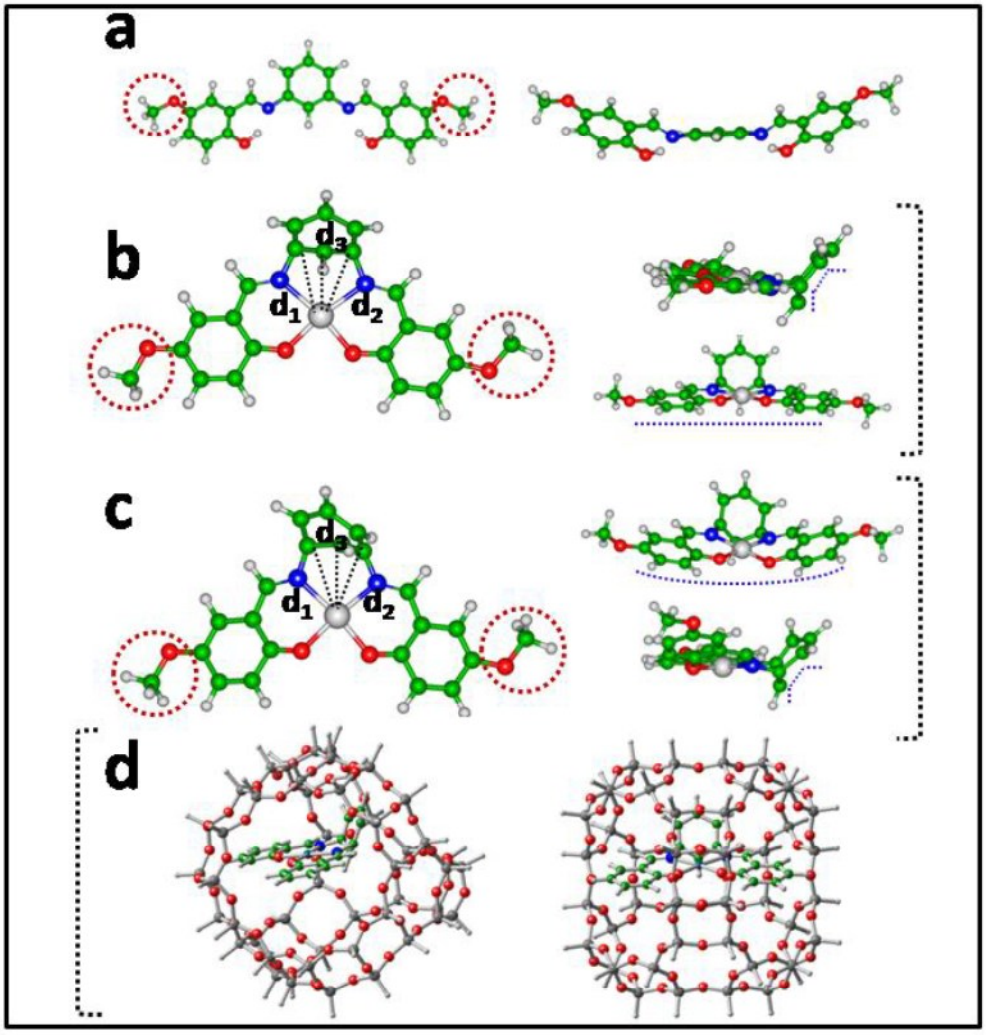

Figure 5A.13: (a) Ligand N, N'-bis(5-methoxysalicylidene)phenylene-1,3-diamine, frontal and side views are shown. Above figure shows the -OMe group marked by red circle for L5′, which is replaced by -NO_2 for L6′ and H for L1′. (b) The neat, singlet state of PdL5′ complex, frontal and side views are shown. (c) The encapsulated and extracted, triplet state of PdL5′ complex, frontal and side views are shown. In the right-hand side two side views are shown to understand the position of the central ring with respect to the plane of the molecule. The distances d_1, d_2 and d_3 are marked on the Pd-complex and are explained in the text. (d) PdL5′ complex encapsulated within zeolite pore, two different views are shown.

Table 5A.7: Important structural parameters from DFT for neat and encapsulated Pd-complexes.

S. No	Bond distances / angles	PdL1′, neat singlet	PdL1′-Y, Encapsulated, extracted triplet	PdL5′, neat singlet	PdL5′-Y, Encapsulated, extracted triplet	PdL6′, neat singlet	PdL6′-Y, Encapsulated, extracted triplet
1	**Pd-O (Å)**	2.01	2.01	2.00	2.00	2.01	2.00
2	**Pd-N (Å)**	2.19	2.06, 2.13	2.19	2.07, 2.13	2.19	2.07, 2.14
3	**O-C (Å)**	1.29	1.29	1.30	1.30	1.28	1.28
4	**N-C(conj) (Å)**	1.30	1.29, 1.33	1.30	1.30, 1.33	1.29	1.28, 1.32
5	**<O-Pd-N**	85.9	88.9	86.1	88.0	85.9	88.4
6	**End to end distance (Å)**	13.18	12.72	13.74	13.33	13.83	13.53
7	**d_1 (Å)**	2.91	2.80	2.91	2.80	2.91	2.80
8	**d_2 (Å)**	2.77	2.93	2.78	2.92	2.79	2.95
9	**d_3 (Å)**	2.91	3.02	2.91	3.01	2.91	3.02

5A.2.8.3 TD-DFT spectra of the ligands (L1′, L5′, L6′)

Firstly, we have calculated the TD-DFT spectra of the ligands L1′, L5′ and L6′, studied the important optical transitions, and compared with PdL1′, PdL5′ and PdL6′ (Figure 5A.14). Frontier molecular orbitals of L1′ (shown in Figure 5A.15) show that the HOMO is fully conjugated and spread over the length of the molecule, but LUMO is only partially spread over the central ring. The HOMO-LUMO gap is calculated to be 3.96 eV (HOMO:-6.21 eV, LUMO: -2.25 eV). For ligand L1′, we observe there are three important peaks, at 349, 308 and 272 nm in the calculated TD-DFT spectra. A close look at the frontier molecular orbitals of the ligands would reveal that it is mainly the overlap of the out of plane p orbitals of the C atoms forming the conjugated pi framework are more important, which only partly includes the central ring positioned out of plane. Thus all these transitions are from HOMO, HOMO-1, HOMO-2 to LUMO or LUMO+1 transitions and are shown in Figure 5A.14. Frontier molecular orbitals of L5′ are shown in Figure 5A.15, and it is seen that HOMO and HOMO-1 are very closely placed in energy, and is only

partially spread over the central ring, but the LUMO is fully conjugated and spread over the length of the molecule. The HOMO-LUMO gap is calculated to be 3.53 eV (HOMO:-5.72 eV, LUMO: -2.19 eV). The presence of -OMe group destabilizes the HOMO and reduces the HOMO-LUMO gap compared to L1′ (see Figure 5A.15). For L5′, the important transitions are around 399, 313-314 and 272 nm in the calculated optical spectrum (Figure 5A.14). There are also prominent peaks around 394, 367 and 373 nm. For L5′ the HOMO to LUMO transition occurs around 395 nm, whereas the HOMO-1 to LUMO transition occurs around 399 nm. The transitions around 373 and 367 nm are HOMO to LUMO+1 and HOMO-1 to LUMO transitions, mixed with other transitions. The transition near 272 nm is due to a transition from inner orbitals to LUMO. Frontier molecular orbitals of L6′ are shown in Figure 5A.15, and it is seen that HOMO and the LUMO are fully conjugated and spread over entire molecule. The HOMO-LUMO gap is calculated to be 4.06 eV (HOMO:-7.02 eV, LUMO: -2.96 eV). The presence of -NO_2 group stabilizes the both the HOMO and LUMO and the HOMO-LUMO gap is increased compared to L1′ or L5′. For L6′, the important transitions with largest f values are around 341, 337, 301 and 289 nm in the calculated optical spectrum (Figure 5A.14). There are also prominent peaks around 335, 325, 310 and 300 nm. For L6′ the HOMO to LUMO transition occurs around 337 nm, whereas the HOMO-1 to LUMO transition occurs around 341 nm. The transitions around 325 and 323 nm are HOMO to LUMO+2 and HOMO to LUMO+1 transitions, mixed with other transitions. The strong peak near 301 nm is due to a transition from inner orbitals to LUMO combined with HOMO-1 to LUMO+2. The transition from HOMO-2 to LUMO+1 is responsible for the peak around 289 nm.

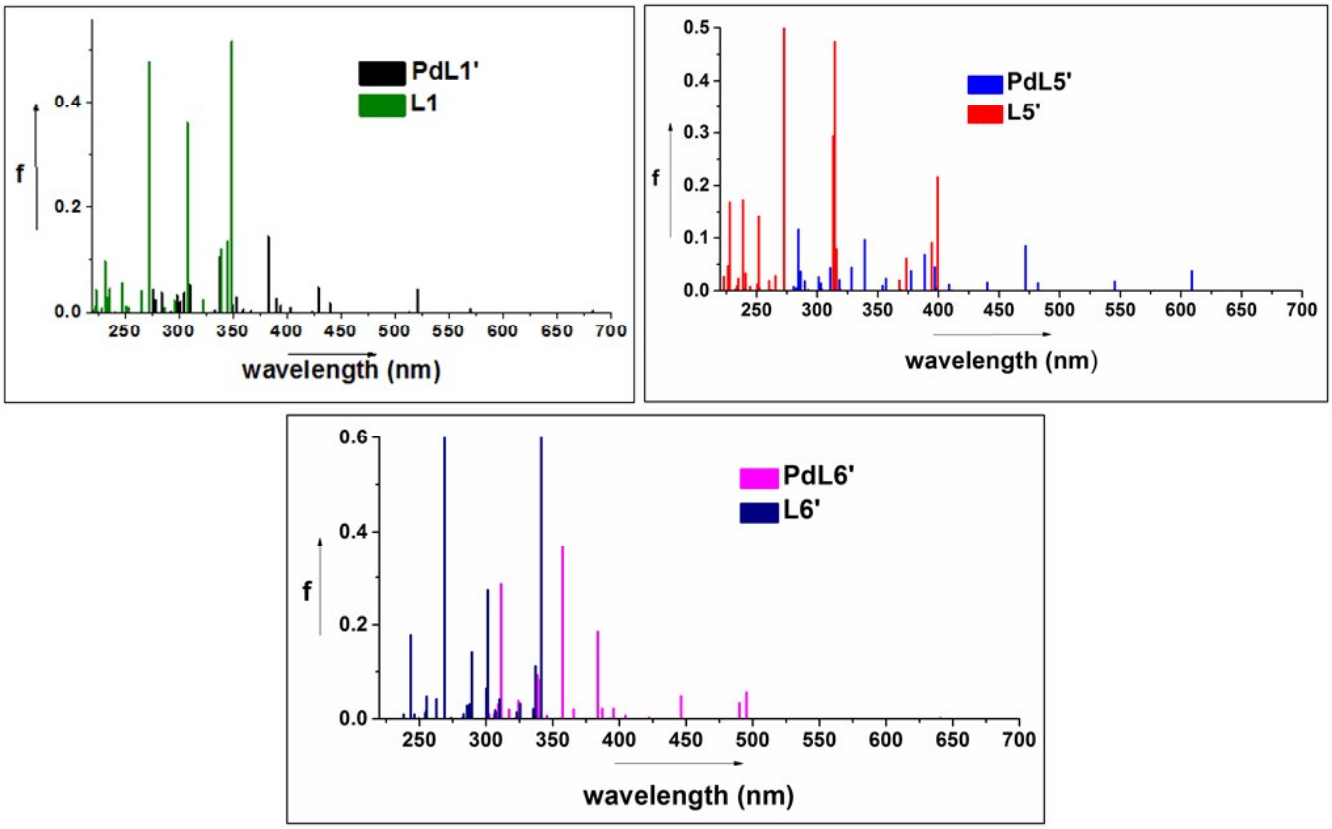

Figure 5A.14: Comparison of optical spectra for L1′ and PdL1′, L5′ and PdL5′, L6′ and PdL6′.

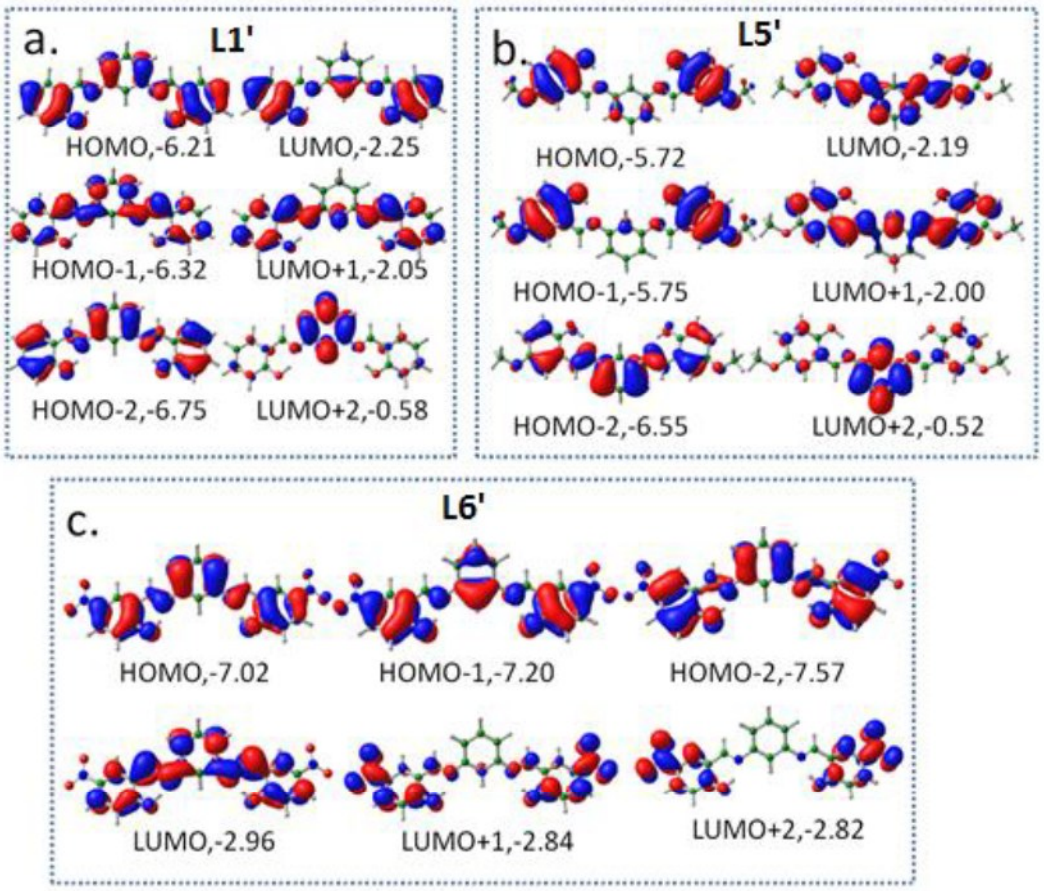

Figure 5A.15: The Molecular orbitals of the free ligands L1′, L5′ and L6′.

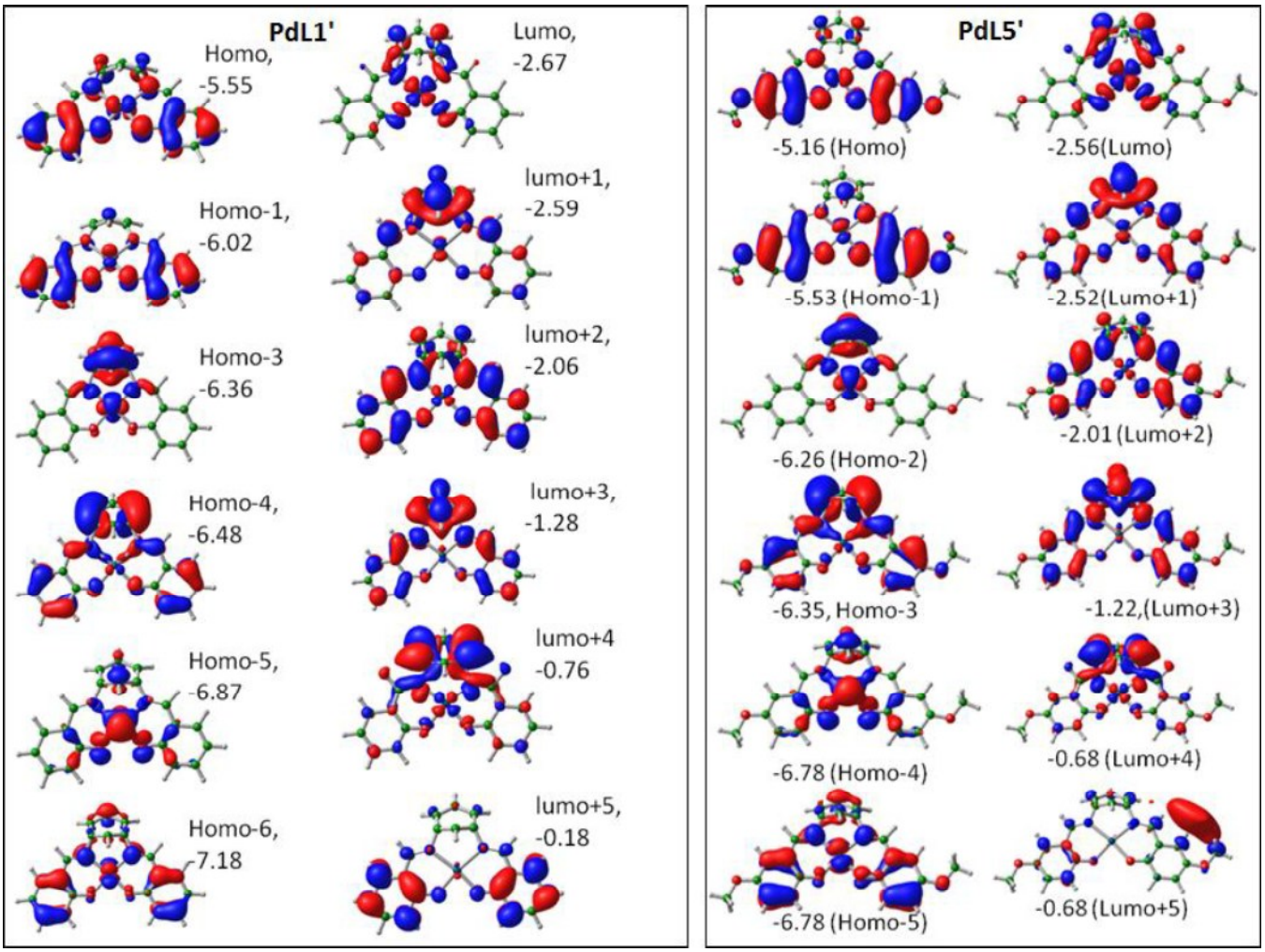

Figure 5A.17: Frontier molecular orbitals of PdL1′ and PdL5′, Energies are reported in eV.

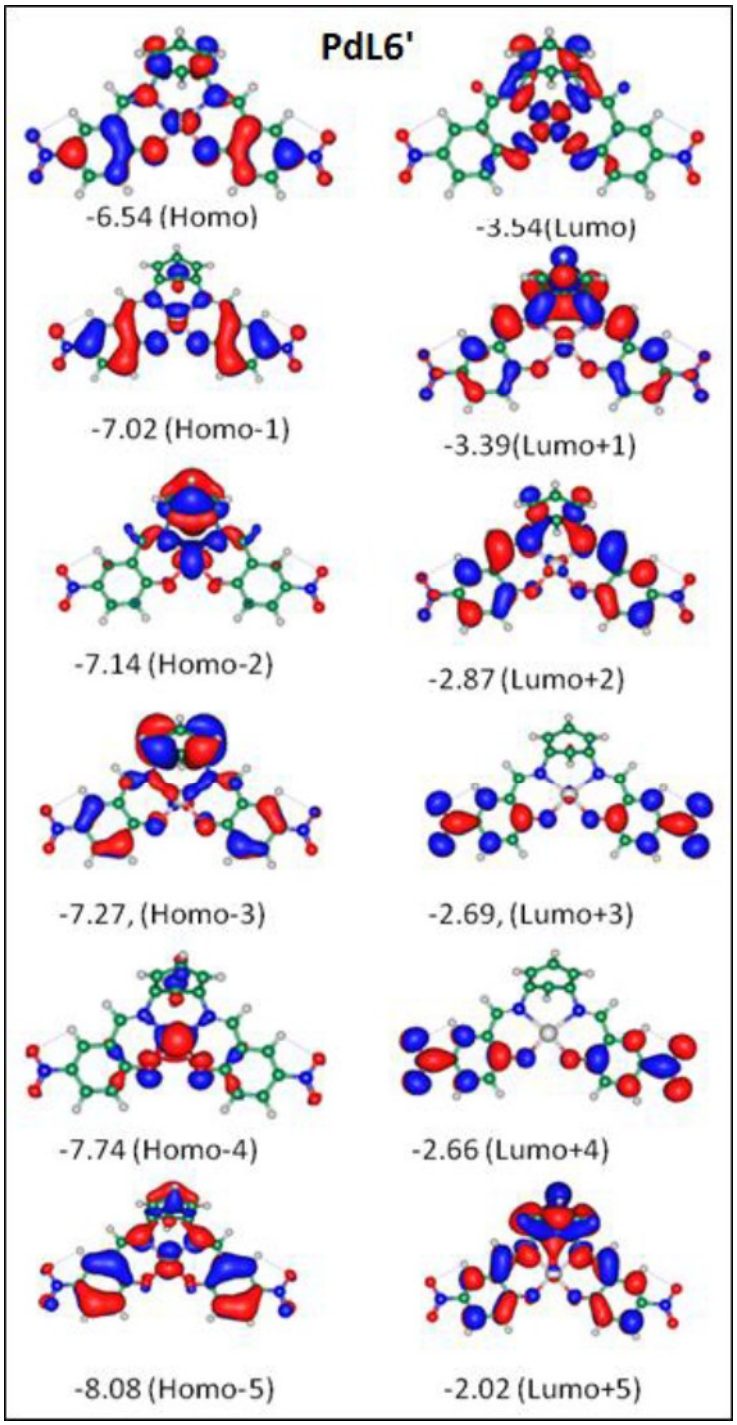

Figure 5A.18: Frontier molecular orbitals of PdL6′, Energies are reported in eV.

5A.2.8.4 TD-DFT spectra of the complexes (neat PdL1′, PdL5′, PdL6′)

In the calculated TD-DFT spectrum of PdL1′ (Figure 5A.14), a weak peak is observed at 569 nm followed by a relatively stronger one at 521 nm. The first one corresponds to occupied HOMO to LUMO+1 which is mixed with other metal to ligand transitions, and the second one corresponds to mostly HOMO to LUMO, i.e Pd d_{xz} to d_{xy} transition. The next important transition occurs at 440 nm Pd d_z^2 (HOMO-2) to metal d_{xy} orbital (LUMO). Again strong peak is seen around 429 nm which corresponds to HOMO-1 to LUMO+1 transition with a contribution from HOMO to LUMO, i.e Pd d_{xz} to d_{xy}. Peaks near 394-382 nm are transitions from ligand to metal d_{xy}, along with HOMO to LUMO transitions.

In the calculated TD-DFT spectrum for PdL5′ two weak peaks are observed at 545 nm and 482 nm followed by a relatively stronger one at 472 nm (Figure 5A.14). The first one corresponds to occupied HOMO to LUMO+1 which is mixed with other metal to ligand transitions, and the second one corresponds to mostly HOMO-1 to LUMO+1, i.e transition within Pd d_{yz} bonding and antibonding with contributions from other MOs. The peak at 472 nm is HOMO (Pd d_{xz}) to LUMO+2 (Pd d_{xy}). The next important transition occurs at 397 nm Pd d_z^2 (HOMO-2) to metal d_{xy} orbital (LUMO). Again strong peak is seen around 388 nm, which corresponds to transitions from ligand orbitals to LUMO.

In the calculated TD-DFT spectrum three consecutive peaks are observed at 495, 489 and 446 nm (Figure 5A.14). The first two correspond to HOMO to LUMO+1 which is mixed with HOMO-1 to LUMO transitions with other transitions in different proportions, and the third one corresponds to Pd d_z^2 (HOMO-4) to metal d_{xy} orbital (LUMO).The peak at 395 nm is HOMO-1 (Pd d_{yz}) to LUMO+1 (Pd d_{yz}) and the next important transition at 387 nm occurs due to transitions from HOMO-1 to LUMO, mixed with others. Another strong peak is seen around 383 nm, which corresponds to transitions from ligand orbitals to LUMO. Figure 5A.16 shows the TD-DFT spectra of the triplet Pd-complexes which are encapsulated and then extracted for the TD-DFT studies. In the Figure 5A.16 we can compare the theoretical TD-DFT spectra of PdL1′-Y, PdL5′-Y and PdL6′-Y.

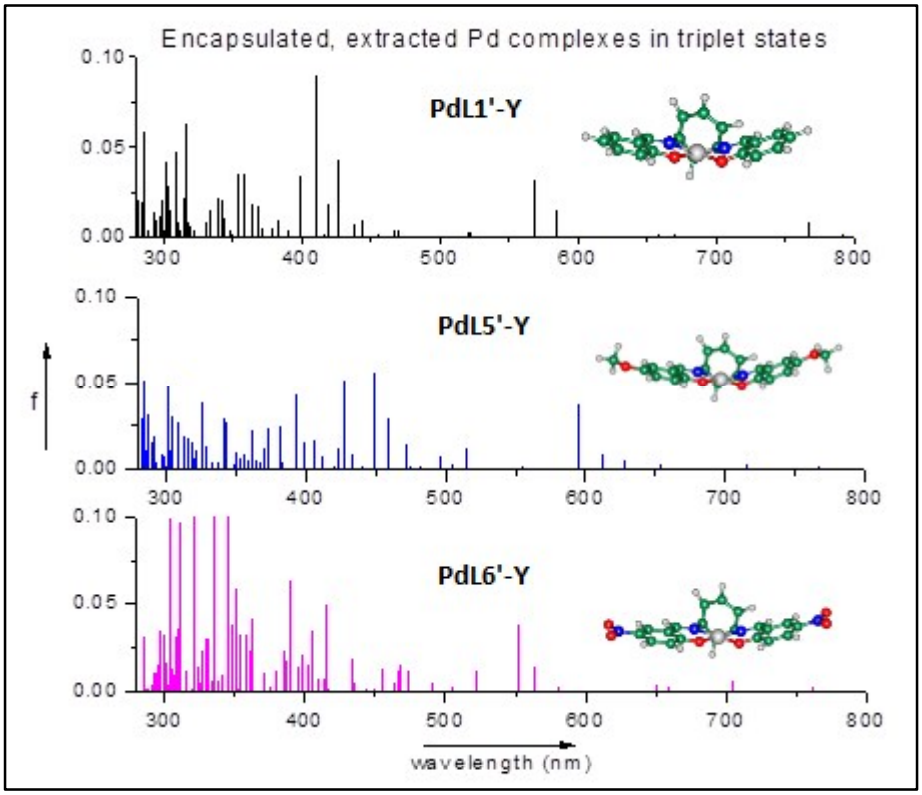

Figure 5A.16: Comparison of optical spectra for PdL1′-Y, PdL5′-Y and PdL6′-Y in encapsulated and extracted triplet state.

5A.2.8.5 Frontier molecular orbitals of the Pd-complexes.

To understand the optical properties and related transitions of the Pd-complexes it is imperative to look into the nature of their frontier molecular orbitals. The present study observes that the HOMO for neat PdL1′ has a modest Pd d_{xz} character hybridized with the pi bonding character of the ligand, and the LUMO has Pd d_{xy} character hybridized with pi antibonding type orbitals from the central 'out-of-plane' aromatic ring of the ligand (Figure 5A.17). The HOMO and LUMO energies for PdL1′ are -5.55 and -2.67 eV respectively with a HOMO-LUMO energy gap of 2.89 eV. Though HOMO-1 also has some contribution from Pd d_{yz} orbital, HOMO-2 comprises primarily of Pd d_z^2 orbital. On the other hand, LUMO+1 orbital has a minimal contribution from Pd d_{yz} while LUMO+2 has a little contribution from Pd d_{xy} orbital. The nature of the molecular orbitals of similar salen complex has been discussed before in literature.[55, 58, 59] A look into the molecular orbitals of PdL5′ (Figure 5A.17) reveals that the HOMO has strong contribution

from Pd d_{xz} orbital hybridized with ligand p orbitals and the LUMO is mainly Pd d_{xy} orbital similar to the case of PdL1′. The HOMO-LUMO gap for PdL5′ is 2.59 eV. HOMO-1 orbital is mainly ligand p with Pd d_{yz} orbital, and HOMO-2 is metal dz^2 orbital, with contributions from the central ring of the ligand. It is also observed that while LUMO+1 has contributions from Pd d_{yz} orbital, LUMO+2 and LUMO+4 both have some contributions of Pd d_{xy} orbital The molecular orbitals of PdL6′ is similar to that of PdL1′ and PdL5′ and the HOMO is mostly Pd d_{xz} orbital hybridized with ligand p orbitals and the LUMO is mainly Pd d_{xy} orbital (Figure 5A.18) with the HOMO-LUMO gap being 3.0 eV. The HOMO-1 orbital is mainly ligand p with Pd d_{yz} orbital, whereas HOMO-2 is metal dz^2 orbital.

The calculated optical spectra for the neat PdL1′, PdL5′ and PdL6′ complexes are given and here we consider only the encapsulated and extracted Pd complexes in triplet states. The molecular orbitals in the triplet states are shown in Figure 5A.19-5A.21 and comprised of alpha and beta sets, due to the presence of unpaired electrons. In the triplet state, the structural distortion of the complexes means more hybridization with the ligand pi orbitals, which makes identification of metal d orbitals difficult. In the triplet state, the HOMO and HOMO-1 are closely placed in energies and located in two different halves of the molecule and each has strong contributions from Pd d_{xz} orbital. The occupied orbitals are dominated by Pd d_{xz}, d_{yz}, and d_z^2 orbitals whereas the unoccupied states are dominated by Pd d_{xy} orbitals. The LUMO is still mainly localized on Pd d_{xy} orbital but strong hybridizations ensure that there are more unoccupied orbitals with Pd d_{xy} character. There are inner occupied orbitals with Pd d_{yz} and Pd d_z^2 character hybridized with ligand p character. A closer look into the TD-DFT spectra (Figure 5A.15 and Figure 5A.16) readily reveals that there is an overall shift towards the higher wavelengths, but identification of the individual transitions are increasingly difficult because the metal d orbitals are mixed up with ligand orbitals in a complicated fashion. In case of neat PdL1′, the first prominent peak is around 521 nm (Figure 5A.14), which shifts to 568 nm in the encapsulated PdL1′-Y case, and this is HOMO-1 to LUMO transition comprising of Pd d_{xz} to Pd d_{xy} orbital. In the case of singlet PdL5′, we see the first important peak around 545 nm (Figure 5A.14), which shifts to 594 in encapsulated triplet case. In the case of PdL6′, important transitions are in the range of 550-470 nm. One may note that in case of PdL6′-Y the prominent peaks are is around 550 nm which were around 495 and 489 nm in case of PdL6′ (Figure 5A.14), indicating a shift towards longer wavelengths upon encapsulation Experimental and DFT simulated UV-Vis spectra of PdL1′, PdL1′-Y, PdL5′ and PdL5′-Y complex are given in Figure 5A.22 for better comparison.

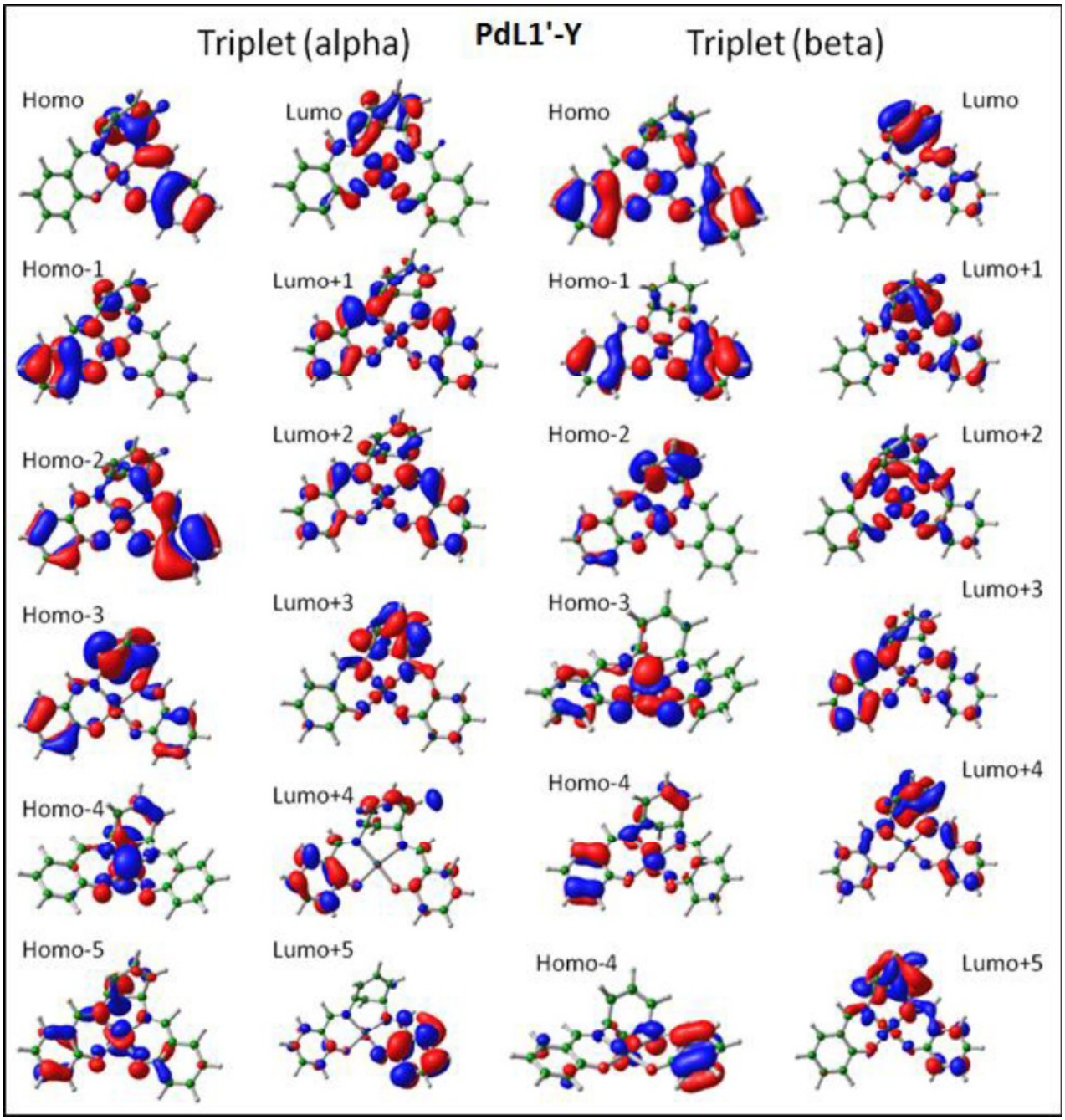

Figure 5A.19: Frontier molecular orbitals of PdL1′ in encapsulated, extracted and triplet state.

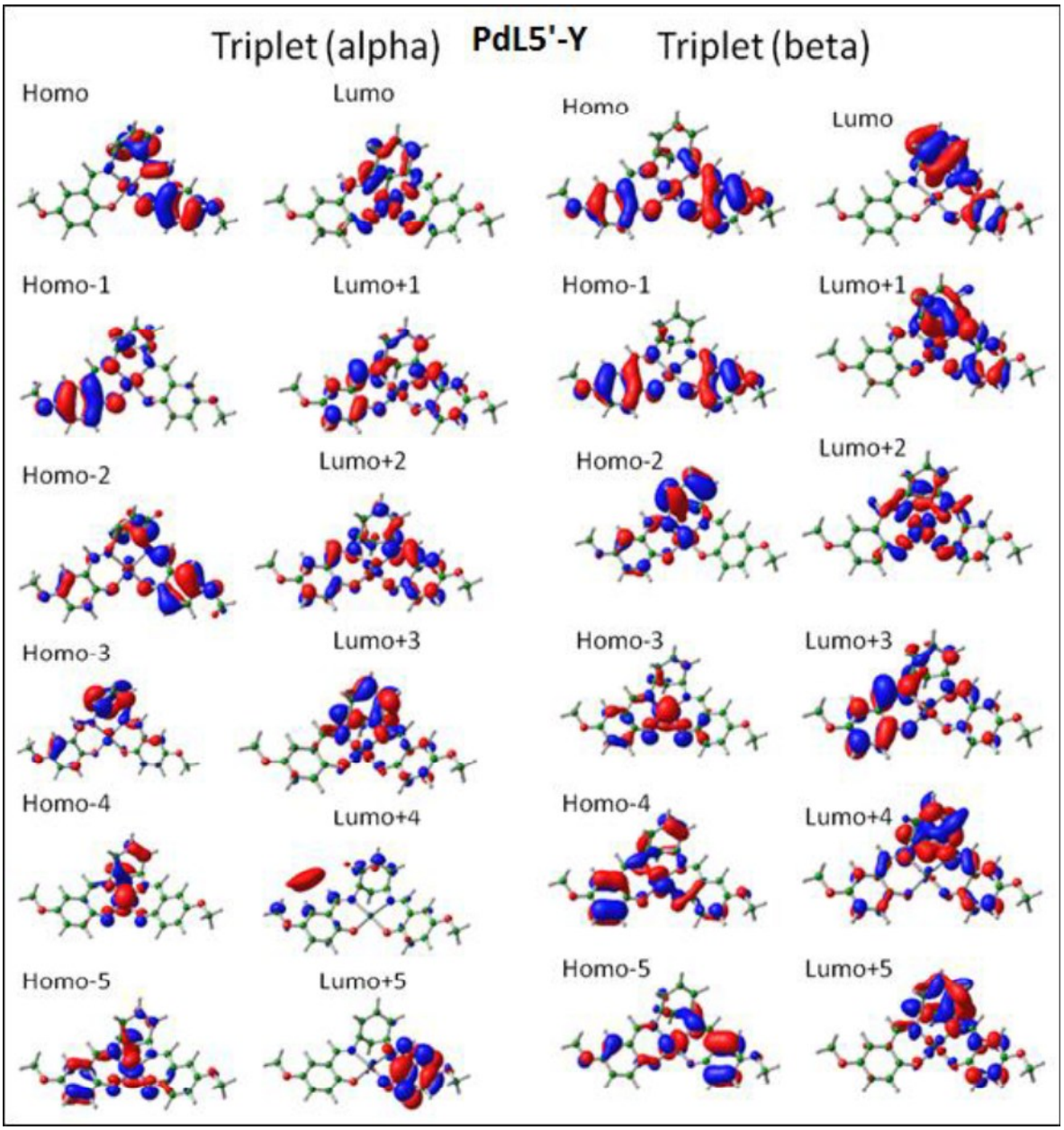

Figure 5A.20: Frontier molecular orbitals of PdL5′ in encapsulated, extracted and triplet state.

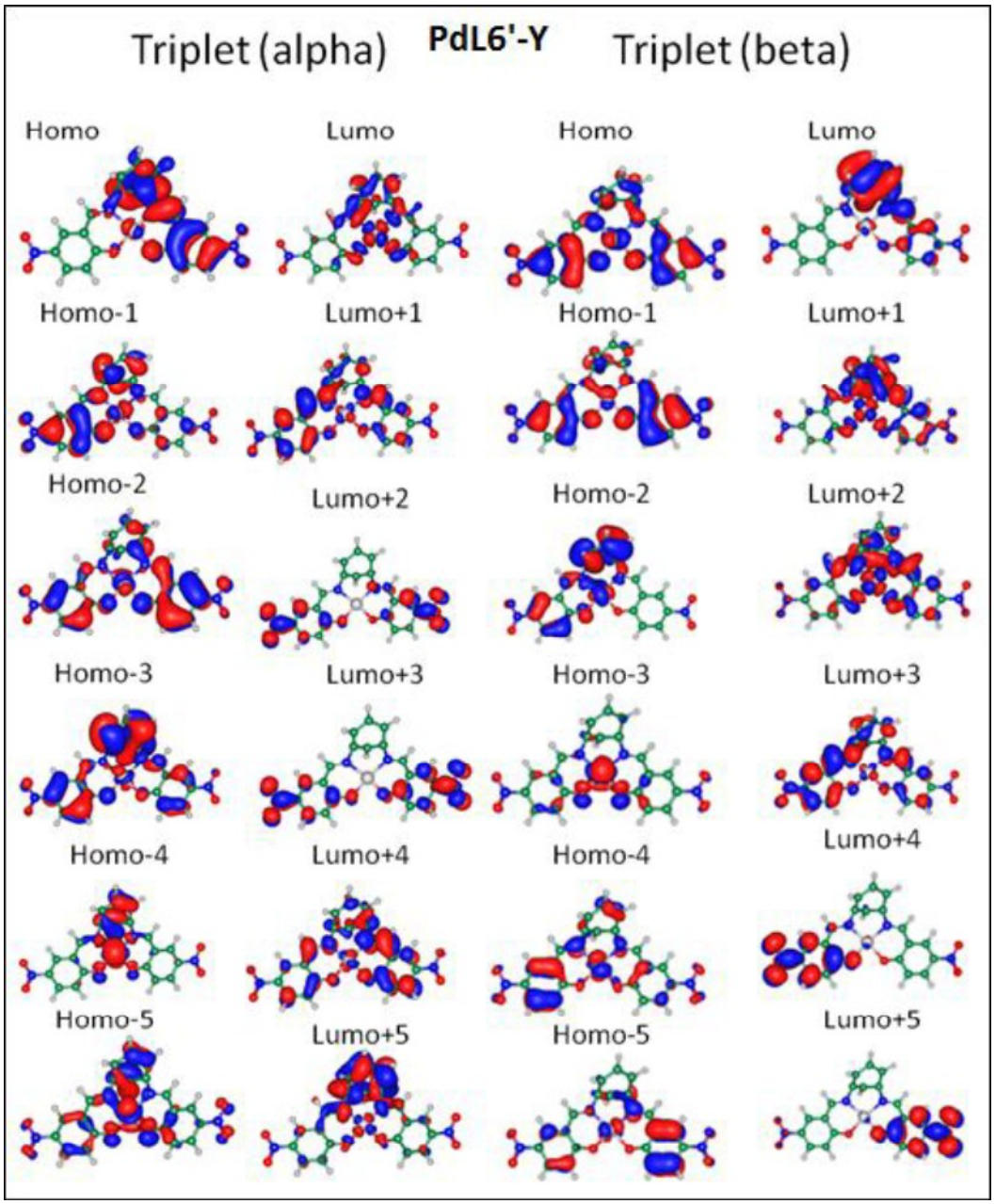

Figure 5A.21: Frontier molecular orbitals of PdL6′ in encapsulated, extracted and triplet state.

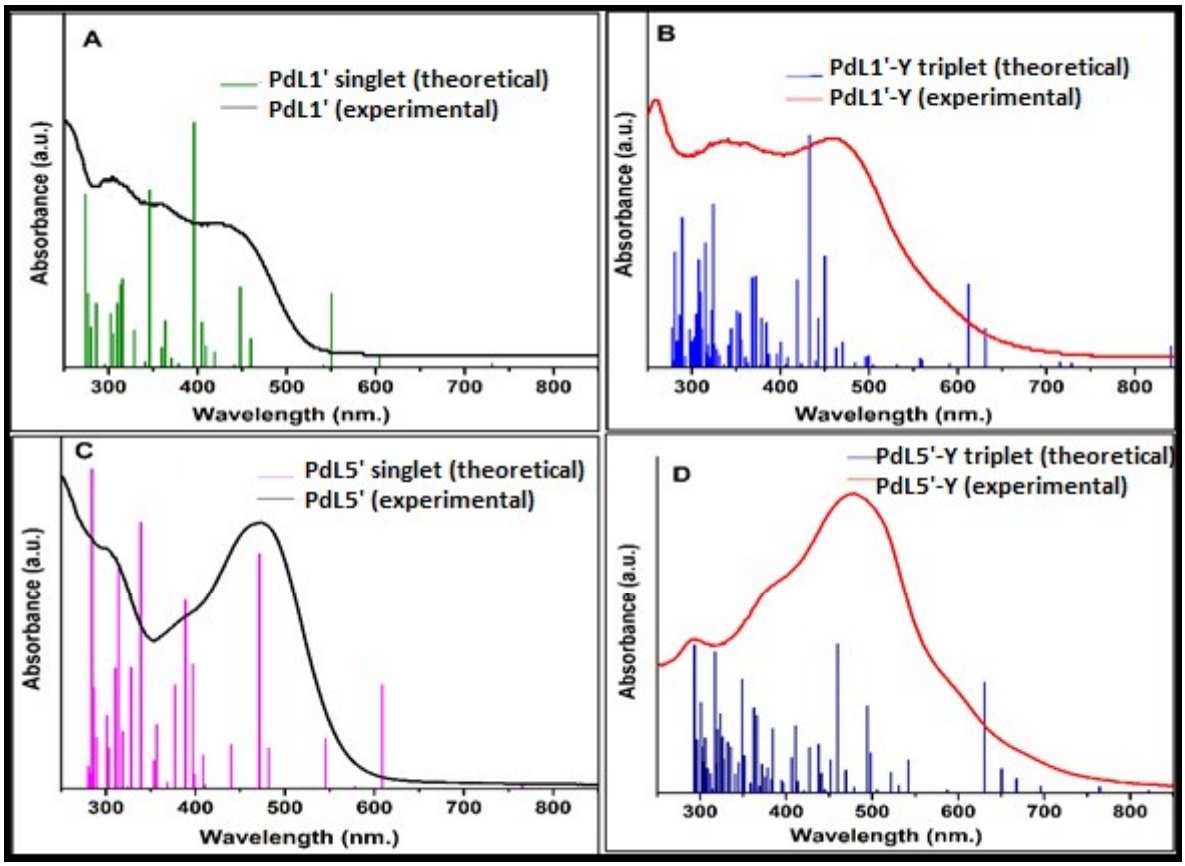

Figure 5A.22: Experimental and DFT simulated UV-Vis spectra of (A) PdL1′, (B) PdL1′-Y, (C) PdL5′ and (D) PdL5′-Y complex.

5A.2.9 Catalytic Study

All neat and encapsulated palladium Schiff base complexes have been explored as catalysts for Heck coupling of bromobenzene with styrene. The results of the Heck reaction are given in Table 5A.8. Calibration curve of bromobenzene is given in Figure 5A.23. Reaction conditions are optimized using PdL1′-Y as a catalyst by varying amount of catalyst and temperature. The effect of temperature on the catalytic activity of PdL1′-Y has been studied up to 140 °C. The % conversion of coupling reaction is increased with temperature, but there is no conversion obtained below 70 °C. As the temperature increased from 100°C to 140°C, the conversion increased from 21.3% to 90.8% (Figure 5A.24). The effect of the amount of catalyst on the Heck reaction is studied and found excellent conversion with 0.70 mmol% of

catalyst. Catalytic data are presented in Figure 5A.25. All catalytic reactions are monitored by gas chromatography and % conversion calculated by using a calibration curve of bromobenzene and n-heptane as an internal standard.

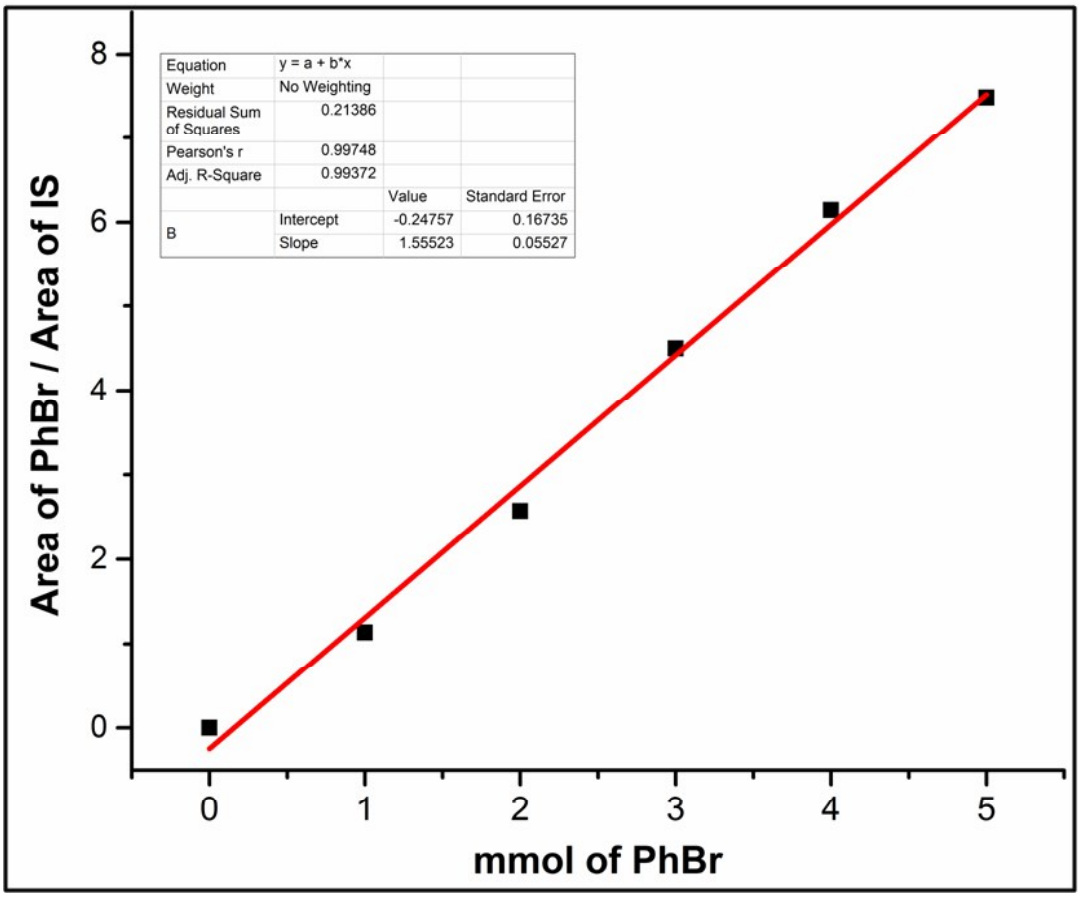

Figure 5A.23: Calibration curve of bromobenzene.

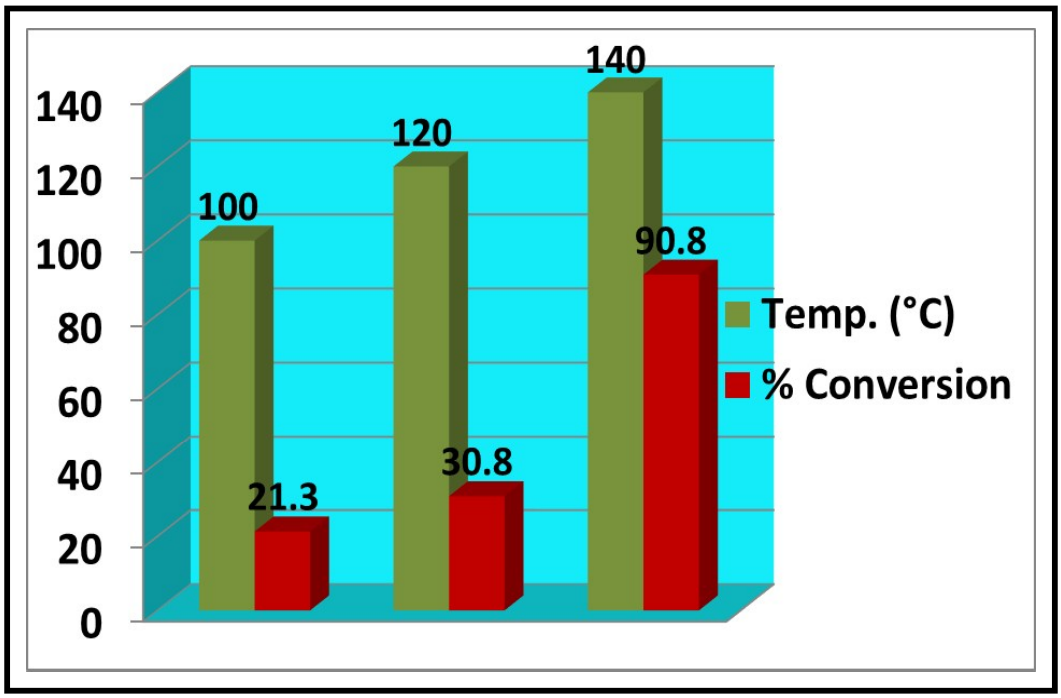

Figure 5A.24: % Conversion of bromobenzene for PdL1′-Y complex with respect to temperature.

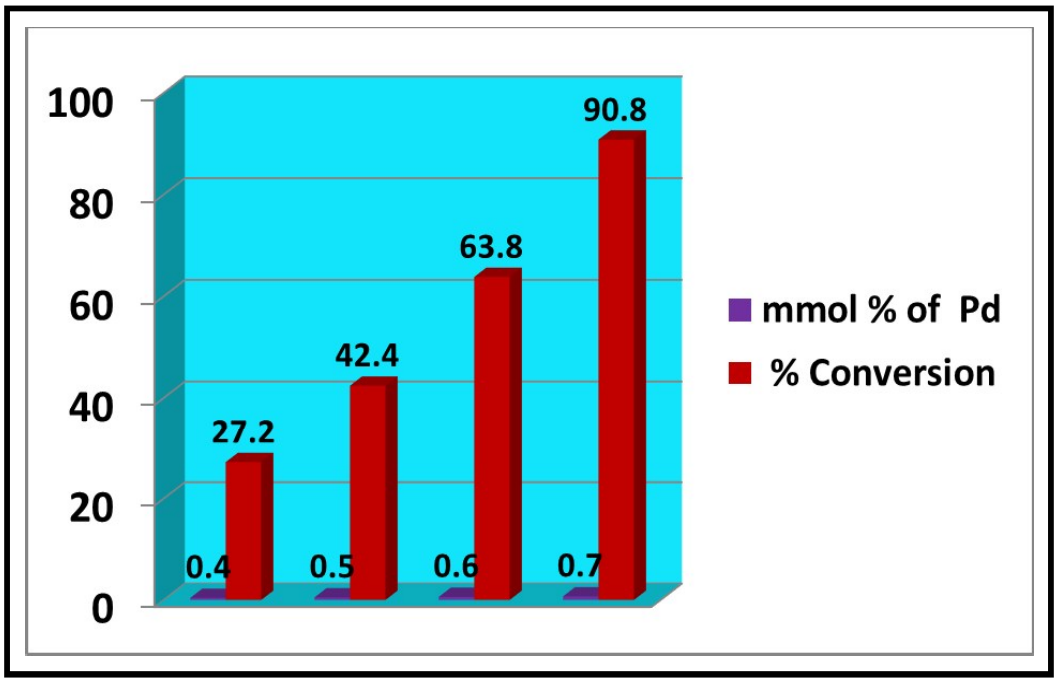

Figure 5A.25: % Conversion of bromobenzene for PdL1′-Y complex with respect to mmol of catalyst.

By using optimized reaction conditions, all neat and encapsulated complexes containing electron-donating and electron-withdrawing substituent have been employed as catalysts. The neat palladium complexes follow the activity order as PdL5′>PdL1′>PdL6′ complex. PdL5′ complex with electron-donating substituent (-OCH_3) is most reactive for the Heck coupling whereas PdL6′ with electron-withdrawing substituent (-NO_2) is least reactive. The activity order of free state palladium complexes is solely controlled by the electronic effects of the substituent group attached, as expected.[60] After the encapsulation of the complexes inside the supercage of zeolite Y, a striking reversal of the reactivity order is observed. Encapsulated palladium complexes follow the order as PdL1′-Y >PdL6′-Y>PdL5′-Y; modified steric environment of the guest complexes imposed by the host zeolite lattice definitely have significant contributions towards it. New modified functionalities towards Heck reaction signify to the substantial structural changes around the metal center under encapsulation inside the host supercage. Pd metal center in these complexes with different substituent provide a different electronic environment for catalysis and additionally on encapsulation they experience differential space constraints, which altogether leads to the modification of the reactivity order. Undoubtedly, the final geometry adopted by the encapsulated complex plays a crucial rule. Upon encapsulation, the metal center in the guest complex can have substantially different electronic charge distribution due to the newly adopted structure. Heterogeneous catalyst can easily be separated from the reaction mixture and reused after washing without loss in activity (Recyclability of the PdL1′-Y catalyst for Heck coupling is presented in Figure 5A.26).

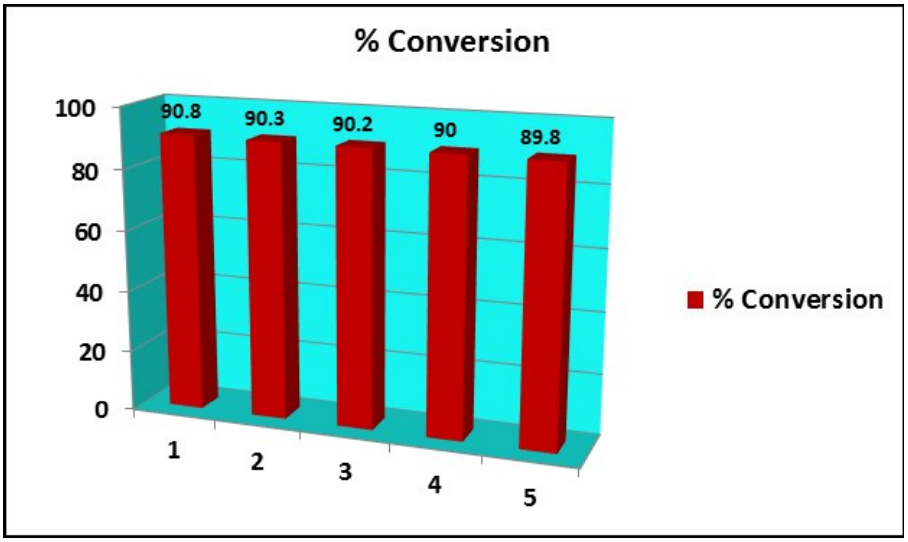

Figure 5A.26: Recyclability of the PdL1′-Y catalyst for Heck coupling reaction.

Table 5A.8: Coupling reaction between bromobenzene and styrene catalyzed by palladium complexes.

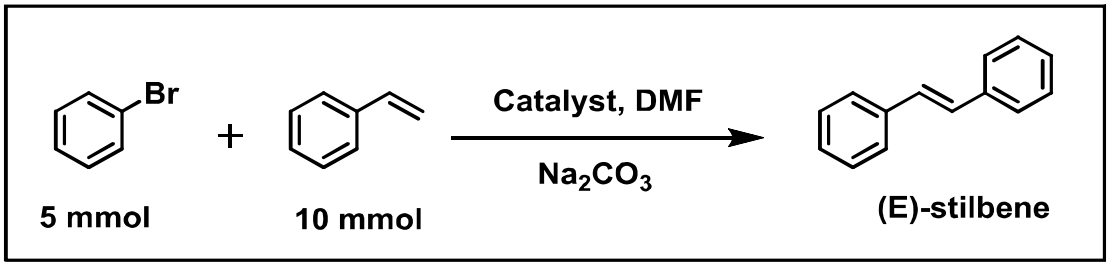

S.No.	Catalyst	mmol % of Pd	Reaction temp. (°C)	% Yield of Product[a]	TON[b]
1	**Zeolite Y**	-	140	Nil	-
2	**Pd-Y**	0.70	140	15.8	122
3	**PdL1′**	0.70	140	56.5	416
4	**PdL5′**	0.70	140	83.6	595
5	**PdL6′**	0.70	140	38.4	281
6	**PdL1′-Y**	0.70	140	90.0	649
7	**PdL5′-Y**	0.70	140	39.2	313
8	**PdL6′-Y**	0.70	140	65.7	474

Reaction conditions: Bromobenzene (5mmol), Styrene (10 mmol), Na_2CO_3 (10 mmol), 10 mL of DMF, catalyst, Reaction time-20 h.

[a] Determined by gas chromatography. [b] Turnover number calculated at the completion of reaction (mol of bromobenzene transformed / mol of palladium metal in catalyst)

5A.2.10 Correlation between structural modification and modified functionality

Palladium complexes are usually efficient catalysts for the coupling reactions though they have some limitations such as difficulties in separation and recovery and thermal instability. However, all these

drawbacks of the homogeneous Pd catalyst could be overcome easily by encapsulating these systems within the pore of zeolites, which provide easy separation, high thermal stability and modified functionality. Hence zeolite encapsulated metal complexes have been studied for various organic transformations.[18, 40, 61] Upon encapsulation, the steric and electrostatic constraints provided by the framework of zeolite Y influence the geometry of complex and consequently modify electronic, magnetic and redox properties, and hence striking changes in the functionality of the enclosed metal complex are observed.[62] The modified functionality for the Heck reaction is an outcome of the modified geometry of the palladium Schiff base complexes.

Neat palladium Schiff base complex has a square planar geometry around the central metal however, the central aromatic ring (m-phenylenediamine) exhibits non-planar arrangement leading to the reduction of π-delocalization. Geometry optimization results directly notify the fact. Therefore, [Pd(sal-1,3-phen)] type systems are subjected to have lesser extent of conjugation from the ligand moiety in comparison to their corresponding [Pd(sal-1,2-phen)] complexes.

The electronic contribution of the substituent in the palladium complexes have been analyzed by electronic spectroscopic studies in a series of complexes (PdL1′, PdL5′, and PdL6′). With the increase in the electron-withdrawing character of the substituent attached, as observed in UV-Vis spectra, the HOMO-LUMO gap of neat Palladium complex is subjected to increase leading to a hypsochromic shift in absorption spectrum pertaining to the metal. The bathochromic shift is in line with the increase in electron density on the ligand.[63] Electron donating group (-OCH_3) enhances π-delocalization and maintains the planarity of the complex whereas an electron-withdrawing group (-NO_2) causes non-planarity. From electronic spectroscopic studies of the neat complexes, we have found that the d-d transition of PdL5′ complex is red shifted and the d-d transition of PdL6′ complex is blue-shifted as compared to that of PdL1′ complex. In the present study, comparative catalytic activities of palladium (sal-1,3-phen) complexes are employed as catalysts for the Heck reaction with aryl bromide and styrene in presence of Na_2CO_3 as base. Observed catalytic results of neat palladium complexes indicate the reactivity order as PdL5′>PdL1′>PdL6′. Electron donating group (-OCH_3) in PdL5′ complex increase the electron density around metal center causing the red-shift of the band appearing from the metal and subsequently, PdL5′ complex is most active as catalyst towards the Heck coupling reaction. PdL6′ complex with electron-withdrawing group (-NO_2) is least reactive among the all neat complexes as expected. Our results have been supported by literature

reports. Saleem and coworkers have already reported the reactivity of the palladium complexes for Heck reaction correlated with the HOMO-LUMO energy gap.[64] Palladium complex with low HOMO-LUMO energy gap shows higher activity towards Heck reaction.

It has also been reported that the presence of electron-withdrawing group, the planarity of salen ligand is disturbed, however an electron-donating group on the same position maintains the planarity of the complex with substantial electron density on the metal center.[65] Higher the electron density around the metal center facilitates the coupling reactions. Upon encapsulation, geometry of these palladium Schiff base complexes is altered significantly due to space constraint imposed by the topology of zeolite Y. For all encapsulated complexes (PdL1′-Y, PdL5′-Y and PdL6′-Y), charge transfer/d-d transition bands are shifted towards higher wavelength. The optimized geometry of the encapsulated complex obtained from theoretical studies clearly indicates an enhanced planarity and hence enhanced π-delocalization induced by the central aromatic ring (m-phenylenediamine) as the topology of the zeolite-Y framework enforces central ring to tilt towards molecular plane. Consequently, red shift in charge transfer/d-d transition is observed. Encapsulation of PdL5′-Y complex with -OCH_3 group, obstructs electron-donating effect to some extent on the other side, zeolite topology imposes planarity to a certain extent. Hence, the effect of the substituent group and electronic effects originating from steric hindrance due to encapsulation oppose each other, therefore, red shift in the d-d transition is marginal as compared to encapsulated PdL1′-Y and PdL6′-Y complexes. However, PdL1′ and PdL6′ complexes when encapsulated in zeolite Y have shown remarkable improvement in reactivity. The enhanced functionality of these systems are the outcome of the enhanced electron density around the metal thereby causing significant red shift in the charge transfer/d-d transition In case of encapsulated PdL6′-Y complex, both the electronic effect of substituent group and that from distorted geometry function in same direction causing much higher red shift. But for PdL1′-Y complex, only steric factor contributes and the wall of zeolite supercage enforces the metal complex to adopt the distorted geometry enhancing the electron density around the metal, hence, reactivity is also enhanced. The functionality of the neat palladium Schiff base complexes is headed by the electronic factor of the substituent present on the phenyl ring and the complexes follow the activity order as PdL5′>PdL1′>PdL6′. However, after the encapsulation, the activity trend is governed by electronic effect originated from the substituent as well as a steric hindrance. The catalytic activity of the encapsulated complexes follow the order of PdL1′-Y>PdL6′-Y>PdL5′-Y. It appears to be an exciting

approach to alteration of HOMO –LUMO energy gap of guest complex by encapsulation of complex inside the rigid zeolite supercage and finally leading to encroach in the field of tunable catalysis. Electron density on palladium metal center can be modified in two ways, either by the attachment of different substituent groups on the ligand moiety or by encapsulating the complexes in the cavities of a rigid host framework. Hence, geometry of these catalysts turns out to be a crucial factor for the enhanced activity towards Heck reaction.

5A.3 CONCLUSION

In summary, zeolite encapsulated palladium Schiff base complexes are synthesized by using 'flexible ligand method' and neat analogs are also studied to compare with their encapsulated states. These complexes are well characterized by the help of different characterization tools like XRD, SEM-EDS, BET, thermal analysis, XPS, IR, and UV-Vis spectroscopic studies. These palladium complexes when employed as catalysts for a Heck coupling reaction, all of them differ significantly from the behavior of their corresponding neat form. The main aim of the present study is to explore the geometry of the palladium complex after encapsulation as well as to rationalize the modified functionality of the systems. The catalytic activity has been explained in the term of electropositive character of metal center. The complex with less electropositive palladium center showing the lowest energy electronic band red-shifted eventually exhibits s higher activity towards Heck coupling reaction. Interestingly, complexes showing blue shift in their free state or encapsulated states are less reactive. From detailed comparative experimental and theoretical electronic data and catalysis studies, it can be concluded that more red shift observed in d-d transition; more is the reactivity of palladium complexes towards Heck coupling reaction. Red shift in d-d transition for particularly this series of palladium complexes can be produced in two ways, either by addition of strong electron-donating substituent groups on the ligand moiety or by encapsulation in zeolite Y. Therefore, the geometry of the catalyst complex plays a key role in Heck coupling reaction for the enhanced activity.

5A.4 REFERENCES

1. S. Pasa, Y. S. Ocak, H. Temel and T. Kilicoglu, *Inorg. Chim. Acta*, 2013, **405**, 493-504.
2. H. A. Dieck and R. F. Heck, *J. Am. Chem. Soc.*, 1974, **96**, 1133-1136.
3. S. Paul and J. H. Clark, *Green Chem.*, 2003, **5**, 635-638.

4. P. Lloyd-Williams and E. Giralt, *Chem. Soc. Rev.*, 2001, **30**, 145-157.
5. S. S. Stahl, *Angew. Chem., Int. Ed.*, 2004, **43**, 3400-3420.
6. D. J. Xuereb and R. Raja, *Catal. Sci. Technol.*, 2011, **1**, 517-534.
7. J. M. Thomas and R. Raja, *Acc. Chem. Res.*, 2008, **41**, 708-720.
8. P. Nehra, B. Khungar, K. Pericherla, S. C. Sivasubramanian and A. Kumar, *Green Chem.*, 2014, **16**, 4266-4271.
9. M. Cai, Y. Huang, R. Hu and C. Song, *J. Mol. Catal. A: Chem.*, 2004, **212**, 151-154.
10. M. M. Miller and D. C. Sherrington, *J. Catal.*, 1995, **152**, 368-376.
11. M. Gruber, S. Chouzier, K. Koehler and L. Djakovitch, *Appl. Catal., A*, 2004, **265**, 161-169.
12. A. Corma, H. Garcia and A. Leyva, *J. Mol. Catal. A: Chem.*, 2005, **230**, 97-105.
13. K. Köhler, M. Wagner and L. Djakovitch, *Catal. Today*, 2001, **66**, 105-114.
14. S. Jana, B. Dutta, R. Bera and S. Koner, *Langmuir*, 2007, **23**, 2492-2496.
15. J. Miao, B. Huang, H. Liu and M. Cai, *RSC Adv.*, 2017, **7**, 42570-42578.
16. T. Selvaraj and R. Rajalingam, *ACS Omega*, 2018, **3**, 9613-9619.
17. F. Li, D. Hu, Y. Yuan, B. Luo, Y. Song, S. Xiao, G. Chen, Y. Fang and F. Lu, *Mol. Catal.*, 2018, **452**, 75-82.
18. A. Choudhary, S. Kumari and S. Ray, *ACS Omega*, 2017, **2**, 6636-6645.
19. C. K. Modi, N. Solanki, R. Vithalani and D. Patel, *Appl. Organomet. Chem.*, 2018, **32**, e3910.
20. S. C. Mohan, R. V. Solomon, P. Venuvanalingam and K. Jothivenkatachalam, *New J. Chem.*, 2017, **41**, 9505-9512.
21. H. Mei, J. Hu, S. Xiao, Y. Lei and G. Li, *Appl. Catal., A*, 2014, **475**, 40-47.
22. N. Wang, Q. Sun, R. Bai, X. Li, G. Guo and J. Yu, *J. Am. Chem. Soc.*, 2016, **138**, 7484-7487.
23. Y. He and C. Cai, *Catal. Commun.*, 2011, **12**, 678-683.
24. P. Das and W. Linert, *Coord. Chem. Rev.*, 2016, **311**, 1-23.
25. C. González-Arellano, A. Corma, M. Iglesias and F. Sánchez, *Adv. Synth. Catal.*, 2004, **346**, 1758-1764.
26. B. Banik, A. Tairai, N. Shahnaz and P. Das, *Tetrahedron Lett.*, 2012, **53**, 5627-5630.
27. M. M. Mogorosi, T. Mahamo, J. R. Moss, S. F. Mapolie, J. C. Slootweg, K. Lammertsma and G. S. Smith, *J. Organomet. Chem.*, 2011, **696**, 3585-3592.
28. A. Dewan, U. Bora and G. Borah, *Tetrahedron Lett.*, 2014, **55**, 1689-1692.
29. R. M. Clarke and T. Storr, *Dalton Trans.*, 2014, **43**, 9380-9391.
30. L. H. Abdel-Rahman, N. M. Ismail, M. Ismael, A. M. Abu-Dief and E. A.-H. Ahmed, *J. Mol. Struct.*, 2017, **1134**, 851-862.
31. T. Kiran, V. G. Prasanth, M. Balamurali, C. Vasavi, P. Munusami, K. I. Sathiyanarayanan and M. Pathak, *Inorg. Chim. Acta*, 2015, **433**, 26-34.
32. S. R. Borhade and S. B. Waghmode, *Tetrahedron Lett.*, 2008, **49**, 3423-3429.
33. B. Karimi and D. Enders, *Org. Lett.*, 2006, **8**, 1237-1240.
34. Y. Heo, Y. Y. Kang, T. Palani, J. Lee and S. Lee, *Inorg. Chem. Commun.*, 2012, **23**, 1-5.
35. Z. Guan, J. Hu, Y. Gu, H. Zhang, G. Li and T. Li, *Green Chem.*, 2012, **14**, 1964-1970.
36. L. Djakovitch, H. Heise and K. Köhler, *J. Organomet. Chem.*, 1999, **584**, 16-26.
37. A. R. Sardarian, M. Kazemnejadi and M. Esmaeilpour, *Dalton Trans.*, 2019, **48**, 3132-3145.
38. M. Jafarian, M. Rashvand avei, M. Khakali, F. Gobal, S. Rayati and M. G. Mahjani, *J. Phys. Chem. C*, 2012, **116**, 18518-18532.
39. W. H. Quayle, G. Peeters, G. L. De Roy, E. F. Vansant and J. H. Lunsford, *Inorg. Chem.*, 1982, **21**, 2226-2231.
40. K. K. Bania, D. Bharali, B. Viswanathan and R. C. Deka, *Inorg. Chem.*, 2012, **51**, 1657-1674.

41. V. Marakatti, *Influence of Alkaline Earth Cation Exchanged X-Zeolites Towards Ortho-Selectivity in Alkylation of Aromatics: Hard-Soft-Acid-Base Concept*, 2015.
42. M. Sharma, B. Das, G. V. Karunakar, L. Satyanarayana and K. K. Bania, *J. Phys. Chem. C*, 2016, **120**, 13563-13573.
43. D. R. Godhani, H. D. Nakum, D. K. Parmar, J. P. Mehta and N. C. Desai, *J. Mol. Catal. A: Chem.*, 2017, **426**, 223-237.
44. B. Kumar Kundu, V. Chhabra, N. Malviya, R. Ganguly, G. S. Mishra and S. Mukhopadhyay, *Microporous Mesoporous Mater.*, 2018, **271**, 100-117.
45. S. L. Hailu, B. U. Nair, M. Redi-Abshiro, R. Aravindhan, I. Diaz and M. Tessema, *J. Porous Mater.*, 2015, **22**, 1363-1373.
46. B. Fan, H. Li, W. Fan, C. Jin and R. Li, *Appl. Catal., A*, 2008, **340**, 67-75.
47. K. K. Bania, D. Bharali, B. Viswanathan and R. C. Deka, *Inorg. Chem.*, 2012, **51**, 1657-1674.
48. R. M. Barrer, *Hydrothermal chemistry of zeolites*, London : Academic press, 1982.
49. B. Dutta, S. Jana, R. Bera, P. K. Saha and S. Koner, *Appl. Catal., A*, 2007, **318**, 89-94.
50. A. P. S. Andrade, L. M. Arantes, J. Y. Kadooca, R. L. Carvalho, Â. de Fátima and A. A. Sabino, *Inorg. Chim. Acta*, 2016, **1**, 886-890.
51. K. Dhara, K. Sarkar, D. Srimani, S. K. Saha, P. Chattopadhyay and A. Bhaumik, *Dalton Trans.*, 2010, **39**, 6395-6402.
52. K. K. Bania and R. C. Deka, *J. Phys. Chem. C*, 2013, **117**, 11663-11678.
53. E. Paez-Mozo, N. Gabriunas, F. Lucaccioni, D. D. Acosta, P. Patrono, A. La Ginestra, P. Ruiz and B. Delmon, *J. Phys. Chem.*, 1993, **97**, 12819-12827.
54. *Clays Clay Miner.*, 1991, **39**, 22-27.
55. A. Choudhary, B. Das and S. Ray, *Dalton Trans.*, 2016, **45**, 18967-18976.
56. M. Salavati-Niasari, M. Shaterian, M. R. Ganjali and P. Norouzi, *J. Mol. Catal. A: Chem.*, 2007, **261**, 147-155.
57. M. Frisch, G. Trucks, H. Schlegel, G. Scuseria, M. Robb, J. Cheeseman, J. Montgomery Jr, T. Vreven, K. Kudin and J. Burant, *Inc.: Wallingford, CT.*
58. A. Choudhary, B. Das and S. Ray, *Dalton Trans.*, 2015, **44**, 3753-3763.
59. A. Choudhary, B. Das and S. Ray, *Inorg. Chim. Acta*, 2017, **462**, 256-265.
60. Z. Beigi, A. H. Kianfar, G. Mohammadnezhad, H. Görls and W. Plass, *Polyhedron*, 2017, **134**, 65-72.
61. M. R. Maurya, A. K. Chandrakar and S. Chand, *J. Mol. Catal. A: Chem.*, 2007, **274**, 192-201.
62. K. K. Bania and R. C. Deka, *J. Phys. Chem. C*, 2011, **115**, 9601-9607.
63. S. Bertini, A. Coletti, B. Floris, V. Conte and P. Galloni, *J. Inorg. Biochem.*, 2015, **147**, 44-53.
64. F. Saleem, G. K. Rao, A. Kumar, S. Kumar, M. P. Singh and A. K. Singh, *RSC Adv.*, 2014, **4**, 56102-56111.
65. M. M. Bhadbhade and D. Srinivas, *Inorg. Chem.*, 1993, **32**, 6122-6130.

Chapter 5B:

An Insight into the Catalytic Activity of Palladium Schiff-Base Complexes towards Heck Coupling Reaction: Routes via Encapsulation in Zeolite-Y

***Abstract**: A small set of palladium Schiff-base complexes have been synthesized and also been entrapped in the supercage of zeolite-Y. All these novel complexes in both the states are systematically characterized with the help of different characterization tools like XRD, SEM-EDS, thermal analysis, XPS, IR, electronic spectroscopic and theoretical studies. These systems are thoroughly studied for the catalytic activities towards the Heck coupling reaction between bromobenzene and styrene. The aim is to meticulously compare the performance of the homogeneous catalysts i.e., neat palladium Schiff-base complexes with that of their heterogeneous encapsulated analogs. The experimental as well as theoretical electronic structure studies suggest a significant structural modification of the guest Pd(II)–Schiff base complexes after encapsulation in zeolite Y. These complexes manifest modified catalytic activities towards Heck coupling reaction. Theoretical studies reinforce to establish the correlation between the modified catalytic properties and structural alteration of these complexes, on encapsulation. These heterogeneous catalysts essentially have shown benefits of easy separation and reusability over the homogeneous analogues.*

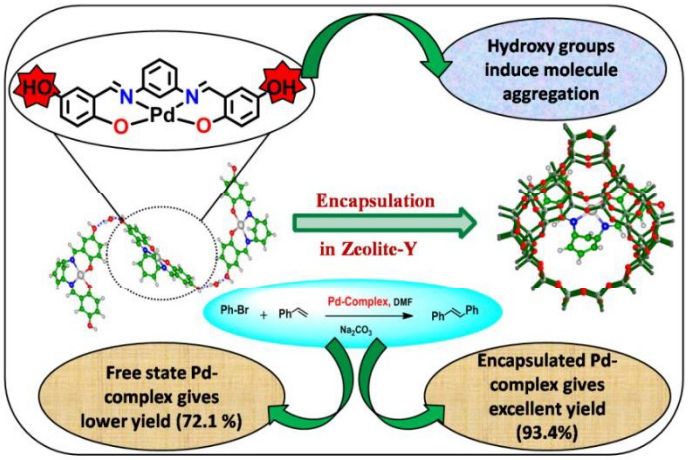

*S. Kumari, B. Das and S. Ray, *Dalton Trans.,* 2019, **48**, 15942-15954.

5B.1 INTRODUCTION

As mentioned earlier (in chapter 5A) palladium (II) Schiff-base complexes of chelating Schiff-base ligands with extended π conjugated architecture, synthetic flexibility and strong binding capacity[1-3] have been widely studied because of their diverse applications in catalysis.[4-9]

In the recent times, the host-guest chemistry involving cobalt, nickel, copper and palladium complexes within the microporous and mesoporous materials, their characterization and catalytic activity were studied in details.[10-15] Zeolite encapsulated palladium complexes are notified as very efficient catalysts for sulfoxidation reactions,[12] aminocarbonylation reaction[15] and for hydrogen generation.[16]

Guan, Z. and co-workers has established an encapsulated $PdCl_2(py)_2$ complex (where py = pyridine) as highly efficient and reusable catalyst for Suzuki–Miyaura cross-coupling reaction between aryl halides and arylboronic acids with Pd loadings of 0.0188 mol% in aqueous medium.[17] Specially, such a low loading level is also remarkably effective as for entrapped complexes, extent of leaching is drastically subsided. Another report on palladium complex entrapped in zeolites with low loading (0.1 mol%) also indicates its high catalytic activity towards the Heck coupling reaction of aryl bromides.[18]

In previous chapter 5A, zeolite encapsulated Pd(II) Schiff-base complexes are found to be efficient catalyst for the Heck coupling reaction and the study mainly explores the origin of modified catalytic reactivity of the encapsulated palladium complex. In continuation of ongoing interest directed towards the design, synthesis and application of new zeolite encapsulated transition metal complexes, the present study focuses on the correspondence between structural and functional modification of the Pd(II) Schiff-base complexes.

Herein, with the continuation of previous work (chapter 5A), synthesis and characterization of the palladium complexes with the L2′, L3′ and L4′ Schiff-base ligands are targeted which follow the order of molecular dimension as PdL2′ < PdL3′ < PdL4′, with L2′; *N,N'*-bis(5-hydroxysalicylidene)phenylene-1,3-diamine, L3′; *N,N'*-bis(5-bromosalicylidene)phenylene-1,3-diamine and L4′; *N,N'*-bis(5-methylsalicylidene)phenylene-1,3-diamine (given in Figure 5B.1). Currently the substituent groups are chosen with relatively milder field strengths (-OH, -Br and $-CH_3$) and with moderately larger molecular dimension as compared to the Pd(II) complexes discussed earlier (in chapter 5A) having $-OCH_3$, $-NO_2$ groups attached. The idea is to figure out upto which level the confinement of the complexes inside the supercage of zeolite, could revamp the electronic structure of the complexes and subsequently the

catalysis. In these complexes with different substituent groups, palladium metal essentially experiences electronic effect differently, as well as steric and electrostatic constraints inside the supercage of the host framework when encapsulated. The topology of zeolite supercage framework enforces structural modification of the guest palladium complex and thereby, alters the electronic, magnetic and redox properties of the complex along with the catalytic reactivity and selectivity of it.

These newly-designed and synthesized palladium Schiff-base complexes presented here are in encapsulated as well as neat forms are employed for the Heck coupling reaction of bromobenzene with styrene. The Heck coupling reaction is supported by the presence of sodium carbonate as a base. The objective of the present study is to investigate the steric effect imposed by the host framework and electronic effect of the substituent group attached to the complex and their equipoise (given in Figure 5B.1).

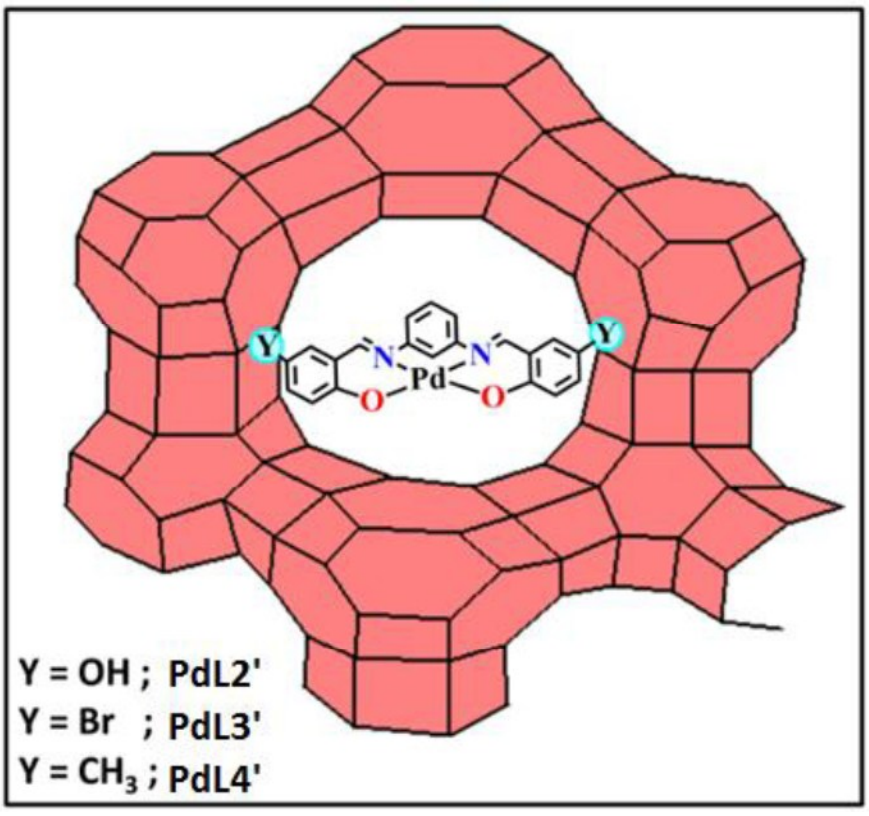

Figure 5B.1: Schematic representation of zeolite-Y encapsulated palladium complexes.

5B.2 RESULTS AND DISCUSSION

Synthesis of ligands and nickel Schiff-base complexes in free or encapsulated states have already discussed in chapter 2 under experimental section (2.2.1-2.2.5).

5B.2.1 Elemental Analysis, Scanning Electron Microscopy (SEM) and X-ray Diffraction (XRD) studies

In order to determine the presence of palladium metal content and other elements in the encapsulated complexes, elemental analysis have been performed with the help of energy dispersive X-ray spectroscopy (EDX) (results of the EDX study given in Table 5B.1). The Si/Al ratio has been found 2.7 corresponding to the unit cell formula as $Na_{52}(AlO_2)_{52}(SiO_2)_{140}.yH_2O$ of parent Na Zeolite-Y. The Si/Al ratio has not been significantly affected while zeolite-Y undergoing Pd(II) exchange and encapsulation processes. However, the amount of palladium content in the encapsulated complexes always is found to be consistently less than that in Pd(II) exchanged zeolite -Y. The target-synthesis of the complex only inside the supercage of host is practically not feasible, as some of the metal complexes or unreacted ligand always be formed or adsorbed on the surface. Therefore, the consistent lowering of the metal content during synthesis of complex inside zeolite Y cavity observed in EDX data can be attributed to the successful entrapment of metal complexes inside the supercage of zeolite-Y as free metal-ions or surface adsorbed complexes are removed uniformly and thoroughly by Soxhlet extraction.

To analyze the surface morphology of the host particularly after encapsulation, SEM micrographs of the encapsulated PdL2′-Y complex have been recorded before (Figure 5B.2A and B) and after Soxhlet extraction (Figure 5B.2C and D). SEM studies confirm that there are some species present on the surface of host before extraction. However, these are completely removed after extraction. The boundaries of the host particles are clearly visible after extraction due to the complete removal of the adsorbed species on the surface in the final product. The pale color of the final product explicitly indicates the successful encapsulation of the metal complex inside the supercage of the zeolite Y.

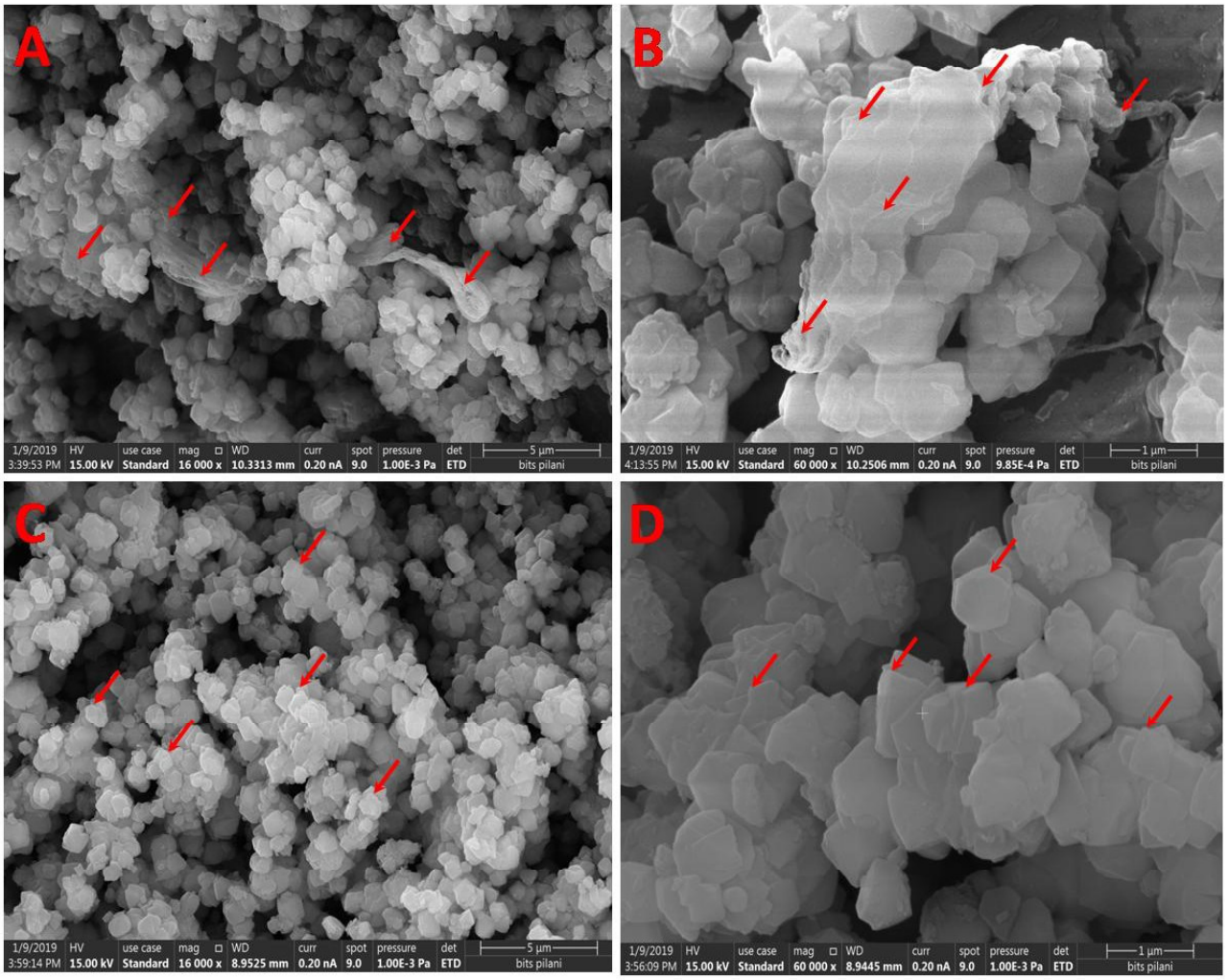

Figure 5B.2: SEM micrograph of the encapsulated PdL2′ in zeolite Y, (A) and (B) (before Soxhlet extraction), (C) and (D) (after Soxhlet extraction).

Detailed powder X-ray diffraction (XRD) studies of parent zeolite-Y, Pd-exchanged zeolite-Y and all encapsulated Pd(II) Schiff-base complexes are presented in Figure 5B.3. In the XRD patterns of parent zeolite-Y and Pd(II)-exchanged zeolite-Y, intensities of peaks for 220 and 311 reflections appearing at $2\theta = 10°$ and 12° respectively shows the relationship as $I_{220} > I_{311}$ which undergoes reversal for zeolites with encapsulated complexes. This reversal in the intensities has already been identified and empirically correlated with the presence of a large complex within the supercage of zeolite-Y.[12, 19-21]This change in the relative intensities may be associated with the redistribution of randomly coordinated free cations in

zeolite- Y at different sites.[22] However, such reversal in the peak intensities is never noticed for the complex forming on the surface.[23, 24] The above observation may suggest the presence of a palladium Schiff-base complex inside the cavity of the host framework. Similar X-ray diffraction patterns have been found for all the systems, indicated that the host framework does not show any considerable structural changes during ion exchange reaction and even after the encapsulation of Pd(II) Schiff-base complex inside the cavity.

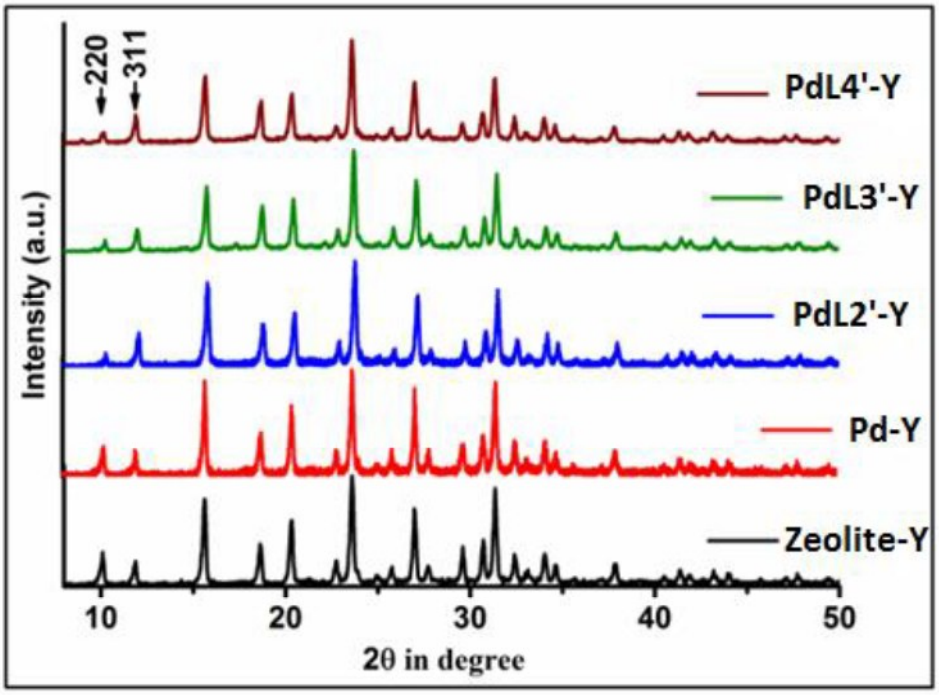

Figure 5B.3: XRD patterns of parent zeolite-Y, Pd(II) zeolite-Y, PdL2′-Y, PdL3′-Y and PdL4′-Y.

5B.2.2 BET surface area analysis

The BET surface area analysis has been performed to know the surface area and pore volume of the parent zeolite-Y and subsequently of the zeolite with palladium Schiff-base complexes entrapped. Figure 5B.4 shows the comparative N_2 adsorption-desorption isotherms of the parent zeolite-Y and zeolites with encapsulated complexes and the results obtained from surface area analysis are given in Table 5B.1. The N_2 adsorption-desorption isotherms for all encapsulated systems and zeolite-Y are of

type I isotherm, typical characteristics of the microporous materials.[25, 26] All the systems exhibit very similar pattern. However, a dominant and vital observation is marked in the comparative studies of surface area and pore volume of the zeolite-Y and zeolite-Y along with encapsulated metal complexes. The BET surface area and pore volume of all the zeolite samples with encapsulated palladium Schiff-base complexes show a dramatic reduction in comparison to those of parent zeolite-Y, suggesting that the palladium Schiff base complexes are not adsorbed on the external surface of host framework rather present inside the cavity of zeolite-Y.[27, 28] The noticeable reduction in the BET surface areas and pore volumes of the encapsulated systems fundamentally depend upon the loading level of metal in zeolite-Y along with the molecular dimension of the complex incorporated inside the supercage of zeolite-Y.

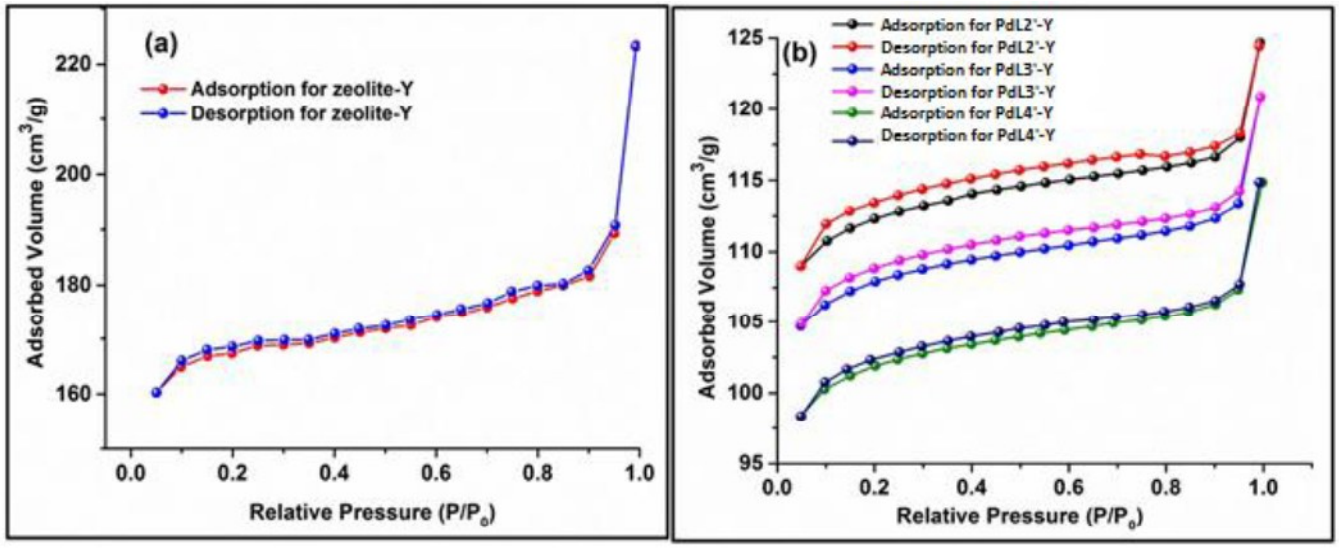

Figure 5B.4: BET isotherms for parent zeolite-Y and zeolite encapsulated complexes: (a) parent zeolite Y, (b) PdL2′-Y, PdL3′-Y and PdL4′-Y.

Table 5B.1: Concentration of palladium (wt %), BET surface area and pore volume of different samples.

S.No.	Samples	Palladium (wt%)	Si/ Al ratio	BET surface area (m^2/g)	Pore volume (cm^3/g)
1	**Zeolite-Y**	-	2.79	535	0.3456
2	**Pd-Y**	0.65	2.79	-	-
3	**PdL2′-Y**	0.42	2.74	349	0.2018
4	**PdL3′-Y**	0.40	2.75	339	0.1917
5	**PdL4′-Y**	0.41	2.73	335	0.1896

5B.2.3 Thermal analysis

Thermo-gravimetric (TGA) analysis has been performed for all neat and encapsulated palladium Schiff-base complexes along with the parent zeolite-Y (shown in Figure 5B.5). Only PdL2′ complex among the all neat-state palladium complexes shows weight loss in the temperature range of (35-110) °C that typically corresponds to the loss of two molecules of water. Parent zeolite-Y shows weight loss in the temperature range of (50-240) °C, which corresponds to the loss of water molecules adsorbed on zeolite framework. In case of encapsulated complex, weight losses occur in two steps. The first weight loss at (50-240) °C parallels to loss of water molecules of zeolite framework[29, 30] and the second weight loss extending up to 800°C is due to the decomposition of the guest molecule. Sharp decomposition of free-state palladium Schiff base complexes when compared with the plateau type TGA curve of the encapsulated analogues it certainly indicates slow and continuous weight loss for the encapsulated systems with the delay in decomposition. Therefore, it could be easily concluded that encapsulation extends the thermal stability to the palladium Schiff-base complexes.[22, 31]

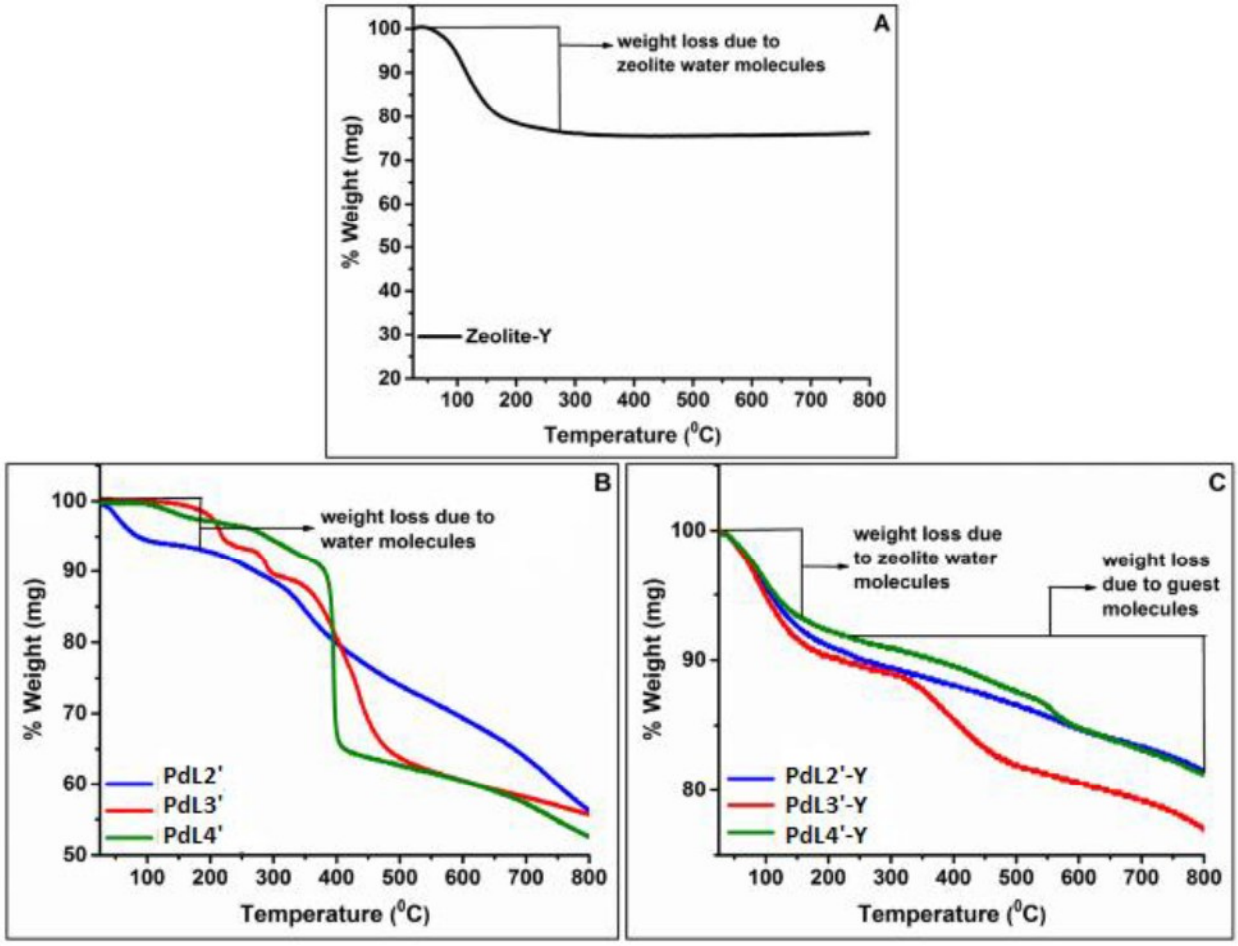

Figure 5B.5: Thermo gravimetric analysis (TGA) results for (A) PdL2′, (B) PdL2′-Y, (C) PdL4′ and (D) PdL4′-Y.

5B.2.4 IR Spectroscopic study

Figure 5B.6 and Table 5B.2 represents the FTIR data for zeolite-Y, free-state palladium complexes and zeolite encapsulated palladium complexes. Observed IR band at 1018 cm^{-1} for parent zeolite Y corresponds to the asymmetric stretching vibrations of $(Si/Al)O_4$ units of framework. Some characteristics IR bands at 560, 717 and 786 cm^{-1}, are the sign of T-O bending mode, double ring and symmetric stretching vibrations respectively.[32] Furthermore, FTIR bands observed at 1643 and 3500 cm^{-1} are correspond to lattice water molecules and surface hydroxylic group, respectively.[33] All these characteristics FTIR bands of pure zeolite Y stay unchanged after metal exchange and even after

encapsulation reaction, revealing that zeolite framework preserves its integrity during the process of encapsulation of palladium complexes. The FTIR range of 1200 to1600 cm^{-1} seems to be an appropriate range for the study of zeolite encapsulated metal complex as in this range, characteristic FTIR bands of zeolite are absent. So, FTIR bands observed are only because of the metal complexes yet the intensity of these FTIR bands is very weak definitely indicating low loading level of palladium metal within the zeolite supercage.

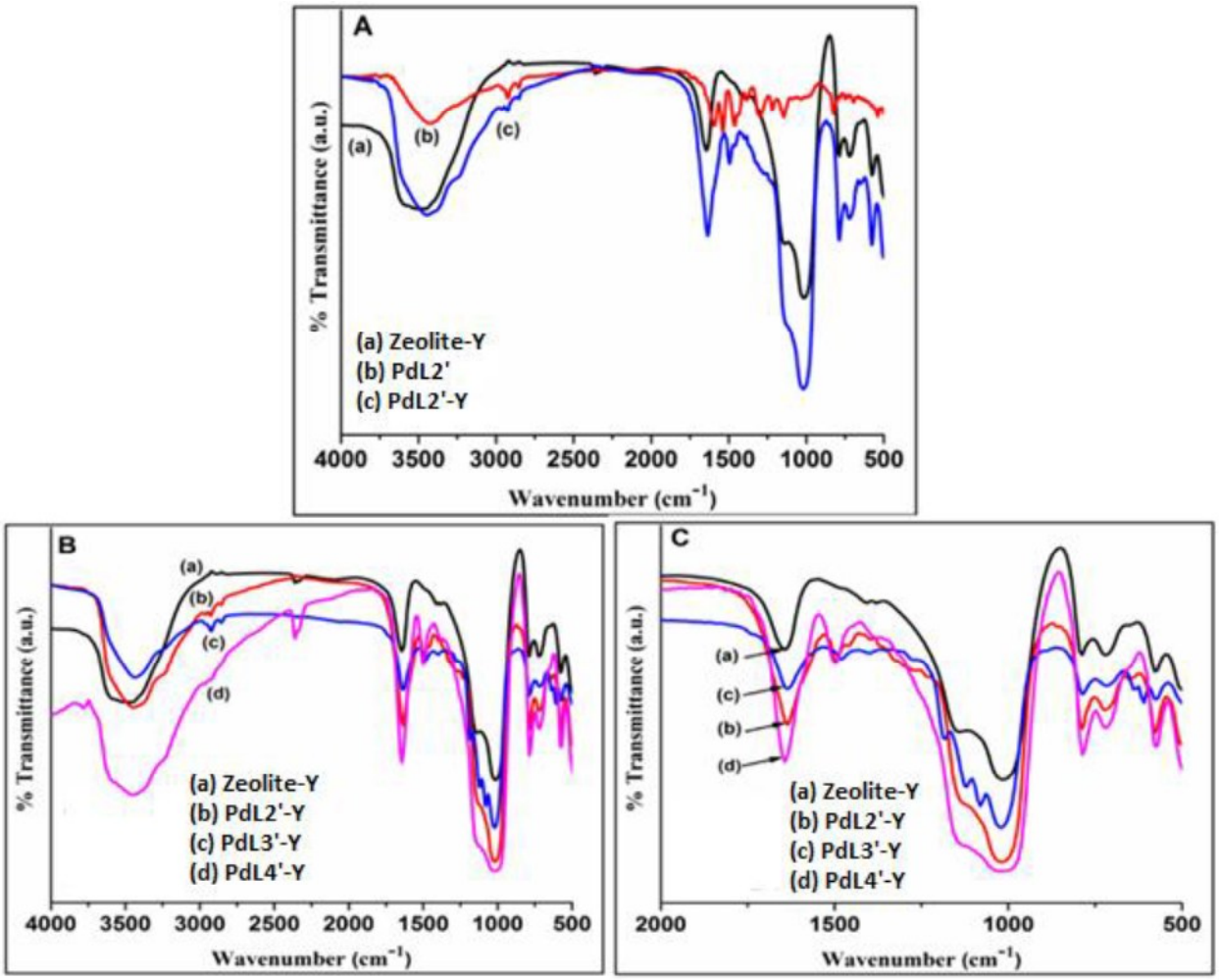

Figure 5B.6: FTIR spectra of (A) parent zeolite-Y, PdL2′ and PdL2′-Y, (B) zeolite-Y, PdL2′-Y, PdL3′-Y and PdL4′-Y and (C) Enlarged view of FTIR spectra in the range of 500 cm^{-1} to 2000 cm^{-1} for (a) parent zeolite-Y, (b) PdL2′-Y, (c) PdL3′-Y and (d) PdL4′-Y.

Characteristic FTIR bands of ligand observed at 1612-1620 cm^{-1} and 1273-1296 cm^{-1} are correspond to the C=N and C-O stretching vibrations and these IR peaks are slightly shifted upon complexation, indicating nitrogen and oxygen coordination within the cavity of zeolite Y. FTIR spectra of free-state palladium Schiff-base complexes indicate important IR peaks at 1528, 1439 cm^{-1} (C=C Stretch.), 1605 cm^{-1} (C=N stretch.), 1278 cm^{-1} (C-O stretch.) and 1358 cm^{-1} (ν_{C-H} deformation).[34] Similar IR peaks with slight shift are also observed in all encapsulated palladium complexes providing indirect evidence for the presence of palladium complexes within the supercage of host framework. Shifts in some characteristics IR peaks upon encapsulation are attributed to the effect of host framework on the guest metal complex. The shift in ν_{C-H} deformation frequencies obtained in all encapsulated complexes, also delivers clear evidence for the encapsulation of palladium complex within the host cavity.

Table 5B.2: FTIR data of neat and encapsulated complexes.

S. No	Samples	C=N stretching	C=C stretching	C-H deformation	C-O stretching
1	**PdL2′**	1593	1539, 1462	1385	1296
2	**PdL2′-Y**	1636	1497, 1458	1396	1292
3	**PdL3′**	1609	1516, 1450	1373	1277
4	**PdL3′-Y**	1636	1481, 1444	1396	1265
5	**PdL4′**	1609	1528, 1481	1373	1257
6	**PdL4′-Y**	1643	1520, 1497	1381	1233

5B.2.5 X-ray Photoelectron Spectroscopy (XPS)

The X-ray Photoelectron Spectroscopy (XPS) provides the information about relative concentration of palladium metal and their oxidation states in the neat and encapsulated systems apart from the detection of the desired elements in the system. The XPS analysis has been carried out for the neat PdL2′ and PdL3′ and encapsulated PdL2′-Y, PdL3′-Y and PdL4′-Y palladium complexes (spectra shown in Figure 5B.7-5B.13). From the comparison of the XPS signal intensities of Pd 3d level in the neat and encapsulated systems, it is found that the encapsulated systems contain very low loading level of

palladium metal. These observations suggest a nice correlation with the EDX and FTIR results. The Table 5B.3 provides the binding energy data for Pd(3d), C(1s), N(1s), O(1s), Si(2p), Al(2p) and Na(1s) in various palladium Schiff-base complexes. The presence of Pd^{+2} metal centre is confirmed by the Pd($3d_{5/2}$) and Pd($3d_{3/2}$) peaks at 337.24 and 342.56 eV respectively. These binding energies data are in well agreement with the literature.[35, 36] Absence of any shake up and satellite peak confirms that the Pd(II) Schiff-base complex present in square planar geometry not in the octahedral geometry.[37] In case of PdL2′ palladium(II) Schiff-base complex, C(1s) XPS signals are appeared at the binding energies of 283.64 and 284.89 eV, N(1s) peak appeared at the binding energy of 398.73 and 400.39 eV and O(1s) XPS peaks at 531.07 eV and 534.36 eV. From the corresponding binding energies data, it is concluded that two different kind of carbon atoms (C-C and C=C) and two types of nitrogen atoms (M-N and C=N) are present in the system. Oxygen binding energies data correspond to M-O and C-O moiety. Encapsulated PdL2′-Y system shows the XPS signals for the Si(2p), Al(2p) and Na(1s) appearing at binding energies of 102.07 eV, 73.70 eV and 1071.55 eV respectively. The appearance of Pd($3d_{5/2}$), Pd($3d_{3/2}$), C(1s), N(1s) and O(1s) peaks in all encapsulated Pd(II) complexes are in agreement with the peaks observed for free-state complexes providing direct proof for the formation of complex inside the supercage of zeolite-Y.

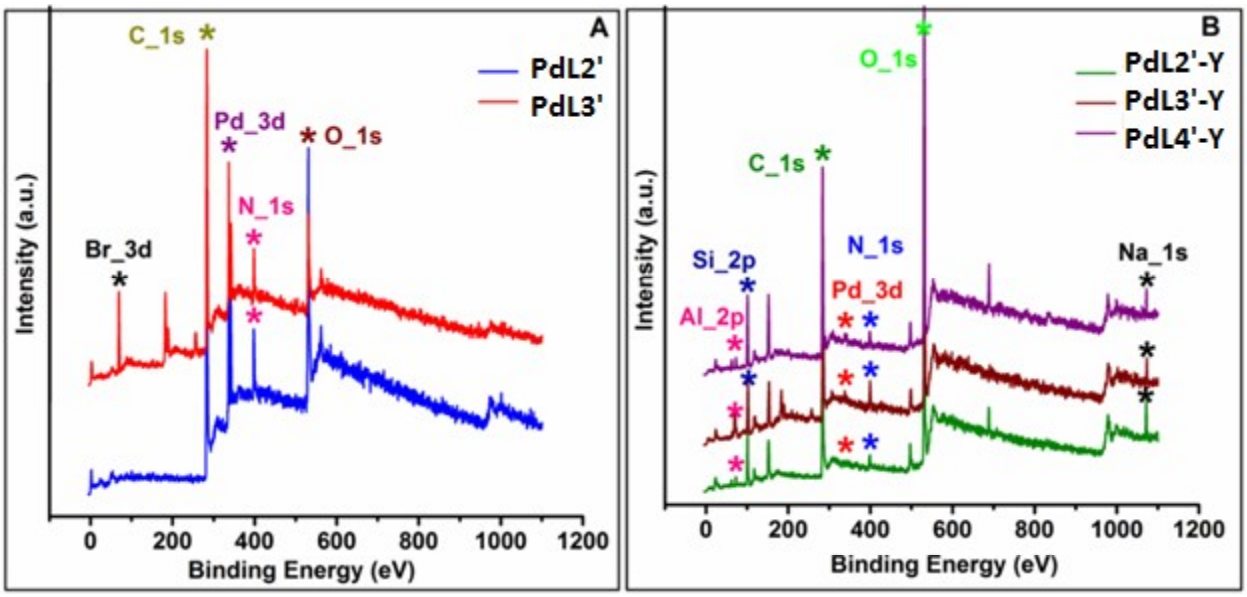

Figure 5B.7: XPS survey spectra for neat and encapsulated complexes (A) PdL2′ and PdL3′, and (B) PdL2′-Y, PdL3′-Y and PdL4′-Y.

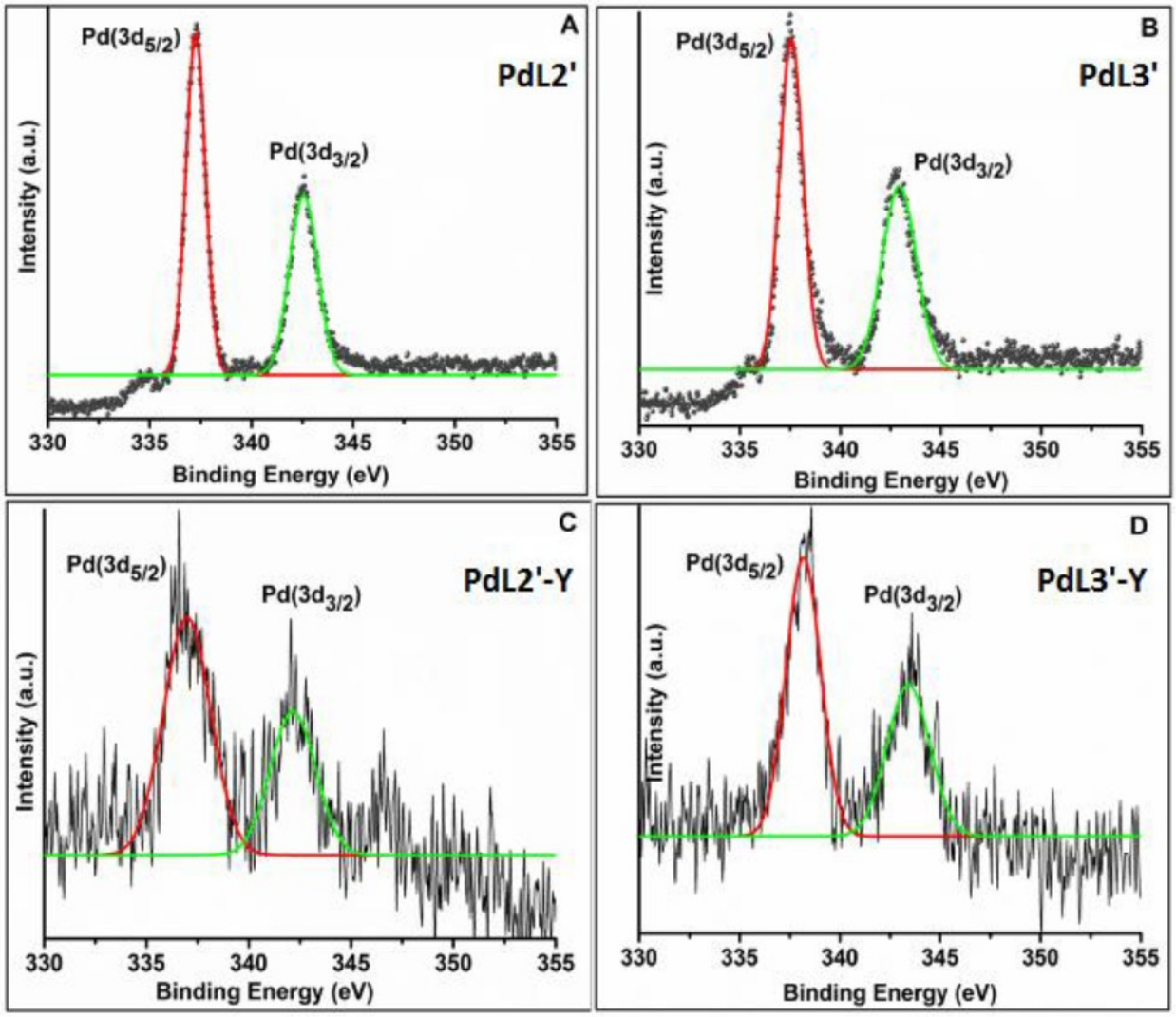

Figure 5B.8: High resolution XPS signals of Pd (3d) for (A) PdL2′, (B) PdL3′ (C) PdL2′-Y and (D) PdL3′-Y complex.

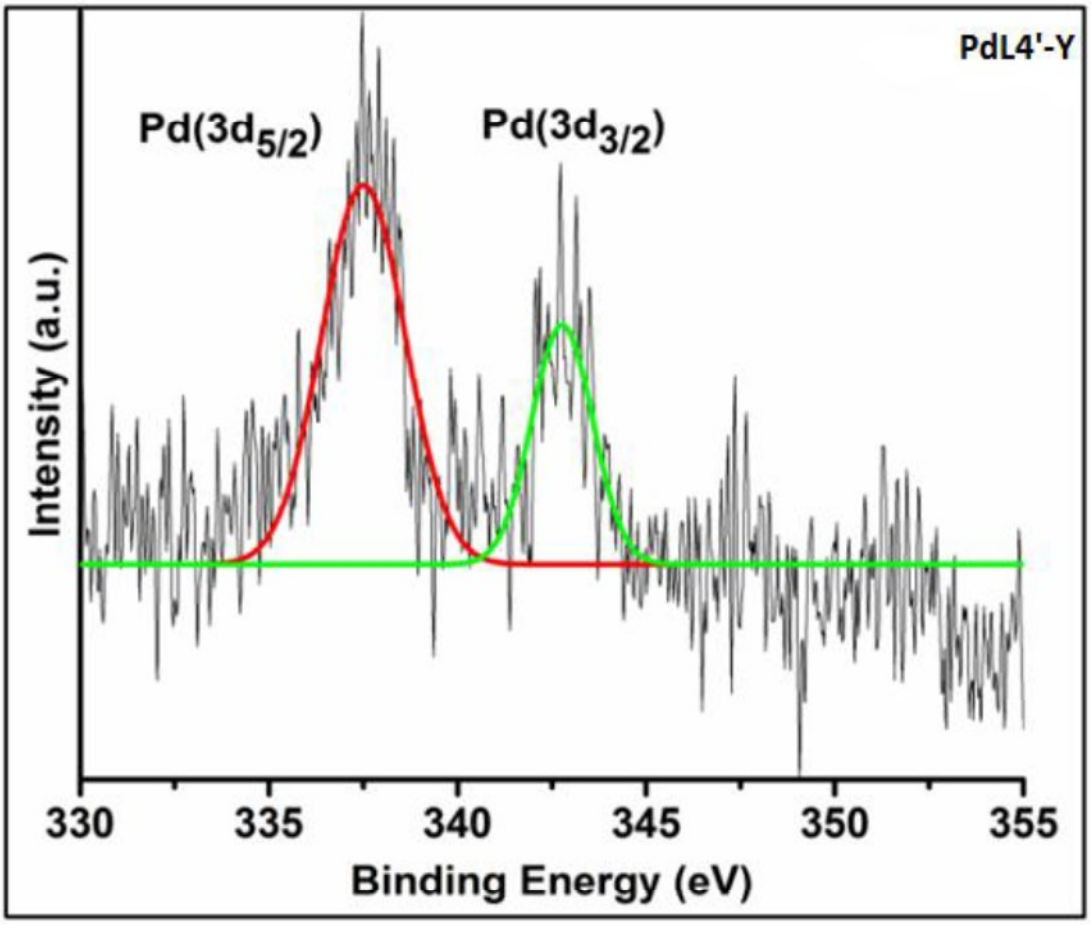

Figure 5B.9: High-resolution XPS signals of Pd (3d) for PdL4′-Y complex.

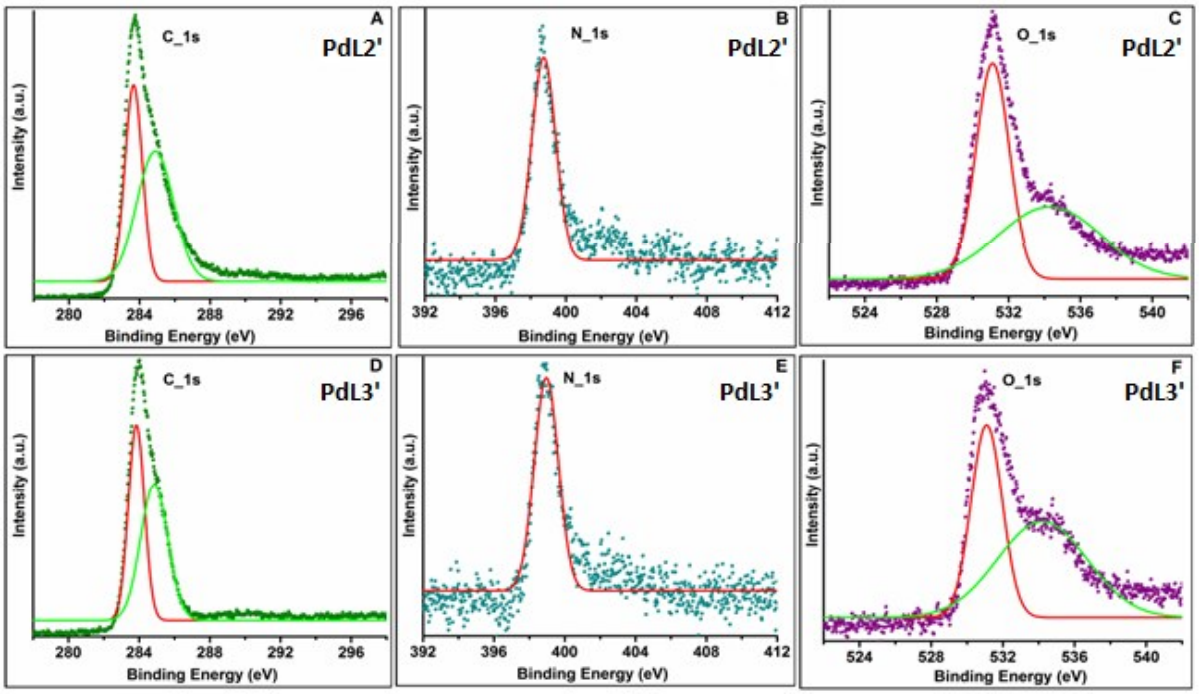

Figure 5B.10: High-resolution XPS spectra of C (1s), N (1s), and O (1s) for PdL2′ and PdL3′ complex.

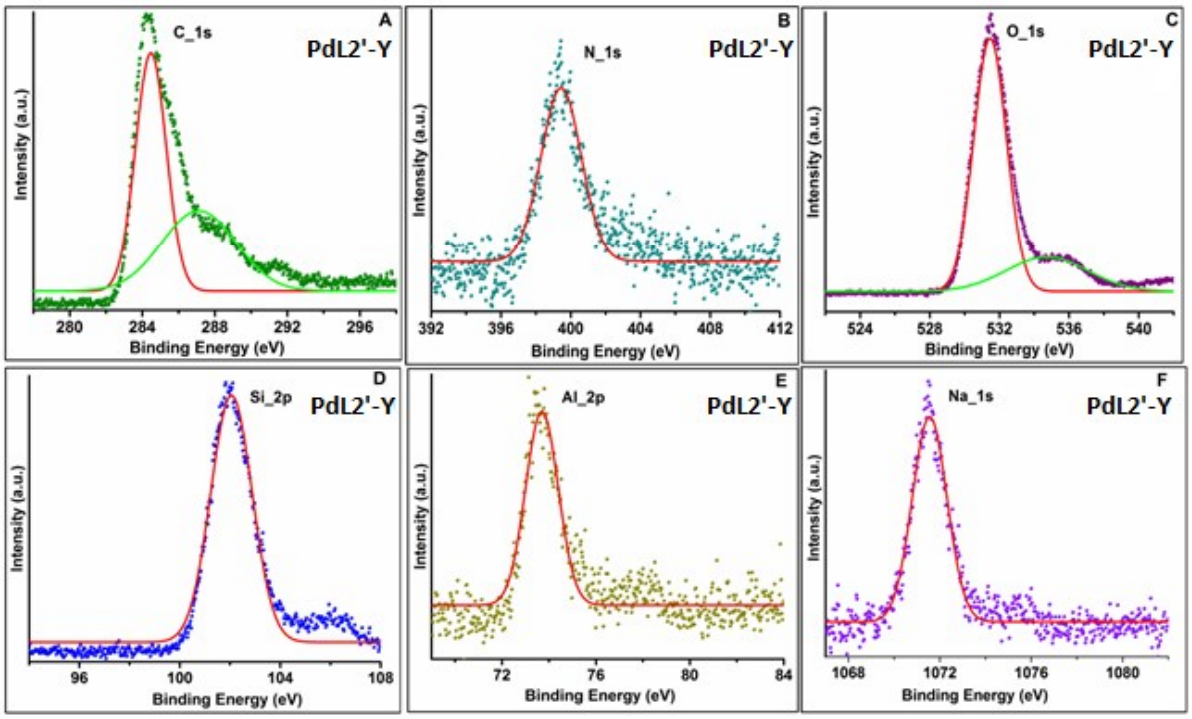

Figure 5B.11: High-resolution XPS spectra of C (1s), N (1s), O (1s), Si (2p), Al (2p) and Na (1s) for PdL2′-Y complex.

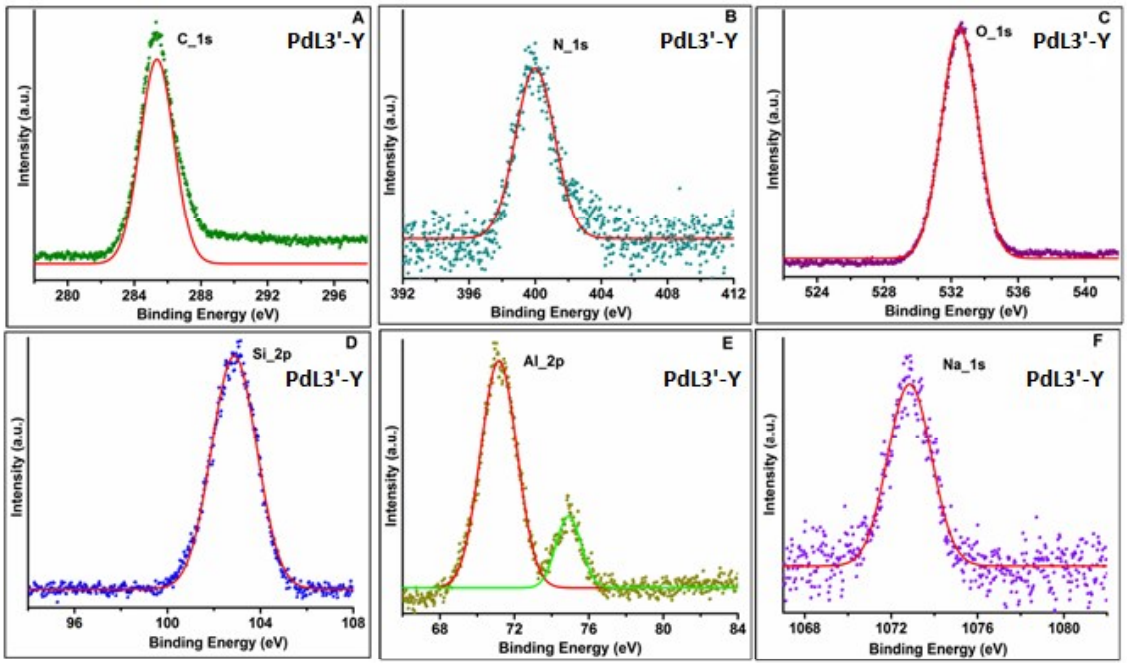

Figure 5B.12: High-resolution XPS spectra of C (1s), N (1s), O (1s), Si (2p), Al (2p) and Na (1s) for PdL3′-Y complex.

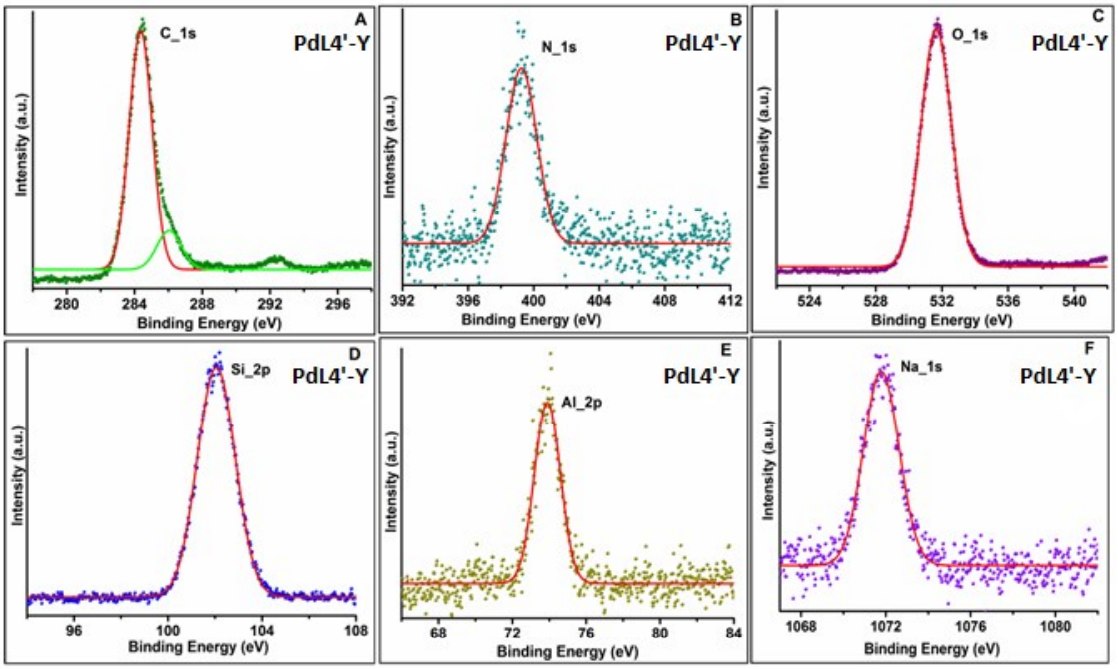

Figure 5B.13: High-resolution XPS spectra of C (1s), N (1s), O (1s), Si (2p), Al (2p) and Na (1s) for PdL4′-Y complex.

Table 5B.3: Binding energy (eV) of neat and encapsulated complexes.

S. No	Samples	Si (2p)	Al (2p)	Na (1s)	C (1s)	N(1s)	O (1s)	Pd (3d5/2)	Pd (3d3/2)
1.	**PdL2′**	-	-	-	283.64, 284.89	398.73	531.07, 534.36	337.24	342.56
2.	**PdL3′**	-	-	-	283.83, 284.89	398.97	531.11, 534.28	337.54	342.91
3.	**PdL2′-Y**	102.07	73.70	1071.55	284.49, 287.19	399.43	531.46, 534.95	337.05	342.18
4.	**PdL3′-Y**	102.87	71.18, 74.90	1072.84	285.36	400.02	532.48	338.17	343.39
5.	**PdL4′-Y**	102.05	73.88	1071.78	284.38, 286.06	399.24	531.66	337.49	342.76

5B.2.6 UV-Vis/Diffuse Reflectance Spectroscopy (UV−Vis/ DRS)

The UV-Vis spectra of the ligands and neat palladium Schiff-base complexes are recorded in $CHCl_3$ however the exceptions are L2′ and PdL2′. UV-Vis spectra of ligand L2′ and corresponding complex PdL2′ are recorded in DMF as both ligand and complex are insoluble in solvent like water, methanol, $CHCl_3$ and many others. The solution spectra of the ligands and neat complexes are shown in Figure 5B.14 and relevant data is given in Table 5B.4. The UV−Vis spectrum of the Schiff-base ligand (L2′) exhibits four intense peaks at 258, 285, 302 and 379 nm attributed to π-π* and n-π* transitions (Figure 5B.14A). The corresponding Pd(II) Schiff base complex (Figure 5B.14A) shows characteristic absorption bands at 265, 304, 360 and 451 nm. The first intense band is due to π-π* intra ligand transitions. The bands at 304 and 360 nm are assigned to the n-π* transitions. The π-π* and n-π* transitions of the ligand are shifted towards higher wavelength upon complexation, indicating the involvement of nitrogen and oxygen in coordination. The lowest energy band at 451 nm is attributed to

either charge transfer or d−d transition from the low-lying fully occupied orbital to the upper unoccupied orbital, suggesting the formation of a square planar PdL2′ complex.

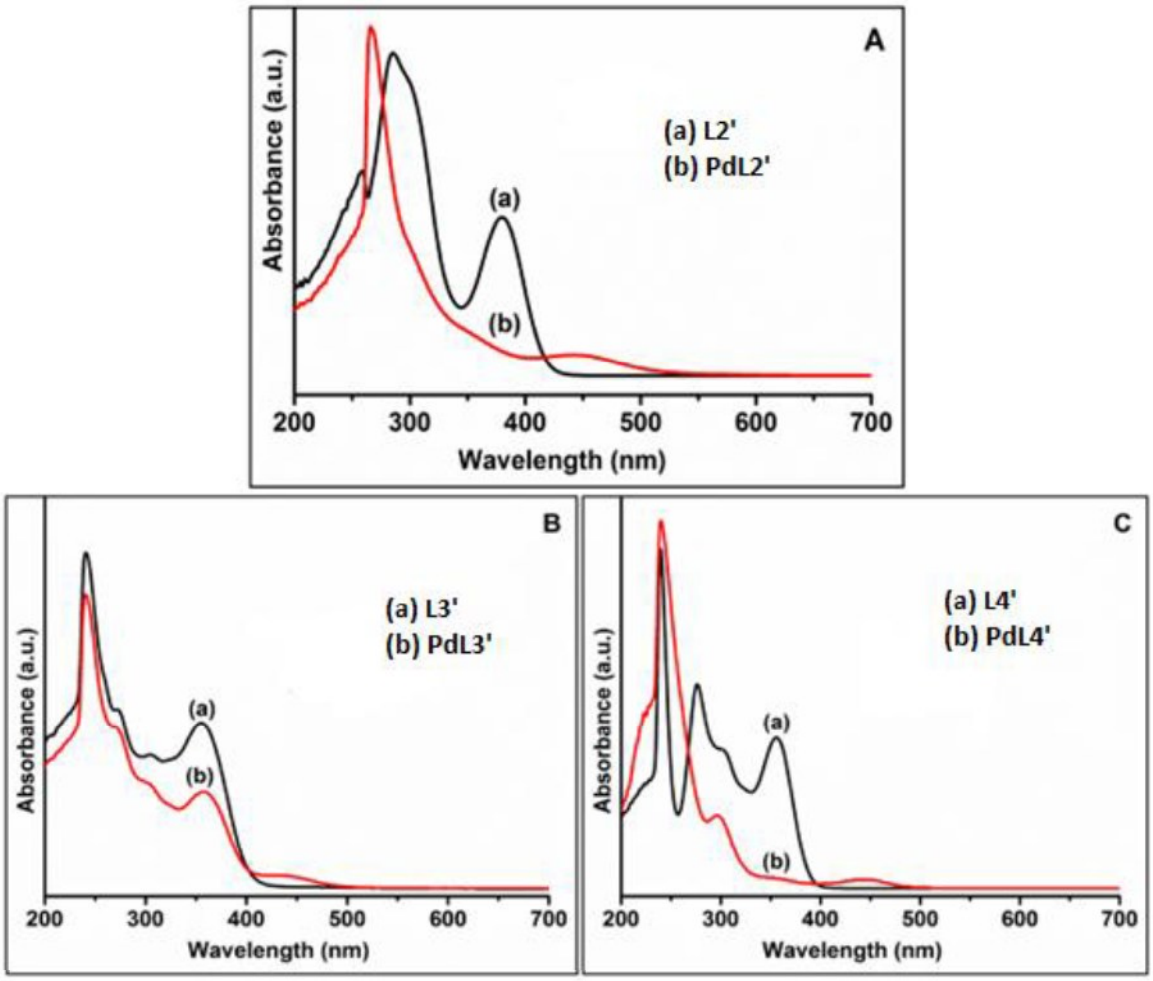

Figure 5B.14: Solution UV-Vis spectra of (A) L2′ and PdL2′, (B) L3′ and PdL3′ and (C) L4′ and PdL4′.

Table 5B.4: Solution UV-Visible data of ligand and neat complexes.

S. No	Samples	π—π^* transitions	n—π^* transitions	CT transitions / d-d Transitions
1	**L2′**	258, 285	302, 379	-
2	**PdL2′**	265	304, 360	451
3	**L3′**	240, 272	304, 355	-
4	**PdL3′**	239, 273	306, 358	440
5	**L4′**	238, 276	305, 356	-
6	**PdL4′**	240	298, 359	446

The solid-state UV-Vis studies of the ligands and their neat complexes also provide specific evidence about the complex formation. The presence of similar electronic bands in the UV-Vis spectra of encapsulated complexes as its free-state analogue indicates the complex formation inside the supercages of host. The DRS/UV−Vis spectra of neat and encapsulated palladium Schiff-base complexes are shown in Figure 5B.15 and data has been presented in Table 5B.5. For PdL2′ complex, the absorption bands in the range of 245−375 nm are due to intraligand transitions. The peak at 458 nm can be attributed to the transition related to the metal Pd.

UV-Vis spectra of all the three free-state complexes when compared, significant shift in absorption band especially for the metal-related transitions emphasizes certain facts. The lowest energy transition at 450 nm for PdL4′ complex appears at longer wavelength (458 nm) in case of PdL2′ complex. It could be well comprehended as PdL2′ complex contains strong electron donating –OH substituent. The observation is just opposite for PdL3′ complex as it contains electron withdrawing –Br groups. Moreover, the lowest energy transition associated with the metal of PdL2′ at 458 nm is found to be red shifted upon encapsulation. Shift in metal-related transition parallels to the modified geometry of metal complex originated by encapsulation. Interestingly, under encapsulation, all the three-palladium Schiff-base complexes show red shift in transition originated from metal. This further administers an intimation

that all the three complexes undergo a similar kind of modification pertaining to the structure inside zeolite-Y. Redshift in transition associated with the metal of palladium Schiff base complexes clearly suggest enhanced π-delocalization around the metal center after encapsulation.

Experimental observations of PdL2′ definitely indicated the need of comprehensive investigation as it behaves quite differently even in neat form compared to all others, starting from its solubility to thermo-gravimetric analysis and reactivity. Surprisingly, its catalytic behavior especially in the encapsulated form does not follow the anticipated trend set by previous studies (chapter 5A). We thus performed a detailed DFT study of PdL2′, to understand its anomalous behavior in neat and encapsulated forms.

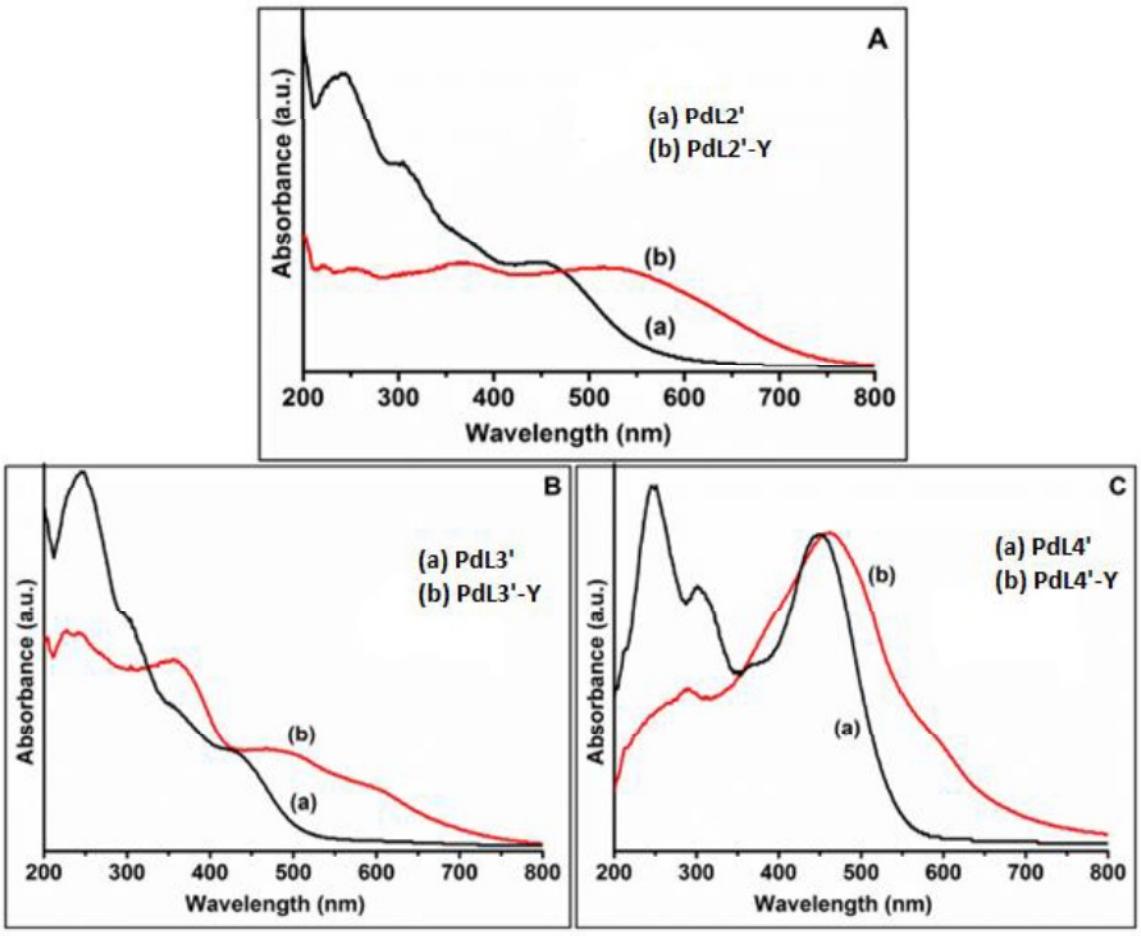

Figure 5B.15: Solid state UV-Vis spectra of (A) PdL2′ and PdL2′-Y, (B) PdL3′ and PdL3′-Y and (C) PdL4′ and PdL4′-Y.

Table 5B.5: Solid-state UV-Visible data of neat and encapsulated complexes

S. No	Samples	π—π^* transitions	n—π^* transitions	CT transitions / d-d transitions
1	**PdL2′**	245	305, 375	458
2	**PdL2′-Y**	258	310, 376	558, 624
3	**PdL3′**	246	306, 368	436
4	**PdL3′-Y**	250	326, 355	504, 608
5	**PdL4′**	248	305, 371	450
6	**PdL4′-Y**	252	289, 385	462, 602

5B.2.7 Theoretical Methods

The electronic structure calculations based on Density Functional Theory (DFT) was used to study and analyze the structural and optical properties of the Pd complexes in neat and zeolite encapsulated states. All results presented here are obtained using GAUSSIAN 09 suite of *ab initio* quantum chemistry programs.[38] The details of the theoretical methods have already discussed in chapter 2 under section 2.3.11.

Density functional theory (DFT) studies for singlet PdL2′ complex show the end-to-end distance (with two -OH groups present in para positions) to be 13.74 Å (Figure 5B.16a, Table 5B.6) in contrast to PdL3′ (14.76 Å) and PdL4′ (14.06 Å) (shown in Table 5B.7). The complexes are all planar molecules with the central phenyl ring connected to two N atoms, behind the Pd centre being nearly perpendicular to the molecular plane. This is reflected in the angle made by the carbon, Pd and carbon atoms, which is ~171 degrees for all complexes (Table 5B.7). We also looked into the <O-Pd-N bond-angle around the Pd atom, which provides some idea about geometry around the Pd centre and for the singlet, neat molecules; the <O-Pd-N bond angle is ~86°, which indicates it is near planarity. In case of the neat molecules, the Pd-O, Pd-N, O-C and N=C bond-distances are 2.0, 2.19, 1.29 and 1.30 Å respectively (Table 5B.6 and Table 5B.7). To understand the unusual properties of PdL2′ even in neat form, we have

looked into the possibility of the terminal -OH groups binding to water molecules, and we indeed find that the two terminals -OH groups can bind to two water molecules *via* hydrogen-bonding (Figure 5B.16a). This kind of binding is not possible for the other complexes.

$PdL2' + 2H_2O \rightarrow H_2O—(PdL2')—H_2O$

The binding energy for the water binding is calculated as:

$E_{bind} = E_{H_2O—(PdL2')—H_2O} - (E_{PdL2'} + 2E_{H_2O})$

It is seen that the binding energy for two water molecules to the PdL2′ complex is ~10 kcal, which indicates that under normal conditions this molecule would bind to two water molecules, which in turn may bind to further Pd-complex molecules in both ends making small oligomeric aggregates mediated by hydrogen bonded water molecules (See Figure 5B.16b). The binding energy for formation of a small aggregate of three PdL2′ complexes mediated by two water molecules is ~16 kcal, indicating a possibility of such aggregation in presence of water/moisture. The formation small aggregates may be the reason of poor solubility of the complex as thermo-gravimetric data indicates two molecules of water loss at the temperature ranging from 35°C to 110°C (shown in Figure 5B.5). It is however important to note that the water molecules bound to PdL2′ complex does not change the geometry of the complex as the structural parameters from Table 5B.6 reveal, but the frontier molecular orbitals are slightly affected. In this connection, it may also noted that the TD-DFT spectra is nearly unchanged by the hydrogen bonded water molecules for PdL2′ (Figure 5B.21). The calculated TD-DFT spectra for PdL3′ and PdL4′ are given in Figure 5B.20. As encapsulation of the PdL2′ complex within zeolite occurs, such small aggregates held loosely by hydrogen bonds are likely to break down and the neat complex is encapsulated within the zeolite pore in triplet state, as our previous studies with similar complexes have shown.[20, 21, 39] This is also favorable from steric point of view as binding to water molecules increase the effective volume of the Pd-complex making it more bulky to fit in within the pore. PdL2′ complex in triplet state is found to be bent (Figure 5B.16c) and its length reduces along with <C-Pd-C angle as shown in Table 5B.6. The optimized structure of zeolite encapsulated triplet PdL2′ complex is shown in Figure 5B.16d.

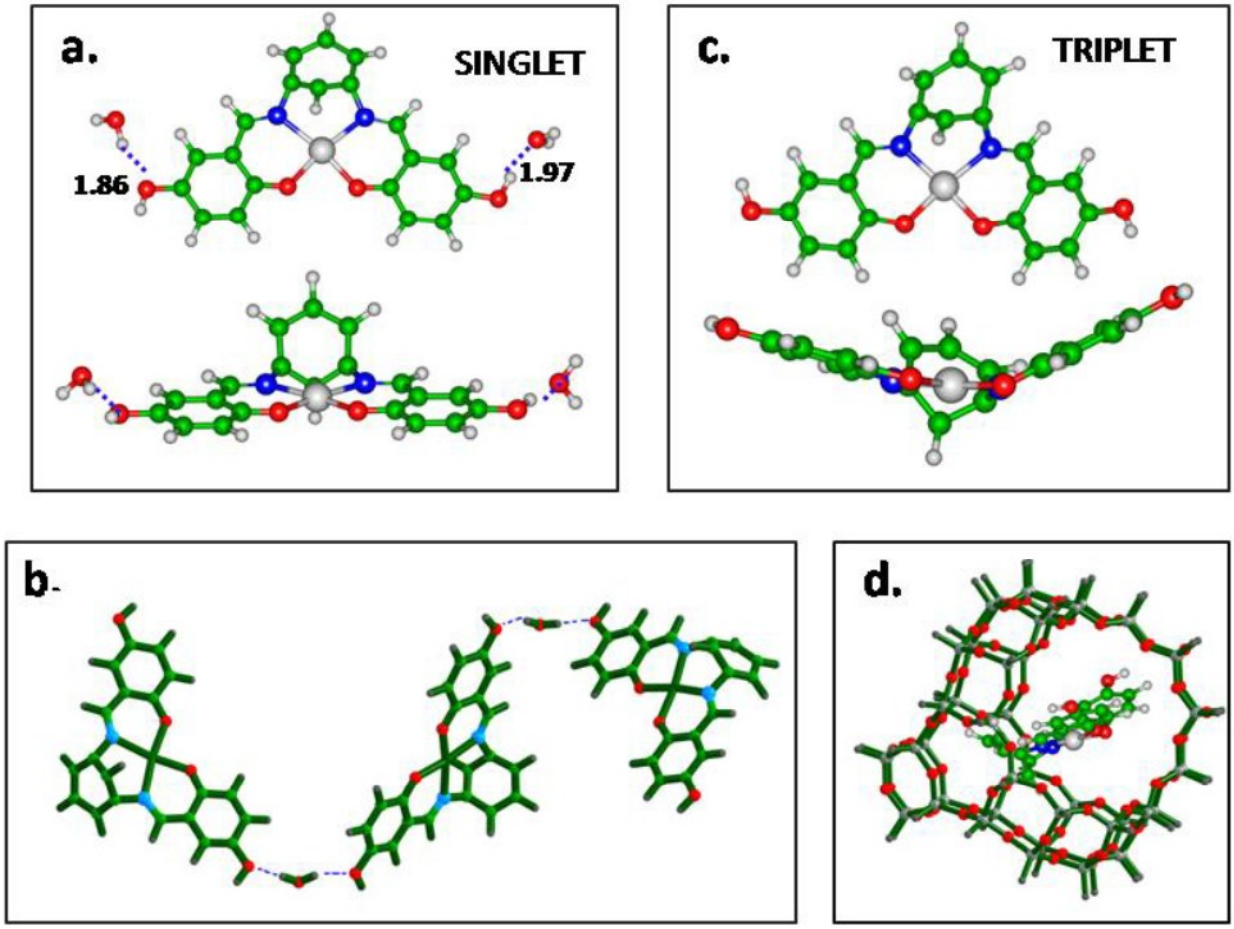

Figure 5B.16: (a) PdL2′ complexes are shown in singlet state. The hydrogen bonded water molecules are also shown. The distances of hydrogen-bonded water molecules from -OH groups are marked. (b) Optimized structure of the hydrogen-bonded singlet, PdL2′ complexes (three), mediated by two water molecules (c) triplet state of PdL2′ complex, two views are shown, (d) The triplet PdL2′ complex encapsulated in zeolite supercage.

Table 5B.6: Important structural parameters from DFT for neat and encapsulated PdL2′ complex.

S. No	Bond distances / angles	PdL2′, neat singlet	PdL2′+2H_2O, neat singlet	PdL2′-Y, Encapsulated, extracted triplet
1	**Pd-O (Å)**	2.00	2.01	2.01
2	**Pd-N (Å)**	2.19	2.19	2.06, 2.14
3	**O-C (Å)**	1.29	1.29	1.29
4	**N-C(conj) (Å)**	1.30	1.29	1.29, 1.32
5	**<O-Pd-N**	85.9	85.6	87.6, 88.9
6	**End to end distance(Å)**	13.74	13.75	12.99
7	**<C-Pd-C**	170.9	170.9	152.4
8	**HOMO,**	-5.24	-5.07	-4.99,-5.33
	LUMO (eV)	-2.62	-2.48	-2.44,-3.49

Table 5B.7: Important structural parameters and HOMO, LUMO energies of neat PdL2′, PdL3′ and PdL4′ complexes obtained from DFT studies.

S. No	Bond distances / angles	PdL2′, Neat singlet	PdL3′, Neat singlet	PdL4′, Neat singlet
1	**Pd-O (Å)**	2.00	2.01	2.01
2	**Pd-N (Å)**	2.19	2.19	2.19
3	**O-C (Å)**	1.29	1.29	1.29
4	**N-C (Å)**	1.30	1.29	1.30
5	**<O-Pd-N**	85.9	85.9	85.9
6	**End to end distance (Å)**	13.74	14.76	14.06
7	**<C-Pd-C**	170.9	170.8	170.8
8	**HOMO,**	-5.24	-5.78	-5.38
	LUMO (eV)	-2.62	-2.98	-2.58

5B.2.7.1 Frontier Molecular orbitals of PdL2′ complex and calculated TD-DFT spectra

To analyze the calculated absorption spectra especially for PdL2′, a detailed investigation of the frontier molecular orbitals of PdL2′ complex were done (shown in Figure 5B.17 and for PdL3′ and PdL4′ in Figure 5B.18). In case of singlet PdL2′ complex, we find that the HOMO is conjugated and spread over the length of the molecule, along with -OH substituents, but LUMO is only spread over the central ring with contributions from Pd atom (Figure 5B.17). A closer look reveals that it is mainly the overlap of the out of plane p orbitals of the C atoms forming the conjugated π framework are more important, which only partly includes the central ring positioned out of plane behind the Pd atom. The d_{xz} orbital of Pd atom partly contributes to the HOMO orbital, which hybridizes with p-orbitals of the ligand. In case of the LUMO, most important contribution comes from Pd d_{xy} orbital (Figure 5B.17). For PdL2′ complex in the TD-DFT spectrum, we observe a few important peaks at 608, 546, 469, 440, 395 nm. The transition around 608 nm is due to a transition from HOMO to LUMO+1. It is thus a transition from Pd d_{xz} orbital to Pd d_{yz} orbital, and both of these orbitals are mixed heavily with π framework of the benzene ring of the ligand. The transition at 546 nm occurs due to the transition from HOMO-2 (Pd d_{z^2}) orbital to LUMO (Pd d_{xy}). The transition at 469 nm is again due to Pd d_{xz} orbital to Pd d_{yz} orbital mixed with few other transitions. The peak at 440 nm is primarily due to Pd d_{z^2} to Pd d_{xy} orbital along with other transitions.

In the triplet state, the complex is bent, and structural distortion leads to more hybridization with the ligand π orbitals, making identification of metal d orbitals difficult (MOs are shown in Figure 5B.19). A closer look into the TD-DFT spectra of the triplet state (Figure 5B.22) readily reveals that there is an overall shift towards the higher wavelengths, though identification of the transitions are difficult due to their mixed nature. There are weak peaks observed at 714 and 658 nm, while stronger peaks appear between 420-470 nm. None of these peaks appear to be pure d-d transitions, but have fairly strong contributions from Pd d orbitals.

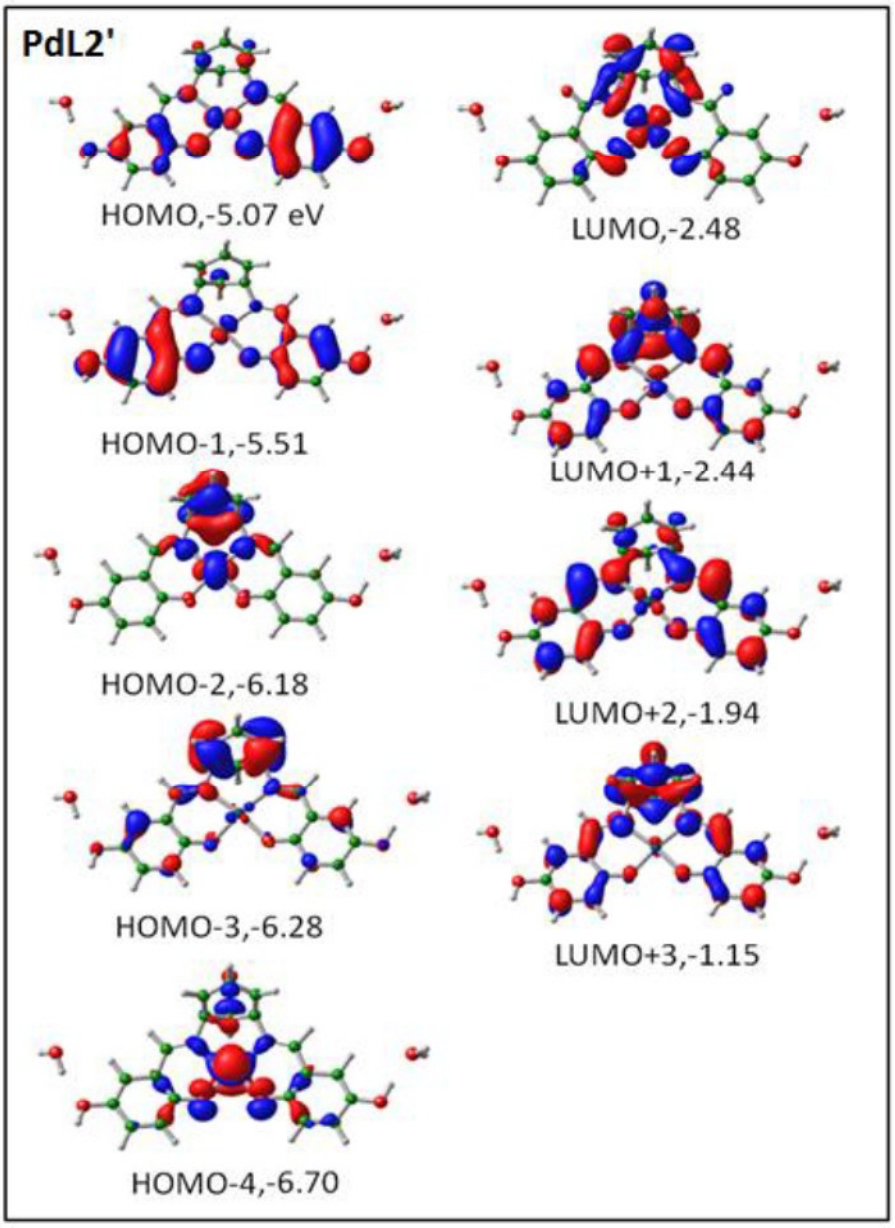

Figure 5B.17: The frontier molecular orbitals of singlet, PdL2′ complex are shown.

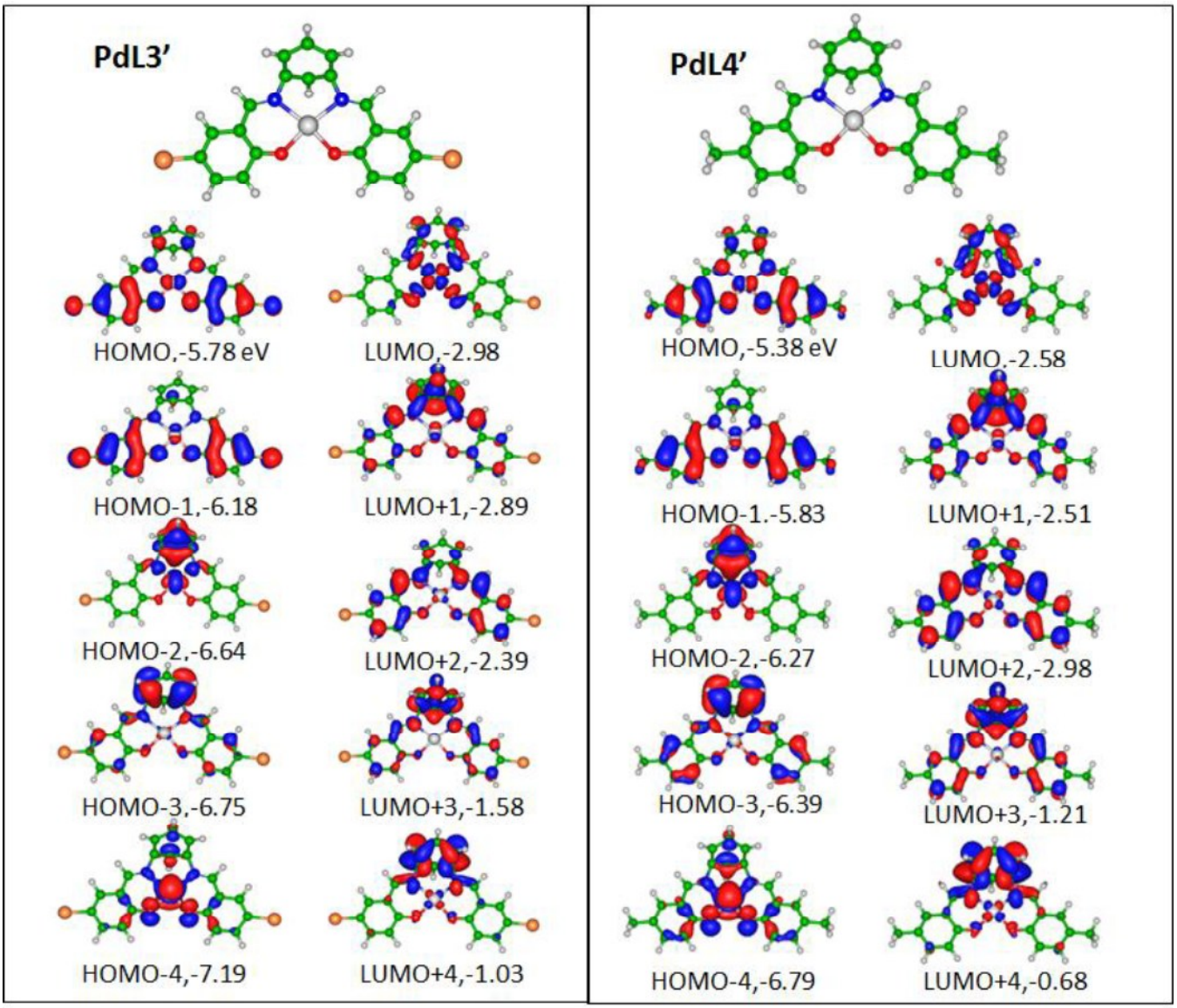

Figure 5B.18: The frontier molecular orbitals for PdL3′ and PdL4′.

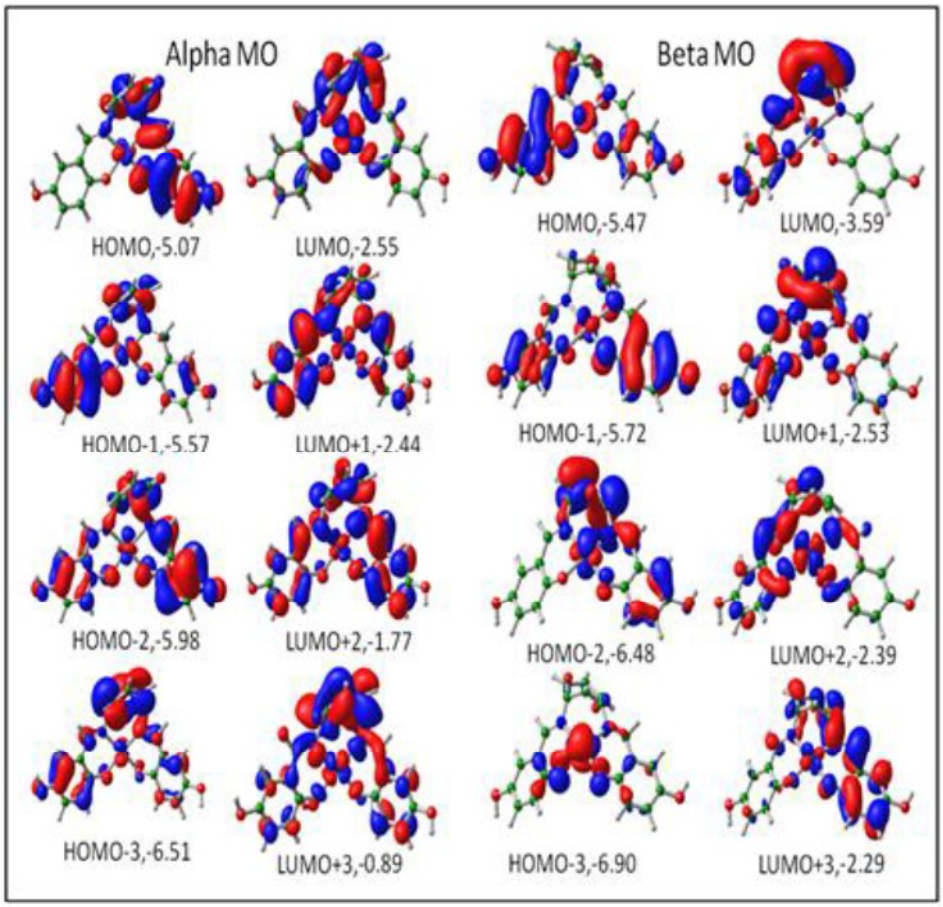

Figure 5B.19: The frontier molecular orbitals of triplet, encapsulated and extracted PdL2′ complex are shown.

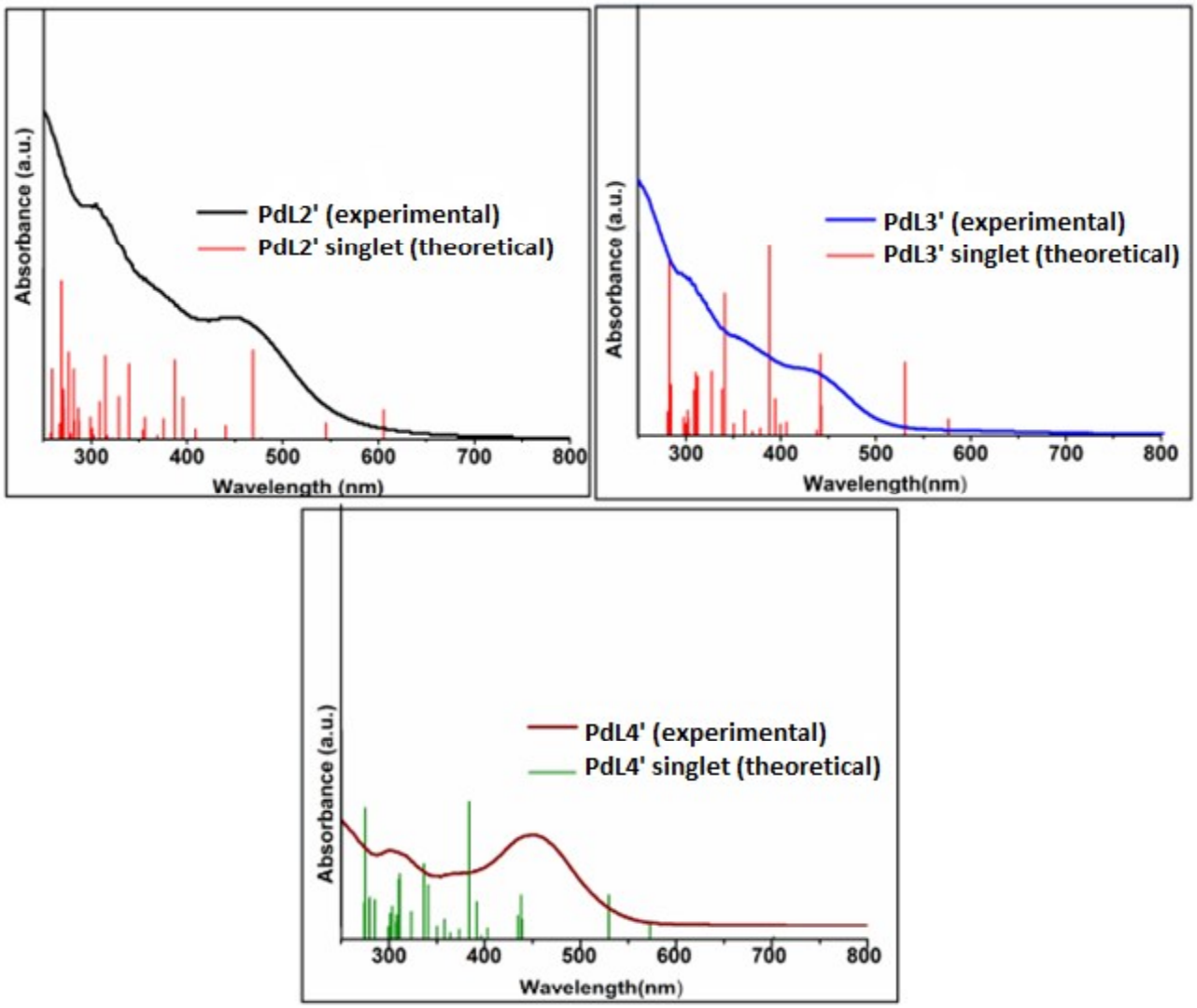

Figure 5B.20: Experimental and TD-DFT spectra for PdL2′, PdL3′ and PdL4′ in neat, singlet state.

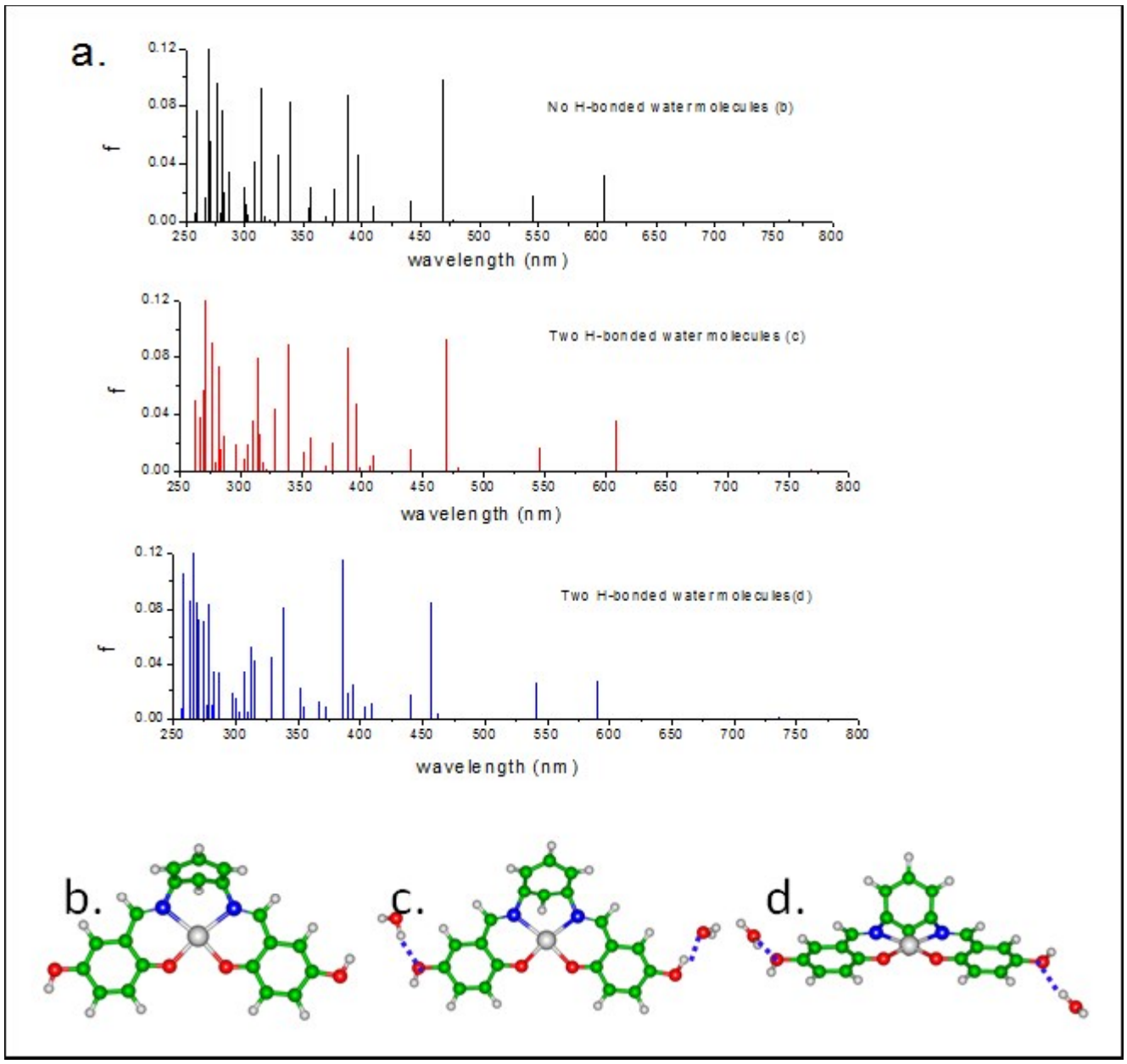

Figure 5B.21: (a) The comparative TD-DFT spectra are shown for neat and water bound singlet PdL2′ complexes. The structures of the singlet complexes studied are given below (b) no water (c) two water molecules hydrogen bonded to Pd complex (c) two water molecules hydrogen bonded to Pd complex in different configuration.

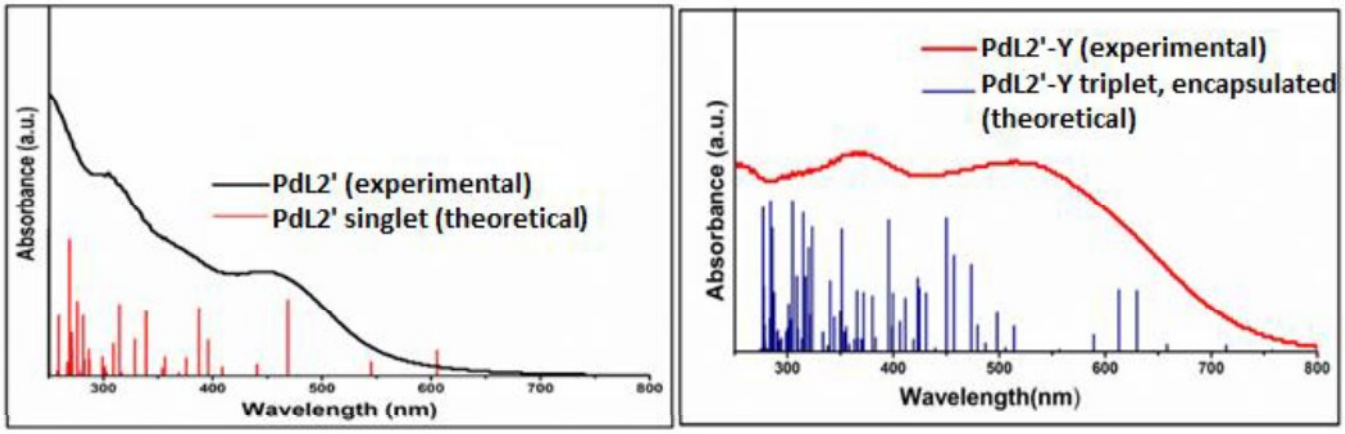

Figure 5B.22: The TD-DFT spectra of the singlet, neat and triplet PdL2′ complexes, which are encapsulated and then extracted.

5B.2.8 Catalytic Study

Catalytic properties of all these free-state and encapsulated systems have been investigated for the Heck coupling reaction between bromobenzene with styrene. The catalysis results for the all systems are presented in Table 5B.8 and the calibration curve of bromobenzene is given in chapter 5A (Figure S14). The reaction conditions have been employed from the previous chapter 5A with respect to encapsulated palladium system and with the variance in amount of catalyst and reaction temperature (Catalytic data given in chapter 5A (Figure S15-S16). All catalytic reactions are monitored by gas chromatography and % conversion calculated by using a calibration curve of bromobenzene with n-heptane as an internal standard.

The reactivity order of free-state homogenous catalysts towards Heck coupling reaction of bromobenzene with styrene follows the reactivity trend as PdL2′ ≥ PdL4′ > PdL3′. The variation of reactivity is governed by the electronic effect of the substituent present. Complexes PdL2′ and PdL4′ bearing electron donating substituent such as -OH and -CH_3 groups respectively show better reactivity towards Heck coupling while the complex with electron withdrawing group shows poor reactivity. Catalysis data of all these three free-state palladium complexes when compared especially with the

previously discussed data of neat palladium complexes without substituent (PdL1′) and with –OCH_3 (PdL5′) and –NO_2 (PdL6′) substituent at the same 5th position, few striking observations are noted deserving further attention. The previous study has identified Pd(II) complex with –OCH_3 group as the most reactive catalyst for the Heck coupling whereas the complex with -NO_2 group as the least reactive one (chapter 5A). The catalysis data of free-state palladium complexes are in well-agreement with the effects of the substituent groups present precisely following the same line of reasoning e.g., stronger the electron donating ability of the substituent present in the complex, more effective would be the complex as catalyst. However, after the encapsulation inside the supercage of zeolite Y, the reactivity order reshuffles. In case of encapsulated systems PdL2′-Y and PdL3′-Y, reactivity is increased after encapsulation as compared to their free-state analogues whereas the reactivity of encapsulated system PdL4′-Y is decreased after encapsulation. Encapsulation triggers inflow of electron density towards Pd in PdL2′-Y and PdL3′-Y cases and opposite is the fact for PdL4′-Y case. Molecular dimension for all these complexes is larger than that of the supercage of zeolite-Y and therefore steric constraints imposed by host cavity must have pronounced contribution towards the reactivity of these complexes. Changes in reactivity of PdL3′-Y and PdL4′-Y systems are just in accordance to the previous study (chapter 5A). Steric constraint of zeolite framework on the guest PdL3′ complex eventually lowers the electron withdrawing effect of the –Br group as encapsulation makes –Br groups non-planar with respect to the molecular plane. Similar though opposite outcome is observed for PdL4′ upon encapsulation. However, we observed that encapsulated PdL2′, is the most efficient catalyst amongst all (% yield and TON are given in Table 5B.8) and is the only one which does not trail the anticipation following the prior study (chapter 5A). This observation definitely points towards the enhancement of electron density on the palladium metal of PdL2′ when it undergoes encapsulation. Heterogeneous catalyst (PdL2′-Y) has been recycled at least five times without significant loss in catalytic activity (Recyclability for the PdL2′-Y catalyst is presented in Figure 5B.23). To know the stability of the catalyst after recyclability, we have done some analysis such as XRD and TGA analysis, which proves the stability of the catalyst (shown in Figure 5B.24).

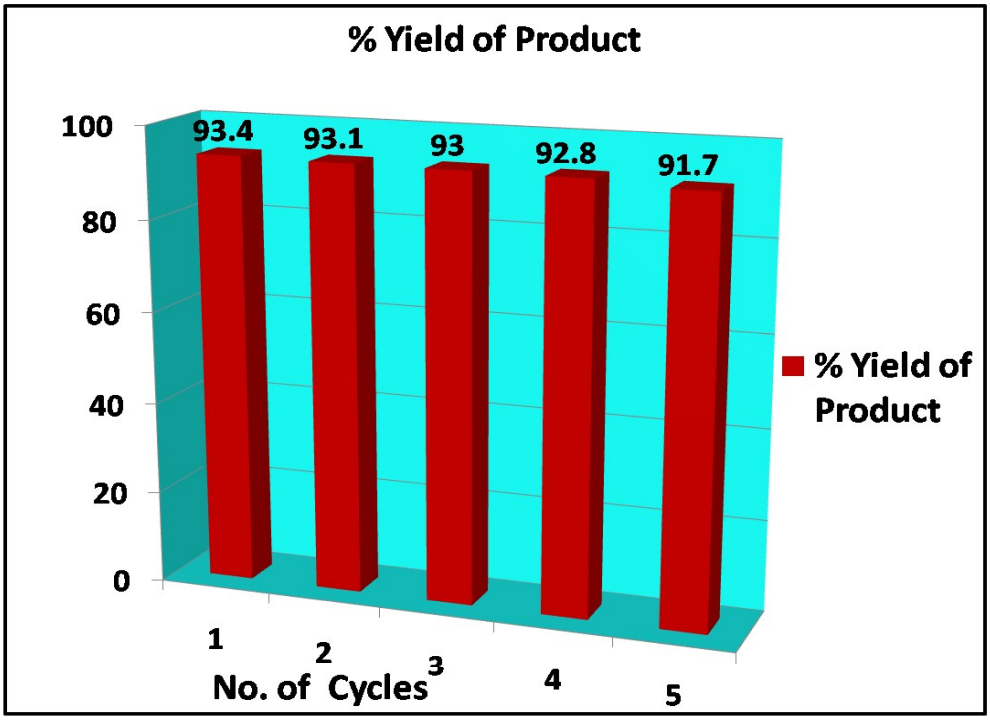

Figure 5B.23: Recyclabili1ty of the PdL2′-Y catalyst for Heck coupling reaction.

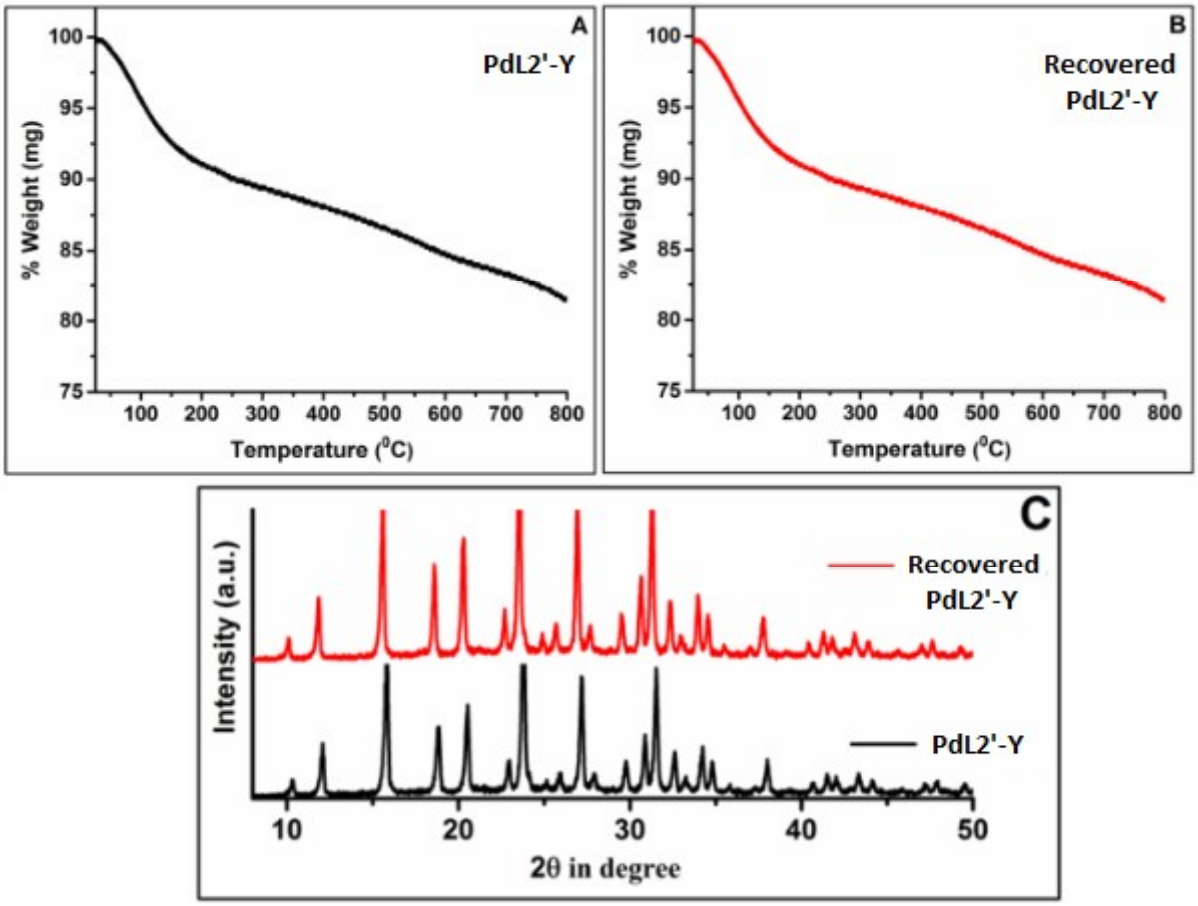

Figure 5B.24: Thermo gravimetric analysis (TGA) results for (A) PdL2′-Y, (B) Recovered catalyst PdL2′-Y and (C) XRD patterns for PdL2′-Y and recovered PdL2′-Y.

Table 5B.8: Coupling reaction between bromobenzene and styrene catalyzed by palladium complexes

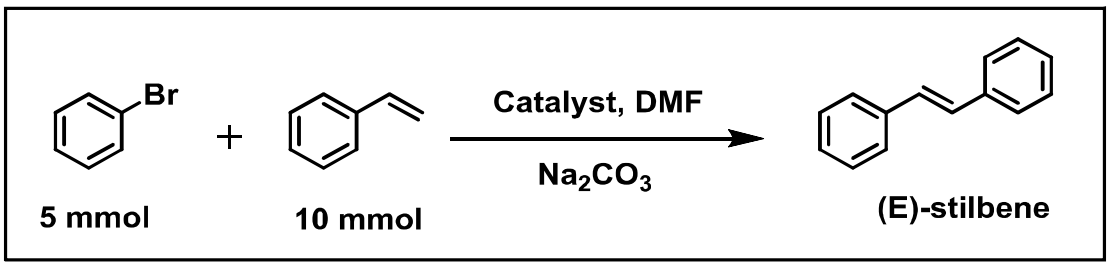

S.No.	Catalyst	mmol % of Pd	Reaction temp. (°C)	% Yield of Product[a]	TON[b]
1	**Zeolite Y**	-	140	Nil	-
2	**Pd-Y**	0.70	140	15.8	122
3	**PdL1′**	0.70	140	56.5	416
4	**PdL5′**	0.70	140	83.6	595
5	**PdL6′**	0.70	140	38.4	281
6	**PdL1′-Y**	0.70	140	90.0	649
7	**PdL5′-Y**	0.70	140	39.2	313
8	**PdL6′-Y**	0.70	140	65.7	474
9	**PdL2′**	0.70	140	72.1	565
10	**PdL3′**	0.70	140	55.5	436
11	**PdL4′**	0.70	140	70.1	549
12	**PdL2′-Y**	0.70	140	93.4	710
13	**PdL3′-Y**	0.70	140	67.9	532
14	**PdL4′-Y**	0.70	140	48.4	379

Entry 1-8 are taken from previous chapter 5A.

Reaction conditions: Bromobenzene (5mmol), Styrene (10 mmol), Na_2CO_3 (10 mmol), 10 mL of DMF, catalyst, Reaction time-20 h.

[a] Determined by gas chromatography. [b] Turnover number calculated at the completion of reaction (mol of bromobenzene transformed / mol of palladium metal in catalyst)

The direct comparison of catalytic results presented in this work with literature data is not very straight-forward as the parameters of interest could be many. The results and the conditions from these studies are summarized in table 5B.9. In terms of the parameters like catalyst used, time taken, % yield and

TON (turn over number), the catalyst of interest for the current study, **PdL2′ -Y** competes well with other such catalysts.

Table 5B.9: Catalytic activity of the present catalyst in comparison to some reported catalysts for the Heck coupling reaction between bromobenzene and styrene.

S.No.	Catalyst	Conditions	Time (h)	Yield (%)	TON	Ref.
1	**Pd-complex anchored GO[a] catalyst (Pd2)**	DMF/Na_2CO_3/150 °C	3	32	323	[40]
2	**[SBA-15/CCMet/Pd(II)]**	DMF/Et_3N/110 °C	3	98	98	[41]
3	**[Pd-TPA/ZrO_2][b]**	DMF/K_2CO_3/120 °C	6	59	123	[42]
4	**Palladium(II) Salophen complex**	DMA/Na_2CO_3/140 °C	12	74	9.3	[43]
5	**Fe_3O_4@SiO_2@Pd(II)-Slp. Comp.[d]**	(H_2O+DMF)[c]/K_2CO_3 /90 °C	6	89	445	[44]
6	**PdL2′-Y**	**DMF/Na_2CO_3/140 °C**	**20**	**93.4**	**710**	**This study**

[a] GO stands for Graphite oxide, [b] Pd exchanged supported 12-tungstophosphoric acid, [c] H_2O/DMF = (2/1) and [d] Bis-salophen palladium complex immobilized on Fe_3O_4@SiO_2 nanoparticles.

5B.2.9 Correlation between structural modification and modified functionality

In transition metal based homogenous catalysis, one of the governing factors is the characteristics/nature of the ligand. Palladium (II) Schiff-base complexes have planar geometry around the metal centre. Activity of the homogeneous catalysts could be varied with the presence of different substituent group attached to the ligand moiety. Upon encapsulation, additionally the steric and electrostatic constraints are imposed by the host, zeolite Y on the guest complexes which subsequently modify electronic, magnetic and redox properties, along with a striking change in the catalytic activity of the enclosed guest complex.[45] The modified catalytic reactivity towards Heck reaction is eventually an outcome of the structural adaptation of the palladium Schiff base complexes upon encapsulation.

[Pd(sal-1,3-phen)] type systems adopt typical structures where central aromatic ring (m-phenylenediamine) shows non-planar arrangement (discussed in chapter 5A). Due to this typical

arrangement of the ring, complete π-delocalization of the ligand system is interrupted. Apart from the π-delocalization, electronic effects of the substituent groups contribute significantly to the reactivity. Electron donating group (-OH and $–CH_3$) favors the π-delocalization and maintains the planarity of the Pd(II) complex whereas an electron withdrawing group (-Br) causes the non-planarity around the palladium metal center. Observations obtained from electronic spectroscopic studies of free-state complexes can be accounted for the fact, as metal-related transition of PdL2′ (with –OH group) complex appears at 458 nm whereas this band is at 450 nm for PdL4′ (with $–CH_3$ group) complex and the same transition for PdL3′ (with –Br group) is blue shifted. Catalysis results observed for free-state Pd(II) complexes indicate the activity order as PdL2′ ≥ PdL4′ > PdL3′. Electron donating group -OH and $–CH_3$ in PdL2′ and PdL4′ complex respectively make the palladium metal center becomes less electropositive causing the red-shift in the d-d transition and subsequently, more catalytically active towards the Heck coupling reaction. PdL3′ complex, on the other end, with electron withdrawing group (-Br group) is least active among the all-neat complexes. After the encapsulation in zeolite-Y, structure of these Pd(II) Schiff-base complexes is modified considerably due to steric and electrostatic constraint provided by the framework of zeolite Y. In case of all encapsulated complexes (PdL2′-Y, PdL3′-Y and PdL4′-Y), lowest energy transition is shifted towards higher wavelength with no exception. In our previous study (chapter 5A), theoretical studies clearly indicate improved planarity in the encapsulated complexes and hence enhanced π-delocalization around the metal center as the topology of the host framework enforces central ring to tilt towards molecular plane. Therefore, all the encapsulated complexes show red shift in the lowest energy transition with comparison to their neat forms. Encapsulation of PdL4′ complex with -CH_3 substituent, obstructs electron-donating effect to some extent and on the other side, host topology enforces partial planarity in the system. The electronic effect of the substituent and that originating from steric constraints due to encapsulation oppose each other; consequently, marginal red shift in the lowest energy metal related transition is observed. In case of encapsulated PdL3′-Y complex, both the electronic effect of –Br substituent group and that from structural modification reinforce each other leading to a significant red shift. Moreover, encapsulated palladium complexes PdL2′-Y and PdL3′-Y have shown remarkable improvement in catalytic activity towards Heck coupling reaction.

The electronic effects from both the sources (substituent and steric constraint) in case of encapsulated PdL2′-Y complex oppose each other very similarly like PdL4′-Y with $–CH_3$ substituent and

subsequently, red shift in metal related low energy transition is expected to be nominal. However, after encapsulation PdL2′-Y complex shows an unexpectedly high red shift. A further striking observation is encapsulated PdL2′-Y is the most efficient catalyst among all even when compared the reactivity of encapsulated Pd(II) Schiff-base complexes with electron donating substituent like –OCH_3 group discussed earlier (in chapter 5A), In this context, Thermo gravimetric (TGA) analysis, poor solubility offers some insight and is well supported by the theoretical studies. Only free-state PdL2′ complex among the all free-state palladium complexes shows weight loss in the temperature range of (35-110) °C corresponding to the loss of two water molecules per molecule of the complex in TGA plot. Not only that, PdL2′ complex shows poor solubility in most of the common protic solvents. All neat complexes except PdL2′ complex show good solubility in chloroform, methanol and water whereas PdL2′ complex is soluble in solvents like DMF and DMSO. These observations directly hint towards the presence of intermolecular hydrogen bonding in between water molecules and hydroxyl substituent of the complex in neat state. Theoretical studies also predict such association with energy stabilization of 16 kcal. However, there is no indication of such association with water molecules in encapsulated state and is well-understood as space constraint imposed by zeolite supercage hinders such association. Therefore, comparative behavior of PdL2′ complex is strikingly different after encapsulation in zeolite-Y and even in neat state from all others. In neat state, electron-donating power of -OH group towards the metal and ring is significantly reduced due to the association with the water molecules however, after encapsulation, both effect (donating power of the free –OH substituent and steric constraints imposed by the walls of zeolite-Y) work parallel resulting large red shift in metal-related transition. Therefore, the neat and encapsulated complexes follow the reactivity order as PdL2′ ≥ PdL4′ > PdL3′ and PdL2′-Y > PdL3′-Y > PdL4′-Y respectively. With encapsulation, electronic effects from substituent –OH group and that imposed by the framework of zeolite finally revamp the electron density around the metal center, and thereby, PdL2′-Y system appears to be the most proficient catalyst amongst the all entries in the Table 5B.8. Hence, structural modifications of these palladium complexes play a central role for the enhanced reactivity towards Heck coupling reaction. Currently discussed PdL2′-Y (complex with –OH substituent) and previously discussed (in chapter 5A) PdL1′-Y (complex without substituent) systems have almost same reactivity for Heck coupling reaction between styrene and bromobenzene. However, currently discussed PdL2′-Y is still marginally better. One more interesting point to note here is, the most active system found currently has -OH group attached and encapsulated whereas the most active

system previously discussed one is also encapsulated but without any substituent. Eventually this particular observation highlights the novelty of the current work. The encapsulated PdL2′-Y system with electron donating (-OH) group is expected to replicate the findings obtained for the PdL5′-Y (encapsulated complex has $–OCH_3$ group) discussed earlier, as both the cases strong electron donating groups are attached to the ligand moiety at the same position. However, these two systems behave oppositely. Encapsulated PdL2′ complex does not follow the expected trend of catalysis as is discussed previously. The electronic spectroscopy and theoretical studies along with other techniques could justify the catalytic behavior of this system. The originality of the present study lies into delivering apprehension of the findings of all the experimental and theoretical studies, which could further be explored to design newer catalysts.

5B.3 CONCLUSION

Three freshly-designed palladium(II) Schiff-base complexes have been successfully synthesized inside the supercage of zeolite-Y. Both neat and encapsulated states are well characterized with the help of various spectroscopic techniques like XRD, SEM-EDS, BET, thermal analysis, XPS, IR, and UV-Vis studies. Electronic effect of the substituent group in neat Pd(II) complexes has been analyzed by using UV-Vis spectroscopy and theoretical studies. Synthesized palladium complexes have been employed as catalyst for the Heck coupling reaction. Existence of an electron donating substituent in the 5^{th}position of the ligand moiety causes red shift in metal-related transition whereas electron-withdrawing group causes blue shift. Square planar palladium Schiff-base complex with electron donating group are proficient catalysts towards the Heck coupling reaction than that of palladium complex with electron withdrawing group. Encapsulated palladium complexes are found to be advantageous over the neat state analogues in terms of recyclability and thermal stability of the catalyst. Catalytic activities of the encapsulated palladium complexes are governed by the structural modification that is induced by the electrostatic environment of the zeolite-Y. It means upon encapsulation, electronic effect of the substituent and structure of the guest complex can be tuned thoroughly by imposing space constraints. The main intend of the study is to know the structural modification of the palladium(II) Schiff-base complex after encapsulation as well as to explore the modified reactivity of the systems. Encapsulated system PdL2′-Y exhibits consequential red shift in lowest energy transition and subsequently manifests exciting reactivity after encapsulation resulting from enhanced π-delocalization in the ligand system.

5B.4 REFERENCES

1. R. M. Clarke and T. Storr, *Dalton Trans.*, 2014, **43**, 9380-9391.
2. L. H. Abdel-Rahman, N. M. Ismail, M. Ismael, A. M. Abu-Dief and E. A.-H. Ahmed, *J. Mol. Struct.*, 2017, **1134**, 851-862.
3. T. Kiran, V. G. Prasanth, M. Balamurali, C. Vasavi, P. Munusami, K. I. Sathiyanarayanan and M. Pathak, *Inorg. Chim. Acta*, 2015, **433**, 26-34.
4. Y. He and C. Cai, *Catal. Commun.*, 2011, **12**, 678-683.
5. P. Das and W. Linert, *Coord. Chem. Rev.*, 2016, **311**, 1-23.
6. C. González-Arellano, A. Corma, M. Iglesias and F. Sánchez, *Adv. Synth. Catal.*, 2004, **346**, 1758-1764.
7. B. Banik, A. Tairai, N. Shahnaz and P. Das, *Tetrahedron Lett.*, 2012, **53**, 5627-5630.
8. M. M. Mogorosi, T. Mahamo, J. R. Moss, S. F. Mapolie, J. C. Slootweg, K. Lammertsma and G. S. Smith, *J. Organomet. Chem.*, 2011, **696**, 3585-3592.
9. A. Dewan, U. Bora and G. Borah, *Tetrahedron Lett.*, 2014, **55**, 1689-1692.
10. T. Selvaraj and R. Rajalingam, *ACS Omega*, 2018, **3**, 9613-9619.
11. F. Li, D. Hu, Y. Yuan, B. Luo, Y. Song, S. Xiao, G. Chen, Y. Fang and F. Lu, *Mol. Catal.*, 2018, **452**, 75-82.
12. A. Choudhary, S. Kumari and S. Ray, *ACS Omega*, 2017, **2**, 6636-6645.
13. C. K. Modi, N. Solanki, R. Vithalani and D. Patel, *Appl. Organomet. Chem.*, 2018, **32**, e3910.
14. S. C. Mohan, R. V. Solomon, P. Venuvanalingam and K. Jothivenkatachalam, *New J. Chem.*, 2017, **41**, 9505-9512.
15. H. Mei, J. Hu, S. Xiao, Y. Lei and G. Li, *Appl. Catal., A*, 2014, **475**, 40-47.
16. N. Wang, Q. Sun, R. Bai, X. Li, G. Guo and J. Yu, *J. Am. Chem. Soc.*, 2016, **138**, 7484-7487.
17. Z. Guan, J. Hu, Y. Gu, H. Zhang, G. Li and T. Li, *Green Chem.*, 2012, **14**, 1964-1970.
18. L. Djakovitch, H. Heise and K. Köhler, *J. Organomet. Chem.*, 1999, **584**, 16-26.
19. W. H. Quayle, G. Peeters, G. L. De Roy, E. F. Vansant and J. H. Lunsford, *Inorg. Chem.*, 1982, **21**, 2226-2231.
20. A. Choudhary, B. Das and S. Ray, *Dalton Trans.*, 2015, **44**, 3753-3763.
21. A. Choudhary, B. Das and S. Ray, *Dalton Trans.*, 2016, **45**, 18967-18976.
22. K. K. Bania, D. Bharali, B. Viswanathan and R. C. Deka, *Inorg. Chem.*, 2012, **51**, 1657-1674.
23. Y. Umemura, Y. Minai and T. Tominaga, *The Journal of Physical Chemistry B*, 1999, **103**, 647-652.
24. K. K. Bania and R. C. Deka, *J. Phys. Chem. C*, 2012, **116**, 14295-14310.
25. H. S. Abbo and S. J. Titinchi, *Top. Catal.*, 2010, **53**, 1401-1410.
26. C. B. Vidal, G. S. Raulino, A. L. Barros, A. C. Lima, J. P. Ribeiro, M. J. Pires and R. F. Nascimento, *J. Environ. Manage.*, 2012, **112**, 178-185.
27. D. R. Godhani, H. D. Nakum, D. K. Parmar, J. P. Mehta and N. C. Desai, *J. Mol. Catal. A: Chem.*, 2017, **426**, 223-237.
28. K. Mori, K. Kagohara and H. Yamashita, *J. Phys. Chem. C*, 2008, **112**, 2593-2600.
29. S. L. Hailu, B. U. Nair, M. Redi-Abshiro, I. Diaz, R. Aravindhan and M. Tessema, *Chinese Journal of Catalysis*, 2016, **37**, 135-145.
30. H. Naeimi and M. Moradian, *Appl. Catal., A*, 2013, **467**, 400-406.
31. S. K. Das, S. P. Mahanta and K. K. Bania, *RSC Adv.*, 2014, **4**, 51496-51509.
32. R. M. Barrer, *Hydrothermal chemistry of zeolites*, London : Academic press, 1982.
33. B. Dutta, S. Jana, R. Bera, P. K. Saha and S. Koner, *Appl. Catal., A*, 2007, **318**, 89-94.

34. A. P. S. Andrade, L. M. Arantes, J. Y. Kadooca, R. L. Carvalho, Â. de Fátima and A. A. Sabino, *Inorg. Chim. Acta*, 2016, **1**, 886-890.
35. A. s. Mollar-Cuni, D. Ventura-Espinosa, S. Martín, Á. Mayoral, P. Borja and J. A. Mata, *ACS Omega*, 2018, **3**, 15217-15228.
36. H. Liu, X. Xue, T. Li, J. Wang, W. Xu, M. Liu, P. Chen and Y. Wu, *RSC Adv.*, 2016, **6**, 84815-84824.
37. K. K. Bania and R. C. Deka, *J. Phys. Chem. C*, 2013, **117**, 11663-11678.
38. M. Frisch, G. Trucks, H. Schlegel, G. Scuseria, M. Robb, J. Cheeseman, J. Montgomery Jr, T. Vreven, K. Kudin and J. Burant, *Inc.: Wallingford, CT.*
39. A. Choudhary, B. Das and S. Ray, *Inorg. Chimi. Acta*, 2017, **462**, 256-265.
40. Á. Mastalir, M. Hancsárik and T. Szabó, *Appl. Organomet. Chem.*, 2020, **34**, e5565.
41. H. Veisi, D. Kordestani and A. R. Faraji, *J. Porous Mater.*, 2014, **21**, 141-148.
42. S. Pathan and A. Patel, *RSC Adv.*, 2012, **2**, 116-120.
43. A. P. Andrade, L. M. Arantes, J. Y. Kadooca, R. L. Carvalho, A. de Fatima and A. A. Sabino, *ChemistrySelect*, 2016, **1**, 886-890.
44. A. R. Sardarian, M. Kazemnejadi and M. Esmaeilpour, *Dalton Trans.*, 2019, **48**, 3132-3145.
45. K. K. Bania and R. C. Deka, *J. Phys. Chem. C*, 2011, **115**, 9601-9607.